

Constraints on the neutrino parameters by future cosmological 21cm line and precise CMB polarization observations

Yoshihiko Oyama¹, Kazunori Kohri^{2,3} and Masashi Hazumi^{2,3,4}

¹ *Institute for Cosmic Ray Research, The University of Tokyo, 5-1-5 Kashiwanoha, Kashiwa, Chiba 277-8582, Japan*

² *Institute of Particle and Nuclear Studies, KEK, 1-1 Oho, Tsukuba, Ibaraki 305-0801, Japan*

³ *The Graduate University for Advanced Studies (SOKENDAI), 1-1 Oho, Tsukuba, Ibaraki 305-0801, Japan*

⁴ *Kavli IPMU (WPI), UTIAS, The University of Tokyo, 5-1-5 Kashiwanoha, Kashiwa, Chiba 277-8583, Japan*

Abstract

Observations of the 21 cm line radiation coming from the epoch of reionization have a great capacity to study the cosmological growth of the Universe. Besides, CMB polarization produced by gravitational lensing has a large amount of information about the growth of matter fluctuations at late time. In this paper, we investigate their sensitivities to the impact of neutrino property on the growth of density fluctuations, such as the total neutrino mass, the effective number of neutrino species (extra radiation), and the neutrino mass hierarchy. We show that by combining a precise CMB polarization observation such as Simons Array with a 21 cm line observation such as Square kilometer Array (SKA) phase 1 and a baryon acoustic oscillation observation (Dark Energy Spectroscopic Instrument:DESI) we can measure effects of non-zero neutrino mass on the growth of density fluctuation if the total neutrino mass is larger than 0.1 eV. Additionally, the combinations can strongly improve errors of the bounds on the effective number of neutrino species $\sigma(N_\nu) \sim 0.06 - 0.09$ at 95 % C.L.. Finally, by using SKA phase 2, we can determine the neutrino mass hierarchy at 95 % C.L. if the total neutrino mass is similar to or smaller than 0.1 eV.

1 Introduction

Due to the discovery of non-zero neutrino masses by Super-Kamiokande through neutrino oscillation experiments in 1998, the standard model of particle physics was forced to be modified so as to theoretically include the neutrino masses.

So far only the mass-squared differences of neutrino species have been measured by neutrino oscillation experiments, which are reported to be $\Delta m_{21}^2 \equiv m_2^2 - m_1^2 = 7.59_{-0.21}^{+0.19} \times 10^{-5} \text{ eV}^2$ [1] and $\Delta m_{32}^2 \equiv m_3^2 - m_2^2 = 2.43_{-0.13}^{+0.13} \times 10^{-3} \text{ eV}^2$ [2]. However, absolute values and their hierarchical structure (normal or inverted) have not been obtained yet although information on them is indispensable to build new particle physics models.

In particle physics, some new ideas and new future experiments have been proposed to measure the absolute values and/or determine the hierarchy of neutrino masses, e.g., through tritium beta decay in KATRIN experiment [3], neutrinoless double-beta decay [4], atmospheric neutrinos in the proposed iron calorimeter at INO [5, 6] and the upgrade of the IceCube detector (PINGU) [7], and long-baseline oscillation experiments, e.g., NO ν A [8], J-PARC to Korea (T2KK) [9, 10] or Oki island (T2KO) [11], and CERN to Super-Kamiokande with high energy (5 GeV) neutrino beam [12].

On the other hand, such nonzero neutrino masses affect cosmology significantly through suppression of growth of density fluctuation because relativistic neutrinos have large thermal velocity and erase their own density fluctuations up to horizon scales due to their free streaming behavior. By measuring power spectra of density fluctuations, we can constrain the total neutrino mass Σm_ν [13–35] and the effective number of neutrino species N_ν [22, 23, 25–38] through observations of cosmic microwave background (CMB) anisotropies and large-scale structure (LSS). We can also obtain additional information about N_ν from the CMB bispectrum [39]. Furthermore, we can constraint on the neutrino isocurvature perturbations from CMB observations [40, 41]. The robust upper bound on Σm_ν obtained so far is $\Sigma m_\nu < 0.23 \text{ eV}$ (95 % C.L.) by the CMB observation by Planck (see Ref. [31, 32]). For forecasts for future CMB observations, see also Refs. [42–45]. For current constraints and forecasts for combinations of cosmological and laboratory experiments (oscillation and neutrinoless double-beta decay), see also Ref. [46].

Moreover, by observing the power spectrum of cosmological 21 cm line radiation fluctuation, we will be able to obtain useful information on the neutrino masses [47–53], and its asymmetry (lepton number asymmetry) [54]. Besides, we can obtain further information about the neutrino masses from observations of the HI distribution in the post-reionization era [55]. That is because the 21 cm line radiation is emitted (1) long after the recombination (at a redshift $z \ll 10^3$) and (2) before an onset of the LSS formation. The former condition (1) gives us information on smaller neutrino mass ($\lesssim 0.1 \text{ eV}$), and the latter condition (2) means we can treat only a linear regime of the matter perturbation, which can be analytically calculated unlike the LSS case.

In actual analyses, it is essential that we combine data of the 21 cm line with those of CMB because the constrained cosmological parameter space is complementary to each other. For example, the former is quite sensitive to the dark energy density, but the latter

is relatively insensitive to it. On the other hand, the former has only a mild sensitivity to the normalization of matter perturbation, but the latter has an obvious sensitivity to it by definition. In pioneering work by [49], the authors tried to make a forecast for constraint on the neutrino mass hierarchy by combining Planck with future 21 cm line observations in case of relatively degenerate neutrino masses $\Sigma m_\nu \sim 0.3$ eV. Additionally, in our previous work [52], we investigate the detectability of the mass hierarchy by combination of a futuristic 21 cm line observation (Omniscope [56, 57]) and CMB polarization observation (POLARBEAR or CMBPol) when the total neutrino mass is relatively small value $\Sigma m_\nu \leq 0.3$ eV. The CMB B-mode polarization produced by CMB lensing gives us more detailed information on the matter power spectrum [58] at later epochs. In that work, we found that the combinations have enough sensitivity to distinguishing the neutrino mass hierarchy when total neutrino mass is $\Sigma m_\nu \sim 0.1$ eV or less.

In this paper, as for 21 cm line observation, we particularly focus on Square Kilometer Array (SKA) [59], which is planned in the 2020s and more realistic observation than Omniscope in near future, and forecast allowed parameter regions for the neutrino masses, the effective number of neutrino species and the mass hierarchy. In our analysis, we consider combinations of SKA with ground-based CMB polarization observations, such as POLARBEAR-2 or Simons Array, which can measure the gravitational lensing of CMB with a high degree of accuracy. Besides, we take into account including the information of baryon acoustic oscillation (BAO) observations, such as Dark Energy Spectroscopic Instrument (DESI) [60].

This paper is organized as follows. In Section 2, we briefly review 21 cm line observation, analytical methods used in this paper, and how neutrino properties are constrained by the 21 cm line observation. In Section 3 and 4, we explain analytical methods of CMB and BAO observation, respectively. We show our results in Section 5, and Section 6 is devoted to our conclusion.

2 21 cm line observation

In this section, we briefly review basic methods to use the 21 cm line observation as a cosmological probe. For further details, we refer to Refs. [61, 62].

2.1 Power spectrum of 21 cm radiation

The 21 cm line of neutral hydrogen atom is emitted by transition between the hyperfine levels of the 1S ground state, and the hyperfine structure is induced by an interaction of magnetic moments between proton and electron. It can be observed as the differential brightness temperature relative to the CMB temperature T_{CMB} :

$$\Delta T_b(\mathbf{r}, z) = \frac{3c^3 h A_{21}}{32\pi k_B \nu_{21}^2} \frac{x_{HI}(\mathbf{r}, z) n_H(\mathbf{r}, z)}{(1+z) H(z)} \left(1 - \frac{T_{\text{CMB}}(\mathbf{r}, z)}{T_S(\mathbf{r}, z)}\right) \left(1 - \frac{1+z}{H(z)} \frac{dv_{p\parallel}(\mathbf{r}, z)}{dr_{\parallel}}\right), \quad (1)$$

where \mathbf{r} is the comoving coordinate of the 21 cm radiation, z represents the redshift, $A_{21} \simeq 2.869 \times 10^{-15} \text{s}^{-1}$ is the spontaneous decay rate of 21 cm line transition, $\nu_{21} \simeq 1.42 \text{ GHz}$ is the 21 cm line frequency, n_H is the number density of hydrogen and x_{HI} is the fraction of neutral hydrogen. T_S is the spin temperature, which is defined by $n_1/n_0 = 3 \exp(-T_{21}/T_S)$, where n_0 and n_1 are the number densities of singlet and triplet states of neutral hydrogen atom, respectively. Here $T_{21} = hc/k_B\lambda_{21}$ is the temperature corresponding to 21 cm line, and λ_{21} is its wavelength. $dv_{p\parallel}/dr_{\parallel}$ is the gradient of peculiar velocity along the line of sight.

From now on, we assume that $T_S \gg T_{\text{CMB}}$ because we focus on the epoch of reionization (EOR) during which this condition is well satisfied. In general, the brightness temperature is sensitive to details of inter-galactic medium (IGM). However, with a few reasonable assumptions, we can eliminate this dependence from the 21 cm line brightness temperature [63–65]. At the epoch of reionization long after star formation begins, X-ray background produced by early stellar remnants heats the IGM. Therefore, gas kinetic temperature T_K becomes much higher than the CMB temperature T_{CMB} . Furthermore, the star formation produces a large amount of Ly α photons sufficient to couple T_S to T_K through the Wouthuysen-Field effect [66, 67]. In this scenario, $T_{\text{CMB}} \ll T_K \sim T_S$ are justified at $z \lesssim 10$, and ΔT_b does not depend on T_S .

Next, we are going to consider fluctuations of $\Delta T_b(\mathbf{r})$. By expanding the hydrogen number density n_H and the ionization fraction x_i ($x_i = 1 - x_{HI}$) as $n_H(\mathbf{r}) = \bar{n}_H(1 + \delta(\mathbf{r}))$ and $x_i(\mathbf{r}) = \bar{x}_i(1 + \delta_x(\mathbf{r}))$, we can rewrite Eq. (1) to be

$$\Delta T_b(\mathbf{r}) = \Delta \bar{T}_b (1 - \bar{x}_i(1 + \delta_x(\mathbf{r}))) (1 + \delta(\mathbf{r})) \left(1 - \frac{1+z}{H(z)} \frac{dv_{p\parallel}(\mathbf{r}, z)}{dr_{\parallel}} \right), \quad (2)$$

where we assume that $T_S \gg T_{\text{cmb}}$ and neglect the term including spin temperature. $\Delta \bar{T}_b$ is the spatially averaged differential brightness temperature at redshift z and given by

$$\Delta \bar{T}_b \simeq 26.8 \left(\frac{1 - Y_p}{1 - 0.25} \right) \left(\frac{\Omega_b h^2}{0.023} \right) \left(\frac{0.15}{\Omega_m h^2} \frac{1+z}{10} \right)^{1/2} \text{ mK}, \quad (3)$$

where Y_p is the primordial ${}^4\text{He}$ mass fraction.

By denoting the fluctuation of ΔT_b as $\delta(\Delta T_b(\mathbf{x})) \equiv \Delta T_b(\mathbf{x}) - \bar{x}_H \Delta \bar{T}_b$, the 21 cm line power spectrum $P_{21}(\mathbf{k})$ in the k -space is defined by

$$\langle \delta(\Delta T_b^*(\mathbf{k})) \delta(\Delta T_b(\mathbf{k}')) \rangle = (2\pi)^3 \delta^3(\mathbf{k} - \mathbf{k}') P_{21}(\mathbf{k}). \quad (4)$$

By treating the peculiar velocity $\delta_v \equiv (1+z)(dv_{p\parallel}/dr_{\parallel})/H(z)$ as a perturbation and using that its Fourier transform is given by $\delta_v(\mathbf{k}) = -\mu^2 \delta(\mathbf{k})$ ($\mu = \hat{\mathbf{k}} \cdot \hat{\mathbf{n}}$ is the cosine of the angle between the wave vector and the line of sight), the power spectrum can be written as

$$P_{21}(\mathbf{k}) = P_{\mu^0}(k) + \mu^2 P_{\mu^2}(k) + \mu^4 P_{\mu^4}(k), \quad (5)$$

z	\bar{x}_H	b_{xx}^2	R_{xx} [Mpc]	α_{xx}	γ_{xx}	$b_{x\delta}^2$	$R_{x\delta}$ [Mpc]	$\alpha_{x\delta}$
9.2	0.9	0.208	1.24	-1.63	0.38	0.45	0.56	-0.4
8.0	0.7	2.12	1.63	-0.1	1.35	1.47	0.62	0.46
7.5	0.5	9.9	1.3	1.6	2.3	3.1	0.58	2.0
7.0	0.3	77.0	3.0	4.5	2.05	8.2	0.143	28.0

Table 1: Fiducial values of the parameters in $\mathcal{P}_{xx}(k)$ and $\mathcal{P}_{x\delta}(k)$ (See Eqs. (9) and (10)) [68].

where $k = |\mathbf{k}|$ and

$$P_{\mu^0} = \mathcal{P}_{\delta\delta} - 2\mathcal{P}_{x\delta} + \mathcal{P}_{xx}, \quad (6)$$

$$P_{\mu^2} = 2(\mathcal{P}_{\delta\delta} - \mathcal{P}_{x\delta}), \quad (7)$$

$$P_{\mu^4} = \mathcal{P}_{\delta\delta}. \quad (8)$$

Here, $\mathcal{P}_{\delta\delta} \equiv (\Delta\bar{T}_b)^2\bar{x}_{HI}^2P_{\delta\delta}$, $\mathcal{P}_{x\delta} \equiv (\Delta\bar{T}_b)^2\bar{x}_i\bar{x}_{HI}P_{x\delta}$ and $\mathcal{P}_{xx} \equiv (\Delta\bar{T}_b)^2\bar{x}_i^2P_{xx}$, where $P_{\delta\delta}$, $P_{x\delta}$ and P_{xx} are the power spectra defined in the same manner as Eq. (4) for the fluctuation of hydrogen number density δ and that of ionization fraction δ_x . Therefore, $P_{\delta\delta}$ traces the fluctuation of matter, which includes information on cosmological parameters such as neutrino mass.

$P_{x\delta}$ and P_{xx} can be neglected as long as we consider the era when the IGM is completely neutral. However, after the reionization starts, these two spectra significantly contribute to the 21 cm line power spectrum. Although a rigorous evaluation of these power spectra may need some numerical simulations, we adopt the treatment given in Ref. [68], where it is assumed that $\mathcal{P}_{x\delta}$ and \mathcal{P}_{xx} have specific forms which match simulations of radiative transfer in Refs. [69, 70]. The explicit forms of the power spectra are parametrized to be

$$\mathcal{P}_{xx}(k) = b_{xx}^2 [1 + \alpha_{xx}(kR_{xx}) + (kR_{xx})^2]^{-\gamma_{xx}/2} \mathcal{P}_{\delta\delta}(k), \quad (9)$$

$$\mathcal{P}_{x\delta}(k) = b_{x\delta}^2 e^{-\alpha_{x\delta}(kR_{x\delta}) - (kR_{x\delta})^2} \mathcal{P}_{\delta\delta}(k), \quad (10)$$

where b_{xx} , $b_{x\delta}$, α_{xx} , γ_{xx} and $\alpha_{x\delta}$ are parameters which characterize the amplitudes and the shapes of the spectra. R_{xx} and $R_{x\delta}$ represent the effective size of ionized bubbles. In our analysis, we adopt the values listed in Table 1 as the fiducial values of these parameters.

We note that the power spectrum in the k -space $P_{21}(\mathbf{k})$ are not directly measured by 21 cm line observations. Instead, the angular location on the sky and the frequency are measured by an experiment, and they can be specified by the following vector

$$\Theta = \theta_x \hat{e}_x + \theta_y \hat{e}_y + \Delta f \hat{e}_z \equiv \Theta_\perp + \Delta f \hat{e}_z, \quad (11)$$

where Δf represents the frequency difference from the central redshift z of a given redshift bin. Then, we can define the Fourier dual of Θ as

$$\mathbf{u} \equiv u_x \hat{e}_x + u_y \hat{e}_y + u_{\parallel} \hat{e}_z \equiv \mathbf{u}_\perp + u_{\parallel} \hat{e}_z. \quad (12)$$

Notice that u_{\parallel} has the unit of time since it is the Fourier dual of Δf . By using the flat-sky approximation ^{#1}, we can linearize the relation between \mathbf{r} and Θ , and it is written as

$$\Theta_{\perp} = \mathbf{r}_{\perp}/d_A(z), \quad \Delta f = \Delta r_{\parallel}/y(z), \quad (13)$$

where \mathbf{r}_{\perp} is the vector perpendicular to the line of sight, Δr_{\parallel} is the comoving distance interval corresponding to the frequency intervals Δf , $d_A(z)$ is the comoving angular diameter distance, and $y(z) \equiv \lambda_{21}(1+z)^2/H(z)$. Then, the relation between \mathbf{k} and \mathbf{u} can be written as

$$\mathbf{u}_{\perp} = d_A \mathbf{k}_{\perp}, \quad u_{\parallel} = y k_{\parallel}. \quad (14)$$

The power spectrum of ΔT_b in the u -space can be defined in the same manner as the treatment in the k -space. By replacing \mathbf{k} with \mathbf{u} in Eq. (4) and using the relation between \mathbf{k} and \mathbf{u} , those two spectra are related each other by

$$P_{21}(\mathbf{u}) = \frac{1}{d_A(z)^2 y(z)} P_{21}(\mathbf{k}). \quad (15)$$

We use the u -space power spectrum in the following analysis because this quantity is directly measurable without any cosmological assumptions.

2.2 Forecasting methods

2.2.1 Fisher matrix of 21 cm line observation

Here, we provide a brief review of the Fisher matrix analysis for the 21 cm observations. In order to forecast errors of cosmological parameters, we use the Fisher matrix analysis [71]. The Fisher matrix of 21 cm line observations is given by [47]

$$F_{\alpha\beta}^{(21\text{cm})} = \sum_{\text{pixels}} \frac{1}{[\delta P_{21}(\mathbf{u})]^2} \left(\frac{\partial P_{21}(\mathbf{u})}{\partial \theta_{\alpha}} \right) \left(\frac{\partial P_{21}(\mathbf{u})}{\partial \theta_{\beta}} \right), \quad (16)$$

where $\delta P_{21}(\mathbf{u})$ is the error in the power spectrum measurements for a Fourier pixel \mathbf{u} , and θ_i represents a cosmological parameter with its index "i". The 1σ error of the parameter θ_i is evaluated by the Fisher matrix, and it is given by

$$\Delta \theta_{\alpha} \geq \sqrt{(F^{-1})_{\alpha\alpha}}. \quad (17)$$

When we differentiate $P_{21}(\mathbf{u})$ with respect to the cosmological parameters, we fix $\mathcal{P}_{\delta\delta}(k)$ in Eqs. (9) and (10) so that we get conservative evaluations for errors of cosmological parameters. In this situation, the information of the matter distribution only comes from

^{#1} Even if we consider all-sky experiments, the flat-sky approximation can be valid as long as we analyze the data in a lot of small patches of the sky [68].

	N_{ant}	$A_e(z = 8)$ [m 2]	L_{\min} [m]	L_{\max} [km]	FoV($z = 8$) [deg 2]	t_0 [hour per field]	z
SKA1	$911 \times 1/2$	443	35	6	13.12	1000	$6.8 - 10$
SKA2	911×4	443	35	6	13.12	1000	$6.8 - 10$

Table 2: Specifications for 21 cm line experiments adopted in the current analysis. We assume that for SKA phase 1 (SKA1) (re-baseline design), the number of antennae is half as many as that of the originally planned SKA1, which has 911 antennae, and for SKA phase 2 (SKA2), the number of antennae is 4 times as many as that of originally planned SKA1. Additionally, for SKA 1 and 2, we assume that multiple fields are observed by using these experiments, and the number of fields is $N_{\text{filed}} = 4$ or 8 in our analyses. Then, the effective field of view is $\text{FoV}_{\text{SKA}} = 13.21 \times N_{\text{filed}}$ [deg 2].

the $\mathcal{P}_{\delta\delta}(k)$ terms in P_{μ^0} , P_{μ^2} and P_{μ^4} . The error of the power spectrum $\delta P_{21}(\mathbf{u})$ consists of sample variances and experimental noises, and is written by

$$\delta P_{21}(\mathbf{u}) = \frac{P_{21}(\mathbf{u}) + P_N(u_{\perp})}{N_c^{1/2}}, \quad (18)$$

where the first term on the right hand side represents the contribution from sample variance, and the second term gives that of experimental noise, respectively. Here, $N_c = 2\pi k_{\perp} \Delta k_{\perp} \Delta k_{\parallel} V(z)/(2\pi)^3$ is the number of independent cells in an annulus summing over the azimuthal angle, $V(z) = d_A(z)^2 y(z) B \times \text{FoV}$ is the survey volume, where B is the bandwidth, and $\text{FoV} \propto \lambda^2$ is the field of view of an interferometer.

2.2.2 Specifications of the experiment

We show the specifications of the 21 cm line observation which is considered in this paper.

Survey range

In our analyses, we consider the redshift range $z = 6.75 - 10.05$, which we divide into 4 bins: $z = 6.75 - 7.25$, $7.25 - 7.75$, $7.75 - 8.25$ and $8.25 - 10.05$. For the wave number, we set its minimum cut off $k_{\min\parallel} = 2\pi/(yB)$ to avoid foreground contaminations [47], and take its maximum value $k_{\max} = 2 \text{ Mpc}^{-1}$ in order not to be affected by a nonlinear effect which becomes important on $k \geq k_{\max}$. For methods of foreground removals, see also recent discussions about the independent component analysis (ICA) algorithm (FastICA) [72] which will be developed in terms of the ongoing LOFAR observation [73].

Noise power spectrum

The noise power spectrum, $P_N(u_{\perp})$ appeared in Eq. (18) is given by

$$P_N(u_{\perp}) = \left(\frac{\lambda^2(z) T_{\text{sys}}(z)}{A_e(z)} \right)^2 \frac{1}{t_0 n(u_{\perp})}, \quad (19)$$

where, the system temperature T_{sys} is estimated to be $T_{\text{sys}} = T_{\text{sky}} + T_{\text{rcvr}}$, and is dominated by the sky temperature due to synchrotron radiation. Here, $T_{\text{sky}} = 60(\lambda/[m])^{2.55}$ [K] is the sky temperature, and $T_{\text{rcvr}} = 0.1T_{\text{sky}} + 40$ [K] is the receiver noise [59]. In addition, the effective collecting area is proportional to the square of the observed wave length $A_e \propto \lambda^2$. The number density of the baseline $n(u_\perp)$ depends on an actual antenna distribution.

To obtain the future cosmological constraints from 21 cm experiments, we consider SKA (phase 1 and phase 2) [59, 74], whose specifications are shown in Table 2. In order to calculate the number density of the baseline $n(u_\perp)$, we have to determine a realization of antenna distributions. Recently, SKA phase 1 re-baseline design was determined, and its total collecting area is one-half as large as that of the originally planned SKA phase 1. Therefore, for SKA1 (re-baseline design), we assume that the number of antennae is half as many as that of the originally planned SKA1, which has 911 antennae, and for SKA phase 2 (SKA2), the number of antennae is 4 times as many as that of the originally planned SKA1.

The number density of the baseline of the originally planned SKA1 is determined as follows. We take 95% (866) of the total antennae (stations) distributed with a core region of radius 3000 m, and the distribution has an antenna density profile of the originally planned SKA1 $\rho_{\text{origSKA1}}(r)$ (r : a radius from center of the array) as follows [58],

$$\rho_{\text{origSKA1}}(r) = \begin{cases} \rho_0 r^{-1}, & \rho_0 \equiv \frac{13}{16\pi(\sqrt{10}-1)} \text{ m}^{-2} \\ \rho_1 r^{-3/2}, & \rho_1 \equiv \rho_0 \times 400^{1/2}, \\ \rho_2 r^{-7/2}, & \rho_2 \equiv \rho_1 \times 1000^2, \\ \rho_3 r^{-9/2}, & \rho_3 \equiv \rho_2 \times 1500, \\ \rho_4 r^{-17/2}, & \rho_4 \equiv \rho_3 \times 2000^4, \end{cases} \begin{array}{ll} r \leq 400 \text{ m}, & \\ 400 \text{ m} < r \leq 1000 \text{ m}, & \\ 1000 \text{ m} < r \leq 1500 \text{ m}, & \\ 1500 \text{ m} < r \leq 2000 \text{ m}, & \\ 2000 \text{ m} < r \leq 3000 \text{ m}. & \end{array} \quad (20)$$

Here, we assume an azimuthally symmetric distribution of antennae in SKA. In this analysis, we ignore measurements from the sparse distribution of the remaining 5% of the total antennae that are outside this core region. This distribution agrees with the specification of the originally planned SKA1 baseline design.

By using this distribution, we can calculate the number density of baseline of the originally planned SKA1 $n_{\text{origSKA1}}(u_\perp)$. For SKA1 (re-baseline design) and SKA2, we assume that these number densities of baseline are

$$n_{\text{SKA1}}(u_\perp) = n_{\text{origSKA1}}(u_\perp) \times \left(\frac{1}{2}\right)^2, \quad (21)$$

$$n_{\text{SKA2}}(u_\perp) = n_{\text{origSKA1}}(u_\perp) \times 4^2, \quad (22)$$

where $n_{\text{SKA1}}(u_\perp)$ is the number density of baseline of SKA1, and $n_{\text{SKA2}}(u_\perp)$ is that of SKA2, respectively.

2.3 Contribution of residual foregrounds

Here, we consider the some existing residual foregrounds. For the 21 cm line observation, we take account of the most dominant galactic foreground, namely the synchrotron radi-

ation. We assume that the foreground subtraction can be done down to a given level, and treat the contribution of residual foreground as the Gaussian random field. Then, we introduce the following effective noise including the contribution of residual foreground [53],

$$P_{N,\text{eff}}(\mathbf{u}_\perp) = \left(\frac{\lambda^2 T_{sys}}{A_e} \right)^2 \frac{1}{n_b(\mathbf{u}_\perp)t_0} + (\sigma_{21\text{cm}}^{\text{RFg}} \times 1 \text{ MHz}) C^{\text{Fg}}(\mathbf{u}_\perp, \nu_*), \quad (23)$$

where ν_* is the central frequency value in the frequency band, and $C^{\text{Fg}}(\mathbf{u}_\perp, \nu)$ is the power of foreground. In Eq.(23), we introduce a foreground removal parameter $\sigma_{21\text{cm}}^{\text{RFg}}$, and assume $\sigma_{21\text{cm}}^{\text{RFg}} = 10^{-7}$ in forecasts of constraints on Σm_ν and N_ν (Sec. 5.2), and $\sigma_{21\text{cm}}^{\text{RFg}} = 10^{-8}$ in those of constraints on Σm_ν and the mass hierarchy (Sec. 5.3). When we include the contribution of residual foregrounds, we use this effective noise as the 21cm noise power spectrum.

As long as we use the flat sky approximation, the u space variable \mathbf{u}_\perp is related to the multipole ℓ of angular power spectrum, $|\mathbf{u}_\perp| = \ell/2\pi$. In our analysis, we use the scale dependence of synchrotron radiation as the foreground power $C^{\text{Fg}}(\mathbf{u}_\perp, \nu) = C_\ell^S(\nu)$, and we model the synchrotron foreground $C_\ell^S(\nu)$ as

$$C_\ell^S(\nu) = A_S \left(\frac{\nu}{\nu_{S,0}} \right)^{2\alpha_S} \left(\frac{\ell}{\ell_{S,0}} \right)^{\beta_S}. \quad (24)$$

where $\alpha_S = -3$, $\beta_S = -2.6$, $\nu_{S,0} = 30$ GHz, $\ell_{S,0} = 350$, $A_S = 4.7 \times 10^{-5} \mu\text{K}^2$. These choices are the values used in the Refs. [84, 85], and match the parameters of foregrounds observed by WMAP [87], DASI [88].

2.4 Effects of neutrino mass on matter power spectrum

The massive neutrinos affect the growth of matter density fluctuation mainly due to the following two physical mechanisms. [75, 76]. First of all, a massive neutrino becomes non-relativistic at $3T_{\nu_i} \sim m_{\nu_i}$, and contributes to the energy density of cold dark matter (CDM). Therefore, the matter-radiation equality time and the expansion rate of the universe are affected by the transition between relativistic and non-relativistic neutrino. When we consider the total mass of neutrinos Σm_ν ($\lesssim 0.2 - 0.3$ eV), only the latter impact is effective because such light neutrinos do not become non-relativistic before the matter-radiation equality time. Secondly, the matter density fluctuation on small scales are suppressed due to the free-streaming effect of neutrino. As long as neutrinos are relativistic, they travel at speed of light, and their free-streaming scales are approximately equal to the Hubble horizon. Then, their own fluctuations within the free-streaming scales are erased, and their energy densities do not contribute to the growth of matter density fluctuation.

In comparison with the standard ΛCDM models in which three massless active neutrinos are assumed, we can introduce two more freedoms. A first additional freedom is the effective number of neutrino species N_ν , which represents generations of relativistic neutrinos

before the matter-radiation equality epoch. N_ν can include other relativistic components, and may not be equal to three. A second additional freedom is the hierarchy of neutrino masses. The difference of the hierarchy of neutrino masses affects both the free-streaming scales and the expansion rate of the Universe [77]. In terms of 21 cm line observations, the minimum cutoff of the wave number is given by $k_{\min} = 2\pi/(yB) \sim 6 \times 10^{-2} h\text{Mpc}^{-1}$ (see 2.2.2). However, the wave number corresponding to the neutrino free-streaming scale is $k_{\text{free}} \lesssim 10^{-2} h\text{Mpc}^{-1}$. Therefore, the main feature due to the difference of the mass hierarchy comes from the modification on the cosmic expansion rate when we focus on the 21 cm line observation. In this paper, we separately study the following two cases:

(A) Effective number of neutrino species

In this analysis, we add the effective number of neutrino species N_ν to the fiducial parameter set, and the fiducial value of this parameter is set to be $N_\nu = 3.046$. Generally N_ν represents three species of massive neutrinos plus an extra relativistic component.

(B) Neutrino mass hierarchy

The normal and inverted mass hierarchies mean $m_1 < m_2 \ll m_3$ and $m_3 \ll m_1 < m_2$, respectively. In a cosmological context, many different parameterizations of the mass hierarchy have been proposed [78–81]. In our analysis, we adopt $r_\nu \equiv (m_3 - m_1)/\Sigma m_\nu$ [81] as an additional parameter to discriminate the true neutrino mass hierarchy from the other. r_ν becomes positive for the normal hierarchy, and negative for the inverted hierarchy. Besides, the difference between r_ν of these two hierarchies becomes larger as the total mass Σm_ν becomes smaller. Therefore, r_ν is particularly useful for distinguishing the mass hierarchies. In Fig 10–13, we plot behaviors of r_ν as a function of Σm_ν .

Note that there is a lowest value of Σm_ν which depends on the mass hierarchy by the neutrino oscillation experiments. The lowest value is $\Sigma m_\nu \sim 0.1$ eV for the inverted hierarchy or $\Sigma m_\nu \sim 0.06$ eV for the normal hierarchy. Therefore, if we obtain a clear constraint like $\Sigma m_\nu \ll 0.10$ eV, we can determine that the mass hierarchy is obviously normal without any ambiguities. However, we can discriminate the mass hierarchy even when the neutrino mass Σm_ν is larger than 0.10 eV if we use r_ν , as will be shown later.

3 CMB

3.1 CMB and neutrino

In this paper, we focus on not only the observations of the 21 cm line but also the CMB observations, especially CMB B-mode polarization produced by gravitational lensing of the matter fluctuation. Although the 21 cm line observation is a power probe of the matter power spectrum, particularly, on small scales, observations of CMB greatly help

to determine other cosmological parameters such as energy densities of the dark matter, baryons and dark energy.

Besides, CMB power spectra are sensitive to neutrino masses through the CMB lensing. Future precise CMB experiments are expected to set stringent constraints on the sum of the neutrino masses and the effective number of neutrino species [44, 45]. Therefore, we propose to combine the CMB experiments with the 21 cm line observations.

3.2 Fisher matrix of CMB

We evaluate errors of cosmological parameters by using the Fisher matrix of CMB, which is given by [71].

$$F_{\alpha\beta}^{(\text{CMB})} = \sum_{\ell} \frac{(2\ell+1)}{2} \text{Tr} \left[C_{\ell}^{-1} \frac{\partial C_{\ell}}{\partial \theta_{\alpha}} C_{\ell}^{-1} \frac{\partial C_{\ell}}{\partial \theta_{\beta}} \right], \quad (25)$$

$$C_{\ell} = \begin{pmatrix} C_{\ell}^{\text{TT}} + N_{\ell}^{\text{TT}} & C_{\ell}^{\text{TE}} & C_{\ell}^{\text{Td}} \\ C_{\ell}^{\text{TE}} & C_{\ell}^{\text{EE}} + N_{\ell}^{\text{EE}} & 0 \\ C_{\ell}^{\text{Td}} & 0 & C_{\ell}^{\text{dd}} + N_{\ell}^{\text{dd}} \end{pmatrix}. \quad (26)$$

Here ℓ is the multipole of angular power spectra, C_{ℓ}^X ($X = \text{TT}, \text{EE}, \text{TE}$) are the CMB power spectra, C_{ℓ}^{dd} is the deflection angle spectrum, C_{ℓ}^{Td} is the cross correlation between the deflection angle and the temperature, $N_{\ell}^{X'}$ ($X' = \text{TT}, \text{EE}$) and N_{ℓ}^{dd} are the noise power spectra, where C_{ℓ}^{dd} is calculated by a lensing potential [82] and is related with the lensed CMB power spectra. The noise power spectra of CMB $N_{\ell}^{X'}$ are expressed with a beam size $\sigma_{\text{beam}}(\nu) = \theta_{\text{FWHM}}(\nu)/\sqrt{8 \ln 2}$, where $\sqrt{8 \ln 2} \sigma_{\text{beam}}$ means the full width at half maximum of the Gaussian distribution, and instrumental sensitivity $\Delta_{X'}(\nu)$ by

$$N_{\ell}^{X'} = \left[\sum_i \frac{1}{n_{\ell}^{X'}(\nu_i)} \right]^{-1}, \quad (27)$$

where ν_i is an observing frequency and

$$n_{\ell}^{X'}(\nu) = \Delta_{X'}^2(\nu) \exp [\ell(\ell+1)\sigma_{\text{beam}}^2(\nu)]. \quad (28)$$

The noise power spectrum of deflection angle N_{ℓ}^{dd} is obtained assuming lensing reconstruction with the quadratic estimator [82], which is computed with FUTURCMB [83]. In this algorithm, N_{ℓ}^{dd} is estimated from the noise $N_{\ell}^{X'}$, and lensed and unlensed power spectra of CMB temperature, E-mode and B-mode polarizations.

Finally, the Fisher matrix in Eq.(25) is modified as follows by taking the multipole range $[\ell_{\min}, \ell_{\max}]$ and the fraction of the observed sky f_{sky} into account,

$$F_{\alpha\beta}^{(\text{CMB})} = \sum_{\ell=\ell_{\min}}^{\ell_{\max}} \frac{(2\ell+1)}{2} f_{\text{sky}} \text{Tr} \left[C_{\ell}^{-1} \frac{\partial C_{\ell}}{\partial \theta_{\alpha}} C_{\ell}^{-1} \frac{\partial C_{\ell}}{\partial \theta_{\beta}} \right]. \quad (29)$$

3.3 Residual foregrounds [84, 85]

We consider synchrotron radiation and dust emission in our galaxy as the dominant sources of foregrounds. These foregrounds are subtracted from each sky pixel of the CMB map. Here, we assume that the foreground subtraction can be performed at a certain level demonstrated in previous foreground separation studies [86]; we assume 2% level in CMB maps. We then model the residual foregrounds in the CMB maps. Note that we only consider the residual foreground of CMB polarization maps as distinct from temperature. That is because it has already been precisely measured by WMAP and Planck.

We model the synchrotron $C_\ell^{S,X}$ and dust $C_\ell^{D,X}$ foregrounds as

$$C_\ell^{S,X}(\nu) = A_S \left(\frac{\nu}{\nu_{S,0}} \right)^{2\alpha_S} \left(\frac{\ell}{\ell_{S,0}} \right)^{\beta_S}, \quad (30)$$

$$C_\ell^{D,X}(\nu) = p^2 A_D \left(\frac{\nu}{\nu_{D,0}} \right)^{2\alpha_D} \left(\frac{\ell}{\ell_{D,0}} \right)^{\beta_D^X} \left[\frac{e^{h\nu_{D,0}/k_B T_{\text{dust}}} - 1}{e^{h\nu/k_B T_{\text{dust}}} - 1} \right]^2, \quad (31)$$

where $X = \text{EE, TE, BB}$, $\alpha_S = -3$, $\beta_S = -2.6$, $\nu_{S,0} = 30$ GHz, $\ell_{S,0} = 350$, $A_S = 4.7 \times 10^{-5} \mu\text{K}^2$, $\alpha_D = 2.2$, $\nu_{D,0} = 94$ GHz, $\ell_{D,0} = 10$, $A_D = 1.0 \mu\text{K}^2$, $\beta_D^X = -2.5$, and the temperature of the dust grains $T_{\text{dust}} = 18\text{K}$. These choices are the values used in the Refs. [84, 85], and match the parameters of foregrounds observed by WMAP [87], DASI [88] and IRAS [89]. The dust polarization fraction, p , is assumed to be 15%, which matches the latest measurement by Planck. We then assume that residual foregrounds are modeled as follows,

$$C_\ell^{X,\text{RFg}}(\nu) = \left[C_\ell^{S,X}(\nu) + C_\ell^{D,X}(\nu) \right] \sigma_{\text{CMB}}^{\text{RFg}} + n_\ell^{\text{RFg},X}(\nu), \quad (32)$$

where $\sigma_{\text{CMB}}^{\text{RFg}}$ is the foreground residual parameter of CMB observations. We assume $\sigma_{\text{CMB}}^{\text{RFg}} = 4 \times 10^{-4}$ (this value corresponds to 2% in the CMB maps), and $n_\ell^{\text{RFg},X}$ is the noise power spectrum of the foreground template maps, which is created by taking map differences and thus are somewhat affected by the instrumental noise. We assume that this noise power spectrum of the template maps is given by

$$n_\ell^{\text{RFg},X}(\nu) = \frac{N_\ell^{\text{RFg},X}}{N_{\text{chan}}(N_{\text{chan}} - 1)/4} \left\{ \left(\frac{\nu}{\nu_{S,\text{ref}}} \right)^{2\alpha_S} + \left(\frac{\nu}{\nu_{D,\text{ref}}} \right)^{2\alpha_D} \right\}, \quad (33)$$

where N_{chan} is the total frequency channels which are used for the foreground removal, $\nu_{D,\text{ref}}$ and $\nu_{S,\text{ref}}$ are the highest and lowest frequency channel included in the removal, respectively, and $N_\ell^{\text{RFg},X}$ is defined by

$$N_\ell^{\text{RFg},X} \equiv \left[\sum_i^{N_{\text{chan}}} \frac{1}{n_\ell^X(\nu_i)} \right]^{-1}, \quad (34)$$

where i represents a frequency channel which is used for the removal. Furthermore, we introduce the following effective noise power spectrum including the residual foregrounds,

$$N_{\ell}^{\text{eff},X} = \left[\sum_i \frac{1}{n_{\ell}^X(\nu_i) + C_{\ell}^{X,\text{RFg}}(\nu_i)} \right]^{-1}, \quad (35)$$

where i represents a frequency channel which is used for the observation of CMB. When we include the effects due to the residual foregrounds in our analysis, we use this effective noise as the CMB noise power spectrum Eq.(27).

By making the modifications given above to FUTURCMB [83], we estimate the errors of the deflection angle of CMB and use them in our Fisher matrix analysis.

3.4 Specifications of the experiments

Now, we show the specifications of the CMB observations. In order to obtain the future constraints, we consider Planck [90], POLARBEAR-2 and Simons Array, whose experimental specifications are summarized in Table 3. The latter two experiments are ground-based precise CMB polarization observations.

For the analysis about Planck and POLARBEAR-2 (or Simons Array), we combine both the experiments, and assume that a part of the whole sky ($f_{\text{sky}} \times 100\%$) is observed by both the experiments, and the remaining region ($65\% - f_{\text{sky}} \times 100\%$) is observed only by Planck. Therefore, we evaluate a total Fisher matrix of CMB $F^{(\text{CMB})}$ by summing the two Fisher matrices,

$$F^{(\text{CMB})} = F^{(\text{Planck})}(65\% - f_{\text{sky}} \times 100\%) + F^{(\text{Planck+PB-2 or SA})}(f_{\text{sky}} \times 100\%), \quad (36)$$

where $F^{(\text{Planck+PB-2 or SA})}$ is the Fisher matrix of the region observed by both Planck and POLARBEAR-2 (PB-2) [or Simons Array (SA)], and $F^{(\text{Planck})}$ is that by Planck only.

In addition, we calculate noise power spectra $N_{\ell}^{X,\text{Planck+PB-2 or SA}}$ of the CMB polarization ($X = \text{EE}$ or BB) in $F^{(\text{Planck+PB-2 or SA})}$ with the following operation.

(1) $2 \leq \ell < 25$

$$N_{\ell}^{X,\text{Planck+PB-2 or SA}} = N_{\ell}^{X,\text{Planck}} \quad (37)$$

(2) $25 \leq \ell \leq 3000$

$$N_{\ell}^{X,\text{Planck+PB-2 or SA}} = [1/N_{\ell}^{X,\text{Planck}} + 1/N_{\ell}^{X,\text{PB-2 or SA}}]^{-1} \quad (38)$$

Since we assume that the CMB temperature fluctuation observed by POLARBEAR-2 or Simons Array is not used for constraints on the cosmological parameters, the temperature noise power spectrum $N_{\ell}^{\text{TT, Planck+PB-2 or SA}}$ is equal to $N_{\ell}^{\text{TT, Planck}}$. This reason is that the CMB temperature fluctuation observed by Planck reaches almost cosmic variance limit. (Planck observation greatly helps to determine other cosmological parameters such as the normalization of power spectra, energy densities of the dark matter, baryons and dark energy). Therefore, the constraints are not strongly improved if we include the CMB temperature fluctuation observed by POLARBEAR-2 or Simons Array.

Experiment	ν [GHz]	Δ_{TT} [$\mu\text{K}-'$]	Δ_{PP} [$\mu\text{K}-'$]	θ_{FWHM} [-']	f_{sky}	ℓ_{min}	ℓ_{max}
Planck	30	145	205	33			
	44	150	212	23			
	70	137	195	14			
	100	64.6	104	9.5	0.65	2	3000
	143	42.6	80.9	7.1			
	217	65.5	134	5			
	353	406	406	5			
POLARBEAR-2 (PB-2) $f_{\text{sky}} = 0.016$	95	-	3.09	5.2	0.016	25	3000
	150	-	3.09	3.5			
PB-2 $f_{\text{sky}} = 0.2$	95	-	10.9	5.2	0.2	25	3000
	150	-	10.9	3.5			
PB-2 $f_{\text{sky}} = 0.65$	95	-	19.7	5.2	0.65	25	3000
	150	-	19.7	3.5			
Simons Array (SA) $f_{\text{sky}} = 0.016$	95	-	2.18	5.2			
	150	-	1.78	3.5	0.016	25	3000
	220	-	6.34	2.7			
SA $f_{\text{sky}} = 0.2$	95	-	7.72	5.2			
	150	-	6.30	3.5	0.2	25	3000
	220	-	21.5	2.7			
SA $f_{\text{sky}} = 0.65$	95	-	13.9	5.2			
	150	-	11.4	3.5	0.65	25	3000
	220	-	38.8	2.7			

Table 3: Experimental specifications of Planck, POLARBEAR-2 and Simons Array assumed in our analysis. Here ν is the observation frequency, Δ_{TT} is the temperature sensitivity per $1' \times 1'$ pixel, $\Delta_{\text{PP}} = \Delta_{\text{EE}} = \Delta_{\text{BB}}$ is the polarization (E-mode and B-mode) sensitivity per $1' \times 1'$ pixel, θ_{FWHM} is the angular resolution defined to be the full width at half-maximum, and f_{sky} is the observed fraction of the sky. For the Planck experiment, we assume that the three frequency bands (70, 100, 143 GHz) are only used for the observation of CMB, and the other bands (30, 44, 217, 353 GHz) are used for foreground removal. For Simons Array, we consider two cases: One case is that 220 GHz band is used for the observation of CMB, and the other is that the band is used for the foreground removal.

4 BAO

In this section, we briefly explain analysis methods about the baryon acoustic oscillation (BAO). In the early Universe, baryons and photons are strongly coupled and their fluctuations (Fourier components) of the mixed fluid oscillate by the pressure of radiation. At the time of the decouple between them, a characteristic peak feature remains at the sound horizon. The scale can be used for a standard ruler of distance. Therefore, we can get the information of the distance and the Hubble expansion rate by measurements of the BAO scale for matter fluctuations. In this paper, we especially consider galaxy surveys for the BAO observation.

4.1 Fisher matrix of BAO [91]

Here we introduce the Fisher matrix of BAO experiments. The observables of BAO are the comoving angular diameter distance $d_A(z)$ and the Hubble parameter $H(z)$ (and more specifically, $\ln(d_A(z))$ and $\ln(H(z))$ are the observables). The Fisher matrix is given by

$$F_{\alpha\beta}^{(\text{BAO})\ d,H} = \sum_i \frac{1}{\sigma_{d,H}^2(z_i) + (\sigma_s^i)^2} \frac{\partial f_i^{d,H}}{\partial \theta_\alpha} \frac{\partial f_i^{d,H}}{\partial \theta_\beta}, \quad (39)$$

$$f_i^d = \ln(d_A(z_i)), \quad (40)$$

$$f_i^H = \ln(H(z_i)), \quad (41)$$

where $\sigma_d(z_i)$ and $\sigma_H(z_i)$ are the variances of $\ln(d_A(z_i))$ and $\ln(H(z_i))$ in the BAO observation respectively, σ_s^i is the error of the systematics, and we assume that the observed redshift range is divided into bins, whose width and central redshift values are represented by Δz_i and z_i , respectively. Here, i is the index of the redshift bins.

Their variances $\ln(d_A(z_i))$ and $\ln(H(z_i))$ are determined by the fitting formulae of BAO presented by [92], and they are given by

$$\sigma_d(z_i) = x_0^d \frac{4}{3} \sqrt{\frac{V_0}{V_i}} f_{nl}(z_i), \quad (42)$$

$$\sigma_H(z_i) = x_0^H \frac{4}{3} \sqrt{\frac{V_0}{V_i}} f_{nl}(z_i). \quad (43)$$

Here, V_i is the comoving survey volume and expressed as

$$V_i = \frac{(d_A(z_i))^2}{H(z_i)} \Omega_{\text{sky}} \Delta z_i, \quad (44)$$

where Ω_{sky} is the survey solid angle. $f_{nl}(z_i)$ is the non-linear evolution factor, which represents the erasure of baryon oscillation features by the non-linear evolution of density fluctuations. In our analysis, we use the following function for $f_{nl}(z_i)$,

$$f_{nl}(z_i) = \begin{cases} 1 & z > z_m, \\ \left(\frac{z_m}{z_i}\right)^\gamma & z < z_m. \end{cases} \quad (45)$$

where z_m is the redshift at which the improvement in the baryon oscillation accuracy saturates (for fixed survey volume and number density). Additionally, in the analysis of the BAO observation, we use the following parameters,

$$x_0^d = 0.0085, \quad (46a)$$

$$x_0^H = 0.0148, \quad (46b)$$

$$V_0 = \frac{2.16}{h^3} \text{Gpc}^3, \quad (46c)$$

$$\gamma = \frac{1}{2}, \quad (46d)$$

$$z_m = 1.4, \quad (46e)$$

where $h \equiv H_0/(100\text{km}/\text{s}/\text{Mpc})$ is the dimensionless Hubble parameter. According to [91], we assume the following systematic error,

$$\sigma_s^i = 0.01 \times \sqrt{\frac{0.5}{\Delta z_i}}. \quad (47)$$

The set of cosmological parameters related to the BAO observation are only $(\Omega_m h^2, \Omega_\Lambda)$ or (h, Ω_Λ) when we assume that the Universe is flat and the dark energy is the cosmological constant.

4.2 Specification of the BAO observation

We estimate the sensitivity of the BAO observation only in the analysis of the neutrino mass, the number of neutrino species and the mass hierarchy. In the analysis, we focus on the Dark Energy Spectroscopic Instrument (DESI) [60, 93], which is a future large volume galaxy survey. The survey redshift range is $0.1 < z < 1.9$ (we do not include the Ly- α forest at $1.9 < z$ for simplicity) and the solid angle is $\Omega_{sky} = 14000[\text{deg}^2]$. In our analysis, we divide the redshift range into 18 bins, in other words $\Delta z_i = 0.1$ [45].

Additionally, in the same manner as [45], when we combine BAO with the other observations, we add a 1% H_0 prior to the Fisher matrix. The prior of the Hubble parameter is achievable in the next decade. The Fisher matrix of the Hubble prior is given by

$$F_{\theta_\alpha \theta_\beta}^{(H_0 \text{ prior})} = \begin{cases} \frac{1}{(1\% \times H_{0,\text{fid}})^2}, & \theta_\alpha = \theta_\beta = H_0, \\ 0, & \text{the other components,} \end{cases} \quad (48)$$

where $H_{0,\text{fid}}$ is the fiducial value of H_0 . If we choose the Hubble parameter as a dependent parameter, it is necessary to translate the Fisher matrix into that of the chosen parameter space. Under the transformation of a parameter space $\theta \rightarrow \tilde{\theta}$, the translated Fisher matrix is given by [91]

$$\tilde{F}_{l,m} = \frac{\partial \theta_j}{\partial \tilde{\theta}_l} \frac{\partial \theta_k}{\partial \tilde{\theta}_m} F_{jk}. \quad (49)$$

By using this formula, under the translation of $(h, \Omega_\Lambda) \rightarrow (\Omega_m h^2, \Omega_\Lambda)$, the Fisher matrix in the new parameter space is written as

$$\tilde{F}^{H_0 \text{ prior}} = \begin{pmatrix} \tilde{F}_{\Omega_m h^2 \Omega_m h^2} & \tilde{F}_{\Omega_m h^2 \Omega_\Lambda} \\ \tilde{F}_{\Omega_\Lambda \Omega_\Lambda} & \tilde{F}_{\Omega_\Lambda \Omega_\Lambda} \end{pmatrix} = \frac{1}{(1\% \times H_{0,\text{fid}})^2} \left(\frac{1}{2\Omega_m h^2} \right)^2 \begin{pmatrix} h^2 & h^4 \\ h^4 & h^6 \end{pmatrix}. \quad (50)$$

5 Results

5.1 Future constraints

In this section, we present our results for projected constraints by the 21cm line, CMB and BAO observations on cosmological parameters, paying particular attention to parameters related to neutrino (the total neutrino mass, the effective number of neutrino species and the neutrino mass hierarchy). When we calculate the Fisher matrices, we choose the following basic set of cosmological parameters: the energy density of matter $\Omega_m h^2$, baryons $\Omega_b h^2$ and dark energy Ω_Λ , the scalar spectral index n_s , the scalar fluctuation amplitude A_s (the pivot scale is taken to be $k_{\text{pivot}} = 0.05 \text{ Mpc}^{-1}$), the reionization optical depth τ , the primordial value of the ${}^4\text{He}$ mass fraction Y_p and the total neutrino mass $\Sigma m_\nu = m_1 + m_2 + m_3$. Fiducial values of these parameters (except for Σm_ν) are adopted to be $(\Omega_m h^2, \Omega_b h^2, \Omega_\Lambda, n_s, A_s, \tau, Y_p) = (0.1417, 0.02216, 0.6914, 0.9611, 2.214 \times 10^{-9}, 0.0952, 0.25)$, which are the best fit values of the Planck result [31].

Here, we numerically evaluate how we can determine the effective number of neutrino species (in section 5.3), and the neutrino mass hierarchy (in section 5.3), by combining the 21 cm line observations (SKA phase 1 or phase 2) with the CMB experiments (Planck + POLARBEAR-2 (PB-2) or Simons Array (SA)) and the BAO observation (DESI). In the former analysis, we fix the neutrino mass hierarchy to be the normal one, and set the fiducial value of the total neutrino mass Σm_ν and the effective number of neutrino species N_ν to be $\Sigma m_\nu = 0.1$ or 0.06 eV and $N_\nu = 3.046$. Next, in the latter analysis, we fix N_ν to be 3.046 , and set the fiducial values of the Σm_ν and the mass hierarchy parameter r_ν to be $(\Sigma m_\nu, r_\nu) = (0.06 \text{ eV}, 0.82)$ (normal hierarchy) or $(\Sigma m_\nu, r_\nu) = (0.1 \text{ eV}, -0.46)$ (inverted hierarchy).

To obtain Fisher matrices we use CAMB [94,95] ^{#2} for calculations of CMB anisotropies C_l and matter power spectra $P_{\delta\delta}(k)$. In order to combine the CMB experiments the 21 cm line and the BAO observations, we calculate the combined Fisher matrix to be

$$F_{\alpha\beta} = F_{\alpha\beta}^{(21\text{cm})} + F_{\alpha\beta}^{(\text{CMB})} + F_{\alpha\beta}^{(\text{BAO})}, \quad (51)$$

In this paper, we do not use information for a possible correlation between fluctuations of the 21 cm and the CMB.

^{#2}In this analysis, we use non-linear power spectra for the calculations by performing a public code HALOFIT [94, 95].

5.2 Constraints on Σm_ν and N_ν

In Figs.1-8, we plot contours of 95% confidence levels (C.L.) forecasts of each combination of CMB, 21cm line and BAO observations in Σm_ν - N_ν plane. Constraints on cosmological parameters are summarized in Tables 4 - 21.

The upper panels of Figs.1-6 show forecasts without residual foregrounds of CMB and 21 cm line (i.e. they are completely removed), and the lower ones show those with given level residual foregrounds, respectively. For Simons Array, we assume that its 220GHz band is used for the foreground removal when we include the contribution of residual foreground, and used for CMB observation when we do not include the residual foreground. The fiducial value of the total neutrino mass is set to be $\Sigma m_\nu = 0.1$ eV (Figs.1, 3 and 5) or $\Sigma m_\nu = 0.06$ eV (Figs.2, 4 and 6). Sky coverages of POLARBEAR-2 and Simons Array are $f_{\text{sky}} = 0.016$ (Figs.1 and 2), $f_{\text{sky}} = 0.2$ (Figs.3 and 4), or $f_{\text{sky}} = 0.65$ (Figs.5 and 6). In the left two panels of Figs.1-6, each contour represents constraints by CMB only or CMB + BAO (DESI) + Hubble prior. In the right two panels of them, each contour represents constraints by Planck only or CMB + BAO (DESI) + Hubble prior + 21cm line (SKA). In these six figures, we assume that the number of the observed fields by SKA is four ($N_{\text{field}} = 4$).

From these figures, adding the BAO experiments to the CMB ones, we see that there is a strong improvement on the sensitivities to Σm_ν and N_ν because several parameter degeneracies are broken by those combinations. Besides, we find that the larger sky coverage improves the constraints more. However, it is difficult to detect the nonzero neutrino mass at 2σ level even by using the combination of Simons Array and DESI.

On the other hand, adding the 21 cm experiments (SKA phase 1) to the CMB observation, we see that there is a substantial improvement. When we neglect the contribution from the residual foreground, the combination of SKA phase 1 and Simons Array ($f_{\text{sky}} = 0.2$ or $f_{\text{sky}} = 0.65$) has enough sensitivity to detect nonzero neutrino mass in the case of $\Sigma m_\nu = 0.1$ eV to be fiducial. Of course, CMB + SKA phase 2 can obviously do the same job. For the effective number of neutrino species, its errors by the combination of CMB and BAO with SKA are several times as small as those of only CMB + BAO. In the case with a given level of residual foregrounds, Planck + Simons Array + BAO + SKA phase 1 can not detect nonzero neutrino mass, and only a combination of SKA phase 2 with Simons Array ($f_{\text{sky}} = 0.2$ or 0.65) can do it. In the case of $\Sigma m_\nu = 0.06$ eV to be fiducial (this value corresponds to the lowest value for the normal hierarchy), it is difficult to detect the nonzero neutrino mass even by the combination with SKA phase 2. For the effective number of neutrino species, its errors in this case are a few times as large as those in the case without the residual foreground. Hence, a stronger foreground removal of the 21 cm line observation is necessary if we want to obtain a stringent constraint on the effective number of neutrino species.

We can find the necessity of the foreground removal of the 21cm line from Figs.7 and 8. These figures show forecasts without the residual foreground of 21 cm line but with that of CMB (i.e. the foreground of the 21 cm line is completely removed). We assume

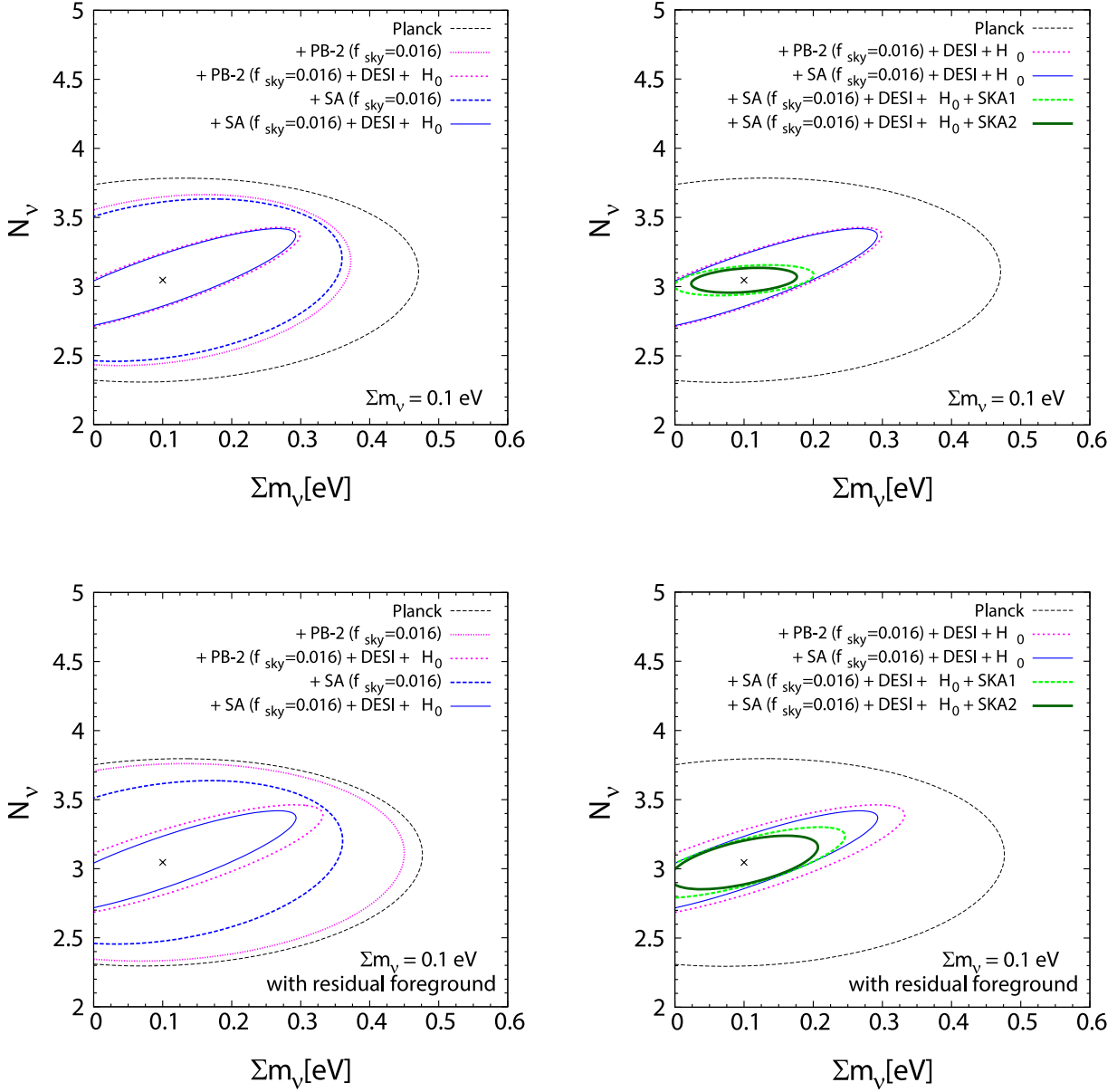


Figure 1: Contours of 95% C.L. forecasts in Σm_ν - N_ν plane. Fiducial values of neutrino parameters, N_ν and Σm_ν , are taken to be $N_\nu = 3.046$ and $\Sigma m_\nu = 0.1$ eV. In the left two panels, the contours are the constraints by adopting Planck (outer dashed line), Planck combined with POLARBEAR-2 (PB-2) ($f_{\text{sky}} = 0.016$) (outer dotted line) or Simons Array (SA) (inner thick dashed line), Planck + BAO(DESI) + Hubble prior + POLARBEAR-2 ($f_{\text{sky}} = 0.016$) (inner thick dotted line) or Simons Array (thin solid line), respectively. In the right two panels, they are the constraints by adopting Planck (outer dashed line), Planck + BAO(DESI) + Hubble prior combined with POLARBEAR-2 ($f_{\text{sky}} = 0.016$) (dotted line) or Simons Array (outer thin solid line), Planck + BAO(DESI) + Hubble prior + Simons Array combined with SKA phase 1 ($N_{\text{filed}} = 4$) (inner thick dashed line) or phase 2 ($N_{\text{filed}} = 4$) (inner thick line), respectively.

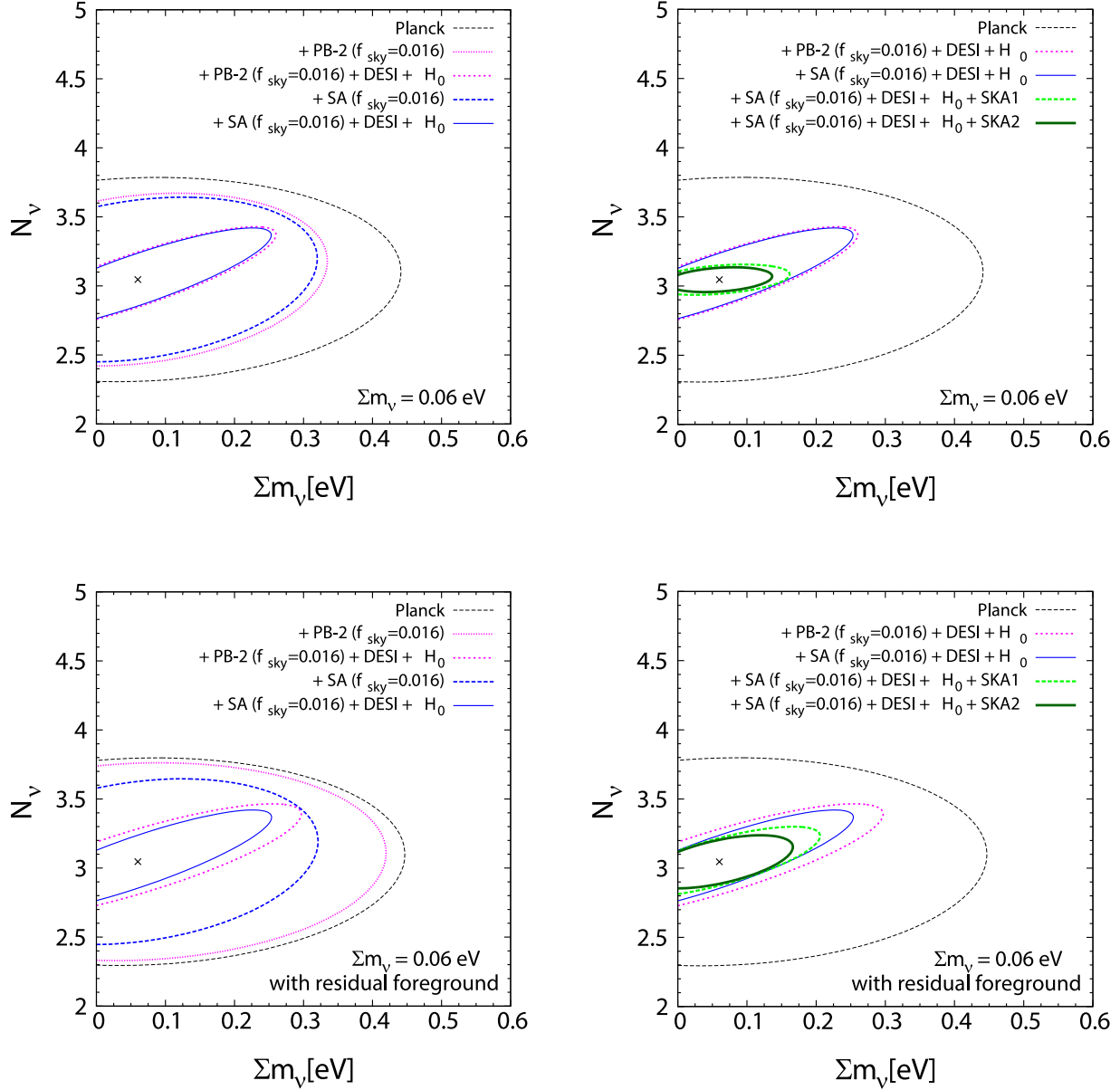


Figure 2: Same as Fig.1, but the fiducial values of neutrino parameters, N_ν and Σm_ν , are taken to be $N_\nu = 3.046$ and $\Sigma m_\nu = 0.06$ eV.

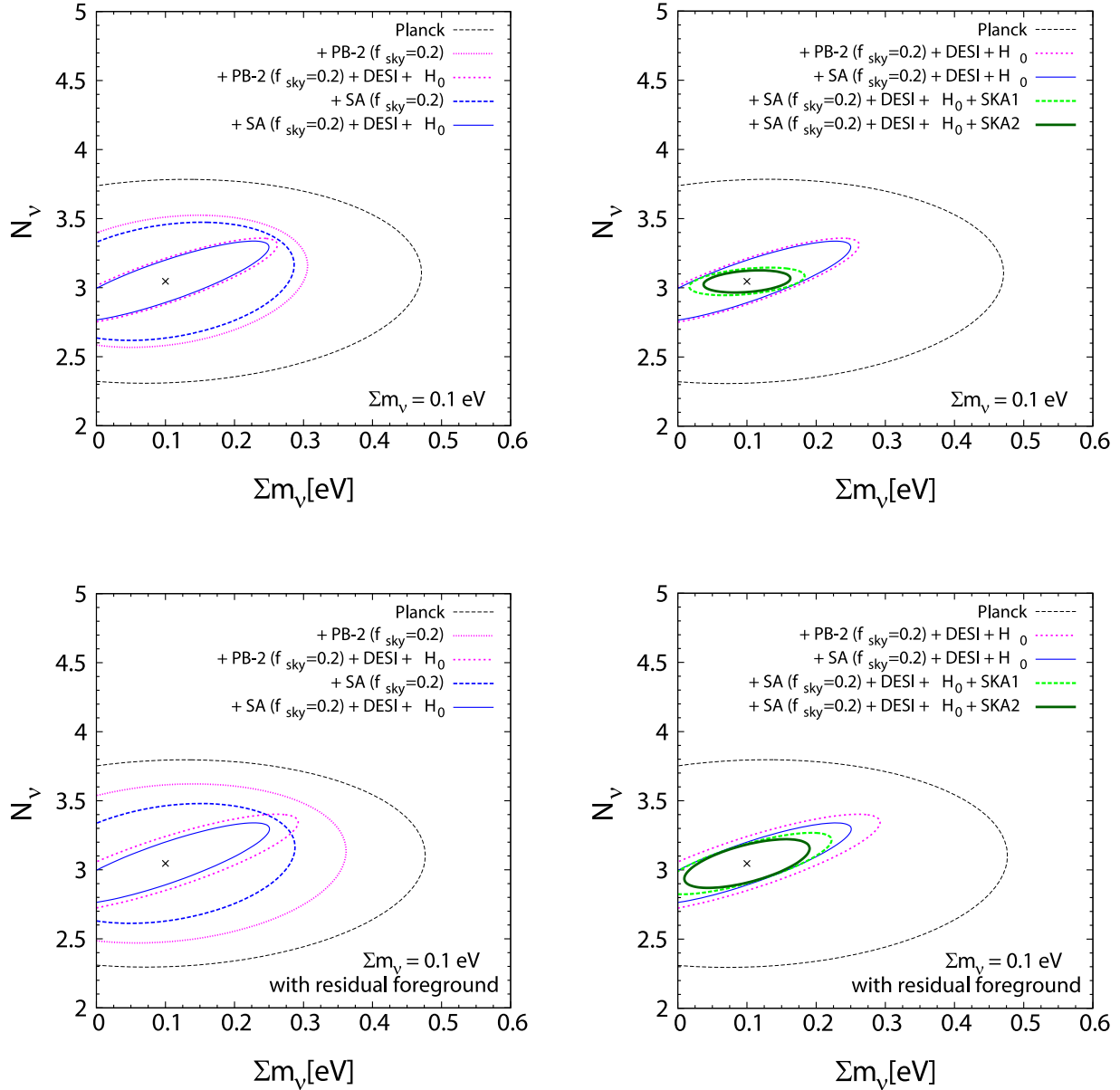


Figure 3: Same as Fig.1, but the sky coverages of POLARBEAR-2 and Simons Array are $f_{\text{sky}} = 0.2$.

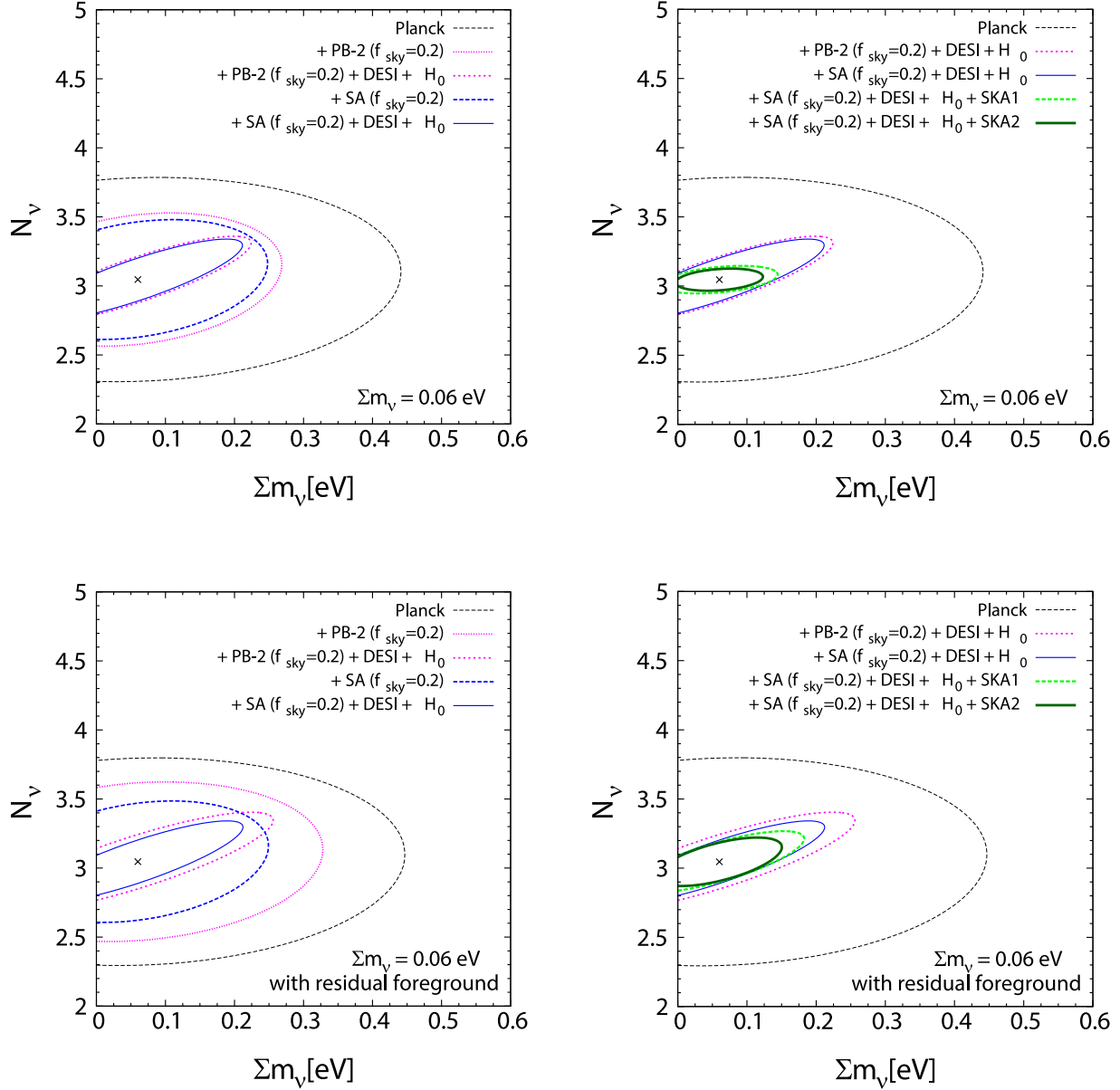


Figure 4: Same as Fig.3, but the fiducial values of neutrino parameters, N_ν and Σm_ν , are taken to be $N_\nu = 3.046$ and $\Sigma m_\nu = 0.06$ eV.

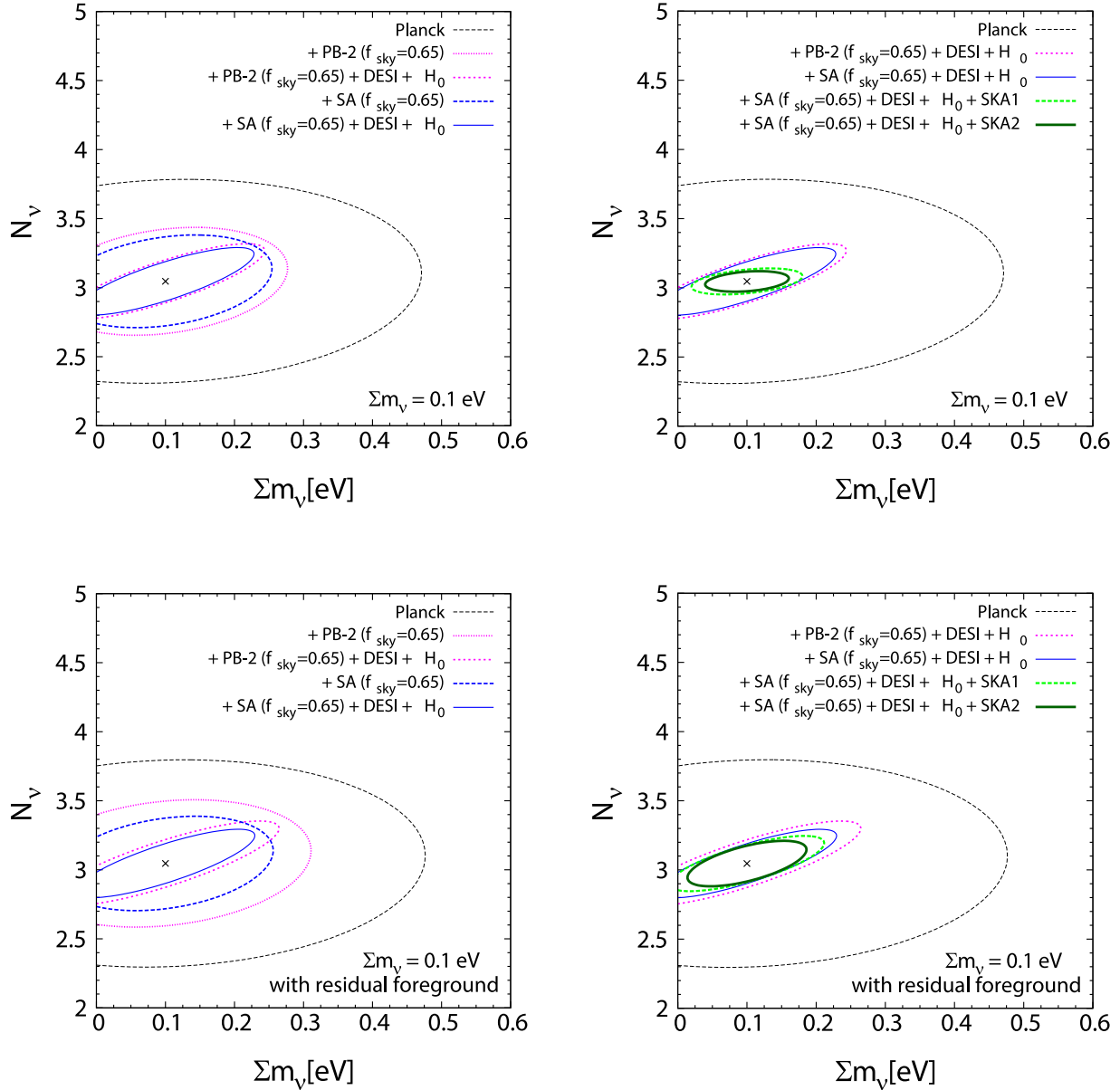


Figure 5: Same as Fig.1, but the sky coverages of POLARBEAR-2 and Simons Array are $f_{\text{sky}} = 0.65$.

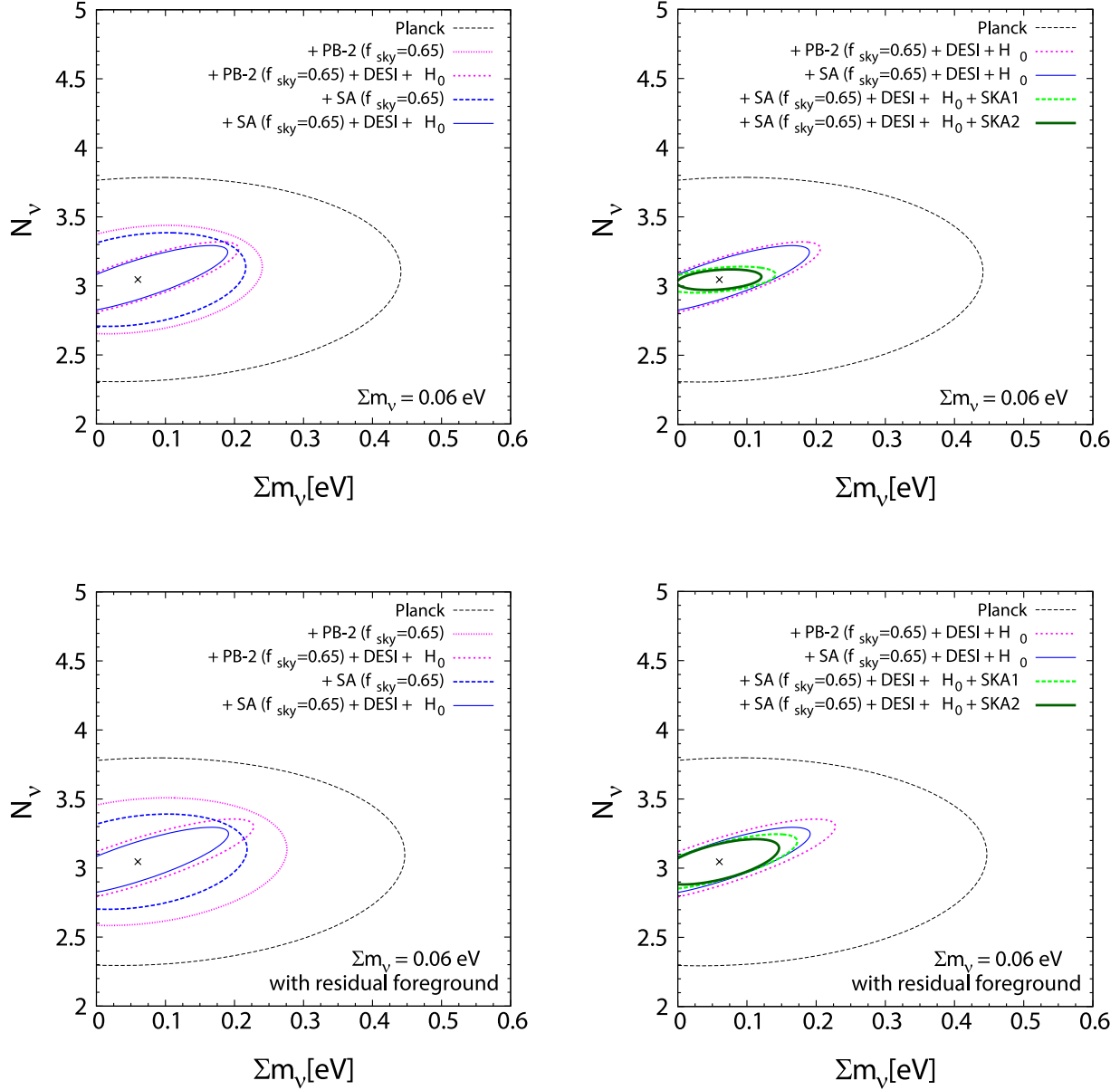


Figure 6: Same as Fig.5, but the fiducial values of neutrino parameters, N_ν and Σm_ν , are taken to be $N_\nu = 3.046$ and $\Sigma m_\nu = 0.06$ eV.

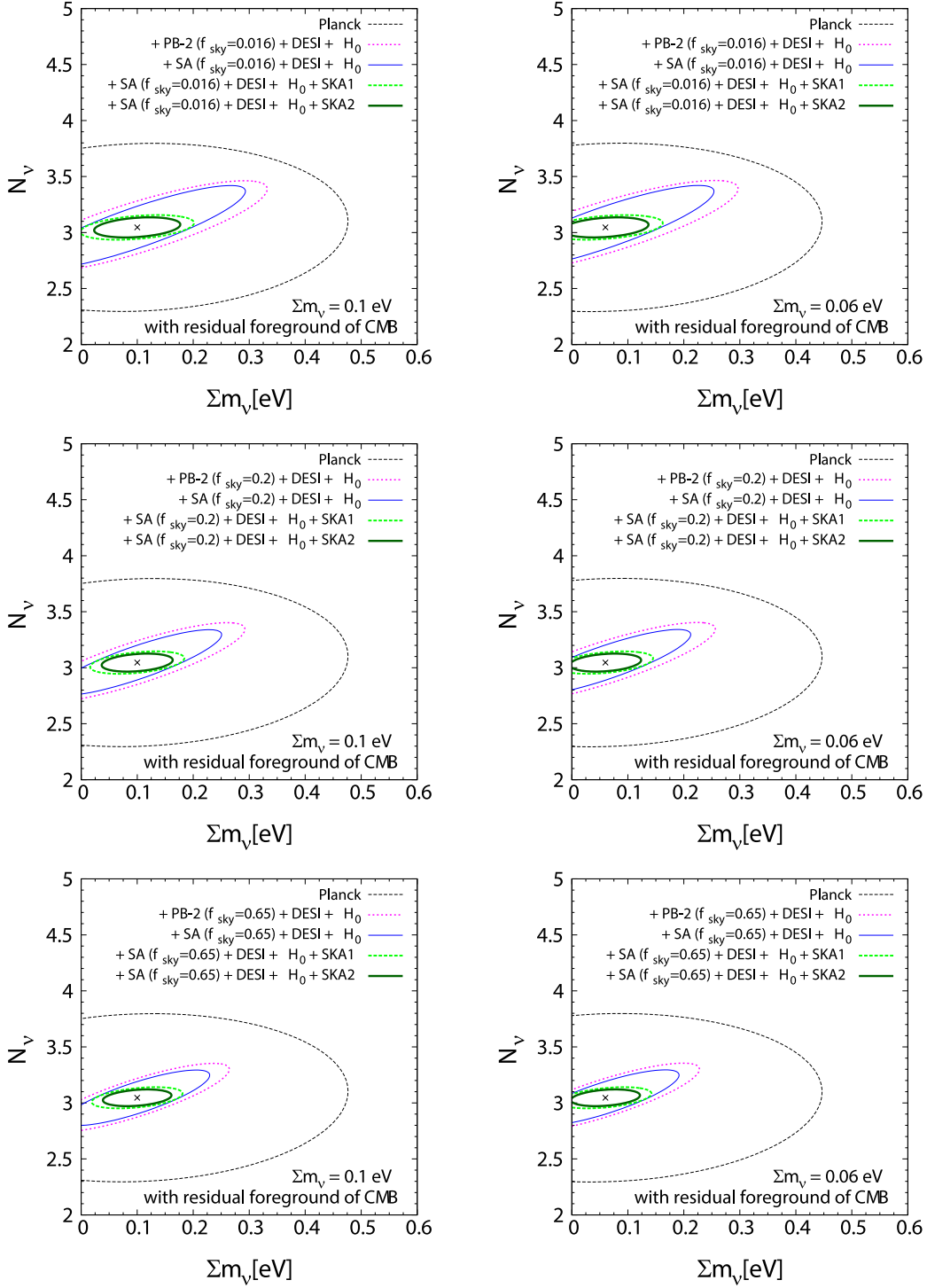


Figure 7: Contours of 95% C.L. forecasts in Σm_ν - N_ν plane without residual foreground of 21 cm line (i.e. the residual foreground of 21 cm line is completely removed, and that of CMB exists only). The fiducial values of neutrino parameters, N_ν and Σm_ν , are taken to be $N_\nu = 3.046$, $\Sigma m_\nu = 0.1$ eV in left panels, and $\Sigma m_\nu = 0.06$ eV in right panels.

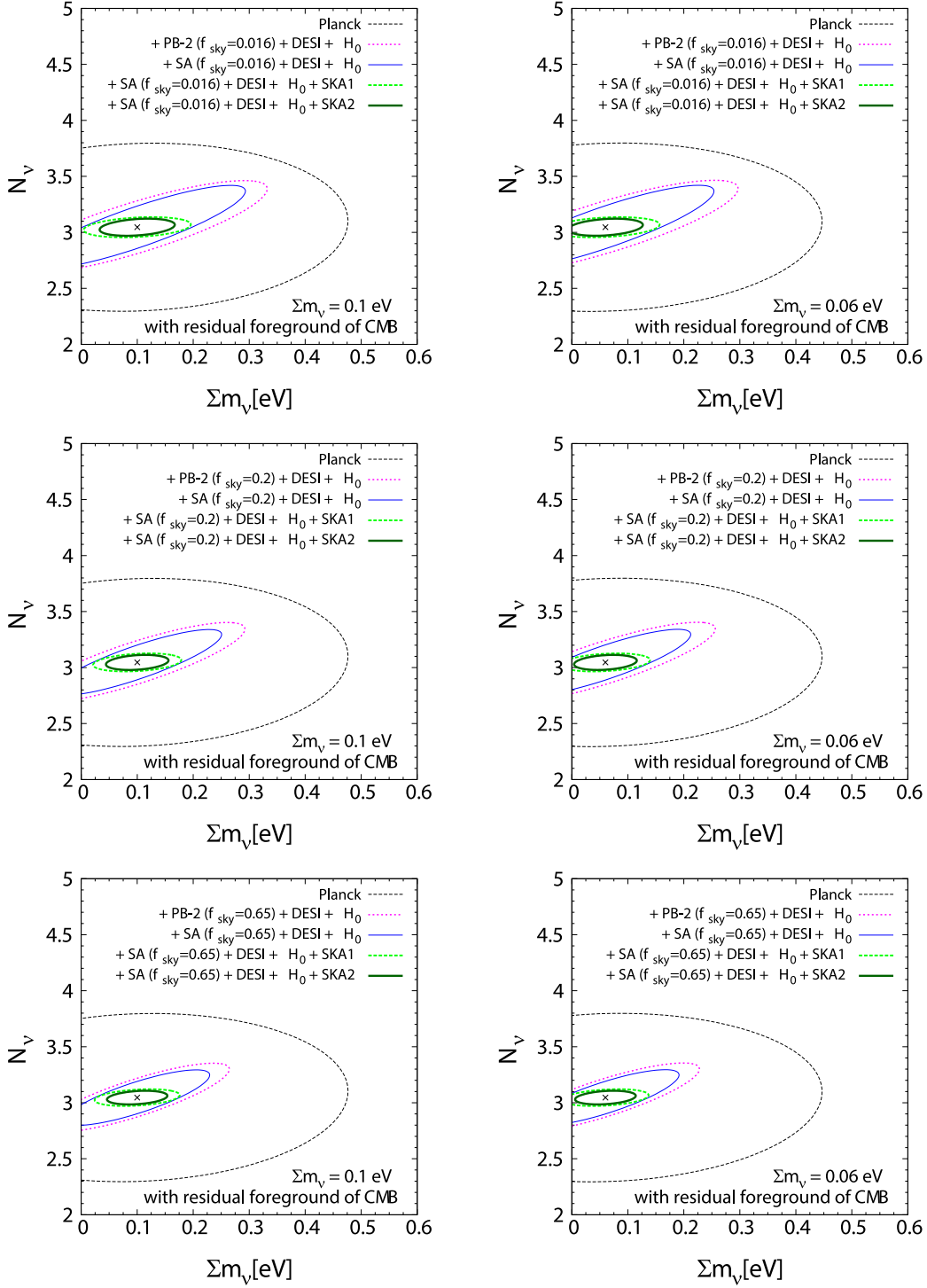


Figure 8: Same as Fig.7, but the observed fields of SKA are twice as large as that of Fig.7 (i.e. $N_{\text{field}} = 8$).

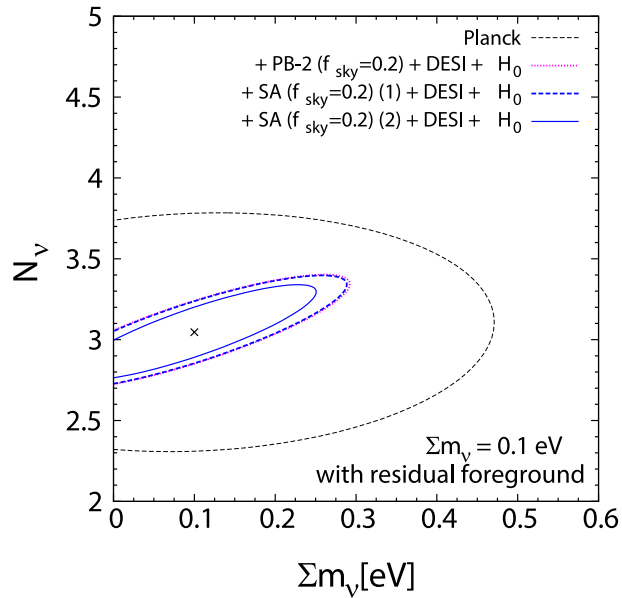


Figure 9: Contours of 95% C.L. forecasts in Σm_ν - N_ν plane. The fiducial values of neutrino parameters, N_ν and Σm_ν , are taken to be $N_\nu = 3.046$ and $\Sigma m_\nu = 0.1$ eV. The contours are the constraints by adopting Planck (outer dashed line), Planck + BAO(DESI) + Hubble prior + POLARBEAR-2 (PB-2) ($f_{\text{sky}} = 0.2$) (outer dotted line). For Simons Array, we plot results of two different cases. At first, we assume that the 220 GHz band of Simons Array is used for only observation of CMB, and not used for the foreground removal (outer thick dashed line, we call this situation Simons Array (1) or SA(1)). Secondary, the 220 GHz band is used for the foreground removal (inner solid line: we call this case Simons Array (2) or SA(2)). The constraint of Simons Array (1) almost laps over that of POLARBEAR-2.

that the number of observed fields of SKA is $N_{\text{field}} = 4$ in Fig.7 and $N_{\text{field}} = 8$ in Fig.8. In these cases, constraints of Σm_ν and N_ν are strongly improved in comparison with the lower panels of Figs.1-6, and the errors of the effective number of neutrino species are approximately $\sigma(N_\nu) \sim 0.06 - 0.09$ or $\sigma(N_\nu) \sim 0.05 - 0.07$ at 2σ by Simons Array + SKA phase 1 or phase 2, respectively. Besides, from Fig.7, by Planck + Simons Array ($f_{\text{sky}} = 0.2$ or 0.65) + BAO + SKA phase 1 and Planck + Simons Array + BAO + SKA phase 2, we can detect the nonzero neutrino mass of $\Sigma m_\nu = 0.1$ eV in this case. Additionally, from Fig.8, we find that more observed fields of 21 cm line observation ($N_{\text{filed}} = 8$) are necessary if we want to detect the nonzero neutrino mass of $\Sigma m_\nu = 0.06$ eV by SKA phase 2.

In Fig.9, we show two different cases about observations of Simons Array. At first, we assume that the 220 GHz band of Simons Array is used for the foreground removal (inner solid line), and this assumption is used for the analysis of Figs.1-8. Secondary, the band is used for only the observation of CMB, and not used for the foreground removal, which is done by only Planck (outer thick dashed line). This figure shows that the latter constraint is almost the same level as that of POLARBEAR-2. The reason is that the strength of the residual foreground depends on only the Planck sensitivity. Therefore, it is better to use the 220 GHz band of Simon Array for the foreground removal. Constraints on cosmological parameters in this situation are summarized in Tables 22 and 23.

5.3 Constraints on neutrino mass hierarchy

Next, we discuss whether we will be able to determine the neutrino mass hierarchies by using the future 21 cm line and the CMB observations. Constraints on cosmological parameters are summarized in Tables 24 - 41. In Figs. 10-13, we plot 2σ errors of the parameter $r_\nu \equiv (m_3 - m_1)/\Sigma m_\nu$ constrained by both the 21 cm line and the CMB observations in case of the inverted hierarchy to be fiducial (left panels), and the normal hierarchy to be fiducial (right panels). In these figure, upper two panels represent results without residual foregrounds, i.e. they are completely removed. On the other hand, middle two panels show the results with given level residual foregrounds. Here, we assume that the amplitude of the residual foreground of the 21 cm line is 10 times as small as that of the previous section, and the 220 GHz band of Simons Array is used for the foreground removal. Lower two panels show the results with only the residual foreground of CMB, i.e. that of the 21 cm line is completely removed. We also assume that the 220 GHz band of Simons Array is used for the foreground removal in these cases. The number of observed field of SKA is $N_{\text{field}} = 4$ in Figs.10-12 and $N_{\text{field}} = 8$ in Fig.13.

It is notable that the difference between r_ν of these two hierarchies becomes larger as the total mass Σm_ν becomes smaller. Therefore, r_ν is quite useful to distinguish a true mass hierarchy from the other. Allowed parameters on r_ν by neutrino oscillation experiments are plotted as two bands for the inverted and the normal hierarchies, respectively. The thin solid lines inside the bands are the central values of the oscillation experiments.

From these figures, we find that it is difficult to determine the neutrino mass hierarchy by the combination of CMB and BAO with SKA phase 1. However, if we use SKA phase 2,

	$\sigma(\Omega_m h^2)$	$\sigma(\Omega_b h^2)$	$\sigma(\Omega_\Lambda)$	$\sigma(n_s)$	$\sigma(A_s \times 10^{10})$
Planck	5.31×10^{-3}	2.44×10^{-4}	2.38×10^{-2}	8.61×10^{-3}	2.83×10^{-1}
+ PB-2 (0.016)	4.57×10^{-3}	2.16×10^{-4}	1.91×10^{-2}	7.69×10^{-3}	2.62×10^{-1}
+ PB-2 + BAO + H_0	3.64×10^{-3}	1.56×10^{-4}	9.77×10^{-3}	5.37×10^{-3}	2.34×10^{-1}
+ PB-2 + BAO + H_0 + SKA1	9.38×10^{-4}	1.46×10^{-4}	4.45×10^{-3}	4.80×10^{-3}	2.07×10^{-1}
+ PB-2 + BAO + H_0 + SKA2	5.76×10^{-4}	1.32×10^{-4}	2.70×10^{-3}	2.89×10^{-3}	1.91×10^{-1}
+ SA (0.016)	4.40×10^{-3}	2.13×10^{-4}	1.84×10^{-2}	7.57×10^{-3}	2.58×10^{-1}
+ SA + BAO + H_0	3.56×10^{-3}	1.54×10^{-4}	9.59×10^{-3}	5.22×10^{-3}	2.32×10^{-1}
+ SA + BAO + H_0 + SKA1	9.37×10^{-4}	1.45×10^{-4}	4.44×10^{-3}	4.69×10^{-3}	2.06×10^{-1}
+ SA + BAO + H_0 + SKA2	5.75×10^{-4}	1.31×10^{-4}	2.69×10^{-3}	2.86×10^{-3}	1.90×10^{-1}
	$\sigma(\tau)$	$\sigma(Y_p)$	$\sigma(\Sigma m_\nu)$	$\sigma(N_\nu)$	
Planck	4.80×10^{-3}	1.69×10^{-2}	1.50×10^{-1}	2.98×10^{-1}	
+ PB-2 (0.016)	4.72×10^{-3}	1.45×10^{-2}	1.10×10^{-1}	2.50×10^{-1}	
+ PB-2 + BAO + H_0	4.68×10^{-3}	1.29×10^{-2}	8.02×10^{-2}	1.54×10^{-1}	
+ PB-2 + BAO + H_0 + SKA1	4.62×10^{-3}	9.88×10^{-3}	4.32×10^{-2}	4.50×10^{-2}	
+ PB-2 + BAO + H_0 + SKA2	4.35×10^{-3}	7.87×10^{-3}	3.29×10^{-2}	3.67×10^{-2}	
+ SA (0.016)	4.71×10^{-3}	1.39×10^{-2}	1.05×10^{-1}	2.37×10^{-1}	
+ SA + BAO + H_0	4.68×10^{-3}	1.25×10^{-2}	7.78×10^{-2}	1.50×10^{-1}	
+ SA + BAO + H_0 + SKA1	4.61×10^{-3}	9.50×10^{-3}	4.06×10^{-2}	4.44×10^{-2}	
+ SA + BAO + H_0 + SKA2	4.34×10^{-3}	7.67×10^{-3}	3.08×10^{-2}	3.62×10^{-2}	

Table 4: $f_{\text{sky}} = 0.016$, $N_{\text{field}} = 4$, $\Sigma m_\nu = 0.1$ eV, without the residual foregrounds.

	$\sigma(\Omega_m h^2)$	$\sigma(\Omega_b h^2)$	$\sigma(\Omega_\Lambda)$	$\sigma(n_s)$	$\sigma(A_s \times 10^{10})$
Planck	5.35×10^{-3}	2.45×10^{-4}	2.41×10^{-2}	8.61×10^{-3}	2.83×10^{-1}
+ PB-2 (0.016)	4.62×10^{-3}	2.16×10^{-4}	1.91×10^{-2}	7.69×10^{-3}	2.64×10^{-1}
+ PB-2 + BAO + H_0	3.68×10^{-3}	1.56×10^{-4}	9.87×10^{-3}	5.37×10^{-3}	2.34×10^{-1}
+ PB-2 + BAO + H_0 + SKA1	9.43×10^{-4}	1.46×10^{-4}	4.46×10^{-3}	4.80×10^{-3}	2.07×10^{-1}
+ PB-2 + BAO + H_0 + SKA2	5.78×10^{-4}	1.31×10^{-4}	2.69×10^{-3}	2.86×10^{-3}	1.91×10^{-1}
+ SA (0.016)	4.46×10^{-3}	2.13×10^{-4}	1.84×10^{-2}	7.58×10^{-3}	2.59×10^{-1}
+ SA + BAO + H_0	3.60×10^{-3}	1.54×10^{-4}	9.69×10^{-3}	5.22×10^{-3}	2.32×10^{-1}
+ SA + BAO + H_0 + SKA1	9.41×10^{-4}	1.45×10^{-4}	4.45×10^{-3}	4.69×10^{-3}	2.06×10^{-1}
+ SA + BAO + H_0 + SKA2	5.77×10^{-4}	1.30×10^{-4}	2.68×10^{-3}	2.84×10^{-3}	1.90×10^{-1}
	$\sigma(\tau)$	$\sigma(Y_p)$	$\sigma(\Sigma m_\nu)$	$\sigma(N_\nu)$	
Planck	4.78×10^{-3}	1.69×10^{-2}	1.54×10^{-1}	2.98×10^{-1}	
+ PB-2 (0.016)	4.70×10^{-3}	1.46×10^{-2}	1.11×10^{-1}	2.52×10^{-1}	
+ PB-2 + BAO + H_0	4.66×10^{-3}	1.29×10^{-2}	8.07×10^{-2}	1.54×10^{-1}	
+ PB-2 + BAO + H_0 + SKA1	4.59×10^{-3}	9.87×10^{-3}	4.37×10^{-2}	4.49×10^{-2}	
+ PB-2 + BAO + H_0 + SKA2	4.33×10^{-3}	7.84×10^{-3}	3.29×10^{-2}	3.66×10^{-2}	
+ SA (0.016)	4.69×10^{-3}	1.39×10^{-2}	1.05×10^{-1}	2.41×10^{-1}	
+ SA + BAO + H_0	4.65×10^{-3}	1.25×10^{-2}	7.79×10^{-2}	1.51×10^{-1}	
+ SA + BAO + H_0 + SKA1	4.59×10^{-3}	9.49×10^{-3}	4.10×10^{-2}	4.43×10^{-2}	
+ SA + BAO + H_0 + SKA2	4.31×10^{-3}	7.64×10^{-3}	3.08×10^{-2}	3.61×10^{-2}	

Table 5: $f_{\text{sky}} = 0.016$, $N_{\text{field}} = 4$, $\Sigma m_\nu = 0.06$ eV, without the residual foregrounds.

	$\sigma(\Omega_m h^2)$	$\sigma(\Omega_b h^2)$	$\sigma(\Omega_\Lambda)$	$\sigma(n_s)$	$\sigma(A_s \times 10^{10})$
Planck	5.37×10^{-3}	2.49×10^{-4}	2.43×10^{-2}	8.82×10^{-3}	2.86×10^{-1}
+ PB-2 (0.016)	5.14×10^{-3}	2.33×10^{-4}	2.26×10^{-2}	8.24×10^{-3}	2.76×10^{-1}
+ PB-2 + BAO + H_0	3.92×10^{-3}	1.70×10^{-4}	1.05×10^{-2}	5.75×10^{-3}	2.34×10^{-1}
+ PB-2 + BAO + H_0 + SKA1	2.49×10^{-3}	1.67×10^{-4}	7.27×10^{-3}	5.63×10^{-3}	2.18×10^{-1}
+ PB-2 + BAO + H_0 + SKA2	1.65×10^{-3}	1.57×10^{-4}	4.59×10^{-3}	4.58×10^{-3}	2.05×10^{-1}
+ SA (0.016)	4.42×10^{-3}	2.14×10^{-4}	1.85×10^{-2}	7.59×10^{-3}	2.55×10^{-1}
+ SA + BAO + H_0	3.57×10^{-3}	1.54×10^{-4}	9.61×10^{-3}	5.23×10^{-3}	2.29×10^{-1}
+ SA + BAO + H_0 + SKA1	2.40×10^{-3}	1.53×10^{-4}	7.01×10^{-3}	5.14×10^{-3}	2.16×10^{-1}
+ SA + BAO + H_0 + SKA2	1.62×10^{-3}	1.46×10^{-4}	4.52×10^{-3}	4.29×10^{-3}	2.02×10^{-1}
	$\sigma(\tau)$	$\sigma(Y_p)$	$\sigma(\Sigma m_\nu)$	$\sigma(N_\nu)$	
Planck	4.84×10^{-3}	1.71×10^{-2}	1.52×10^{-1}	3.03×10^{-1}	
+ PB-2 (0.016)	4.69×10^{-3}	1.62×10^{-2}	1.41×10^{-1}	2.88×10^{-1}	
+ PB-2 + BAO + H_0	4.63×10^{-3}	1.40×10^{-2}	9.37×10^{-2}	1.68×10^{-1}	
+ PB-2 + BAO + H_0 + SKA1	4.61×10^{-3}	1.23×10^{-2}	7.27×10^{-2}	1.09×10^{-1}	
+ PB-2 + BAO + H_0 + SKA2	4.50×10^{-3}	1.08×10^{-2}	5.64×10^{-2}	8.14×10^{-2}	
+ SA (0.016)	4.64×10^{-3}	1.39×10^{-2}	1.05×10^{-1}	2.39×10^{-1}	
+ SA + BAO + H_0	4.60×10^{-3}	1.26×10^{-2}	7.79×10^{-2}	1.51×10^{-1}	
+ SA + BAO + H_0 + SKA1	4.59×10^{-3}	1.12×10^{-2}	5.88×10^{-2}	1.03×10^{-1}	
+ SA + BAO + H_0 + SKA2	4.48×10^{-3}	9.94×10^{-3}	4.31×10^{-2}	7.80×10^{-2}	

Table 6: $f_{\text{sky}} = 0.016$, $N_{\text{field}} = 4$, $\Sigma m_\nu = 0.1$ eV, with the residual foregrounds.

	$\sigma(\Omega_m h^2)$	$\sigma(\Omega_b h^2)$	$\sigma(\Omega_\Lambda)$	$\sigma(n_s)$	$\sigma(A_s \times 10^{10})$
Planck	5.42×10^{-3}	2.50×10^{-4}	2.46×10^{-2}	8.82×10^{-3}	2.86×10^{-1}
+ PB-2 (0.016)	5.18×10^{-3}	2.33×10^{-4}	2.28×10^{-2}	8.23×10^{-3}	2.76×10^{-1}
+ PB-2 + BAO + H_0	3.97×10^{-3}	1.70×10^{-4}	1.06×10^{-2}	5.75×10^{-3}	2.34×10^{-1}
+ PB-2 + BAO + H_0 + SKA1	2.50×10^{-3}	1.67×10^{-4}	7.28×10^{-3}	5.62×10^{-3}	2.18×10^{-1}
+ PB-2 + BAO + H_0 + SKA2	1.64×10^{-3}	1.57×10^{-4}	4.56×10^{-3}	4.55×10^{-3}	2.04×10^{-1}
+ SA (0.016)	4.48×10^{-3}	2.14×10^{-4}	1.84×10^{-2}	7.59×10^{-3}	2.57×10^{-1}
+ SA + BAO + H_0	3.61×10^{-3}	1.54×10^{-4}	9.71×10^{-3}	5.23×10^{-3}	2.29×10^{-1}
+ SA + BAO + H_0 + SKA1	2.40×10^{-3}	1.53×10^{-4}	7.01×10^{-3}	5.13×10^{-3}	2.15×10^{-1}
+ SA + BAO + H_0 + SKA2	1.61×10^{-3}	1.45×10^{-4}	4.49×10^{-3}	4.26×10^{-3}	2.02×10^{-1}
	$\sigma(\tau)$	$\sigma(Y_p)$	$\sigma(\Sigma m_\nu)$	$\sigma(N_\nu)$	
Planck	4.82×10^{-3}	1.72×10^{-2}	1.56×10^{-1}	3.03×10^{-1}	
+ PB-2 (0.016)	4.67×10^{-3}	1.63×10^{-2}	1.45×10^{-1}	2.89×10^{-1}	
+ PB-2 + BAO + H_0	4.60×10^{-3}	1.40×10^{-2}	9.56×10^{-2}	1.69×10^{-1}	
+ PB-2 + BAO + H_0 + SKA1	4.58×10^{-3}	1.23×10^{-2}	7.37×10^{-2}	1.09×10^{-1}	
+ PB-2 + BAO + H_0 + SKA2	4.47×10^{-3}	1.07×10^{-2}	5.66×10^{-2}	8.08×10^{-2}	
+ SA (0.016)	4.61×10^{-3}	1.40×10^{-2}	1.05×10^{-1}	2.42×10^{-1}	
+ SA + BAO + H_0	4.57×10^{-3}	1.26×10^{-2}	7.81×10^{-2}	1.51×10^{-1}	
+ SA + BAO + H_0 + SKA1	4.56×10^{-3}	1.12×10^{-2}	5.87×10^{-2}	1.02×10^{-1}	
+ SA + BAO + H_0 + SKA2	4.45×10^{-3}	9.89×10^{-3}	4.29×10^{-2}	7.73×10^{-2}	

Table 7: $f_{\text{sky}} = 0.016$, $N_{\text{field}} = 4$, $\Sigma m_\nu = 0.06$ eV, with the residual foregrounds.

	$\sigma(\Omega_m h^2)$	$\sigma(\Omega_b h^2)$	$\sigma(\Omega_\Lambda)$	$\sigma(n_s)$	$\sigma(A_s \times 10^{10})$
Planck	5.31×10^{-3}	2.44×10^{-4}	2.38×10^{-2}	8.61×10^{-3}	2.83×10^{-1}
+ PB-2 (0.2)	3.58×10^{-3}	1.50×10^{-4}	1.40×10^{-2}	5.36×10^{-3}	2.38×10^{-1}
+ PB-2 + BAO + H_0	3.03×10^{-3}	1.19×10^{-4}	8.23×10^{-3}	4.13×10^{-3}	2.25×10^{-1}
+ PB-2 + BAO + H_0 + SKA1	9.18×10^{-4}	1.15×10^{-4}	4.35×10^{-3}	3.84×10^{-3}	1.99×10^{-1}
+ PB-2 + BAO + H_0 + SKA2	5.67×10^{-4}	1.07×10^{-4}	2.67×10^{-3}	2.58×10^{-3}	1.85×10^{-1}
+ SA (0.2)	3.26×10^{-3}	1.42×10^{-4}	1.30×10^{-2}	5.04×10^{-3}	2.31×10^{-1}
+ SA + BAO + H_0	2.84×10^{-3}	1.14×10^{-4}	7.77×10^{-3}	3.94×10^{-3}	2.22×10^{-1}
+ SA + BAO + H_0 + SKA1	9.11×10^{-4}	1.10×10^{-4}	4.31×10^{-3}	3.67×10^{-3}	1.98×10^{-1}
+ SA + BAO + H_0 + SKA2	5.65×10^{-4}	1.04×10^{-4}	2.66×10^{-3}	2.52×10^{-3}	1.83×10^{-1}
	$\sigma(\tau)$	$\sigma(Y_p)$	$\sigma(\Sigma m_\nu)$	$\sigma(N_\nu)$	
Planck	4.80×10^{-3}	1.69×10^{-2}	1.50×10^{-1}	2.98×10^{-1}	
+ PB-2 (0.2)	4.58×10^{-3}	1.09×10^{-2}	8.30×10^{-2}	1.93×10^{-1}	
+ PB-2 + BAO + H_0	4.58×10^{-3}	9.69×10^{-3}	6.54×10^{-2}	1.26×10^{-1}	
+ PB-2 + BAO + H_0 + SKA1	4.53×10^{-3}	7.83×10^{-3}	3.70×10^{-2}	4.13×10^{-2}	
+ PB-2 + BAO + H_0 + SKA2	4.28×10^{-3}	6.70×10^{-3}	2.84×10^{-2}	3.32×10^{-2}	
+ SA (0.2)	4.56×10^{-3}	9.95×10^{-3}	7.52×10^{-2}	1.72×10^{-1}	
+ SA + BAO + H_0	4.56×10^{-3}	9.02×10^{-3}	6.05×10^{-2}	1.18×10^{-1}	
+ SA + BAO + H_0 + SKA1	4.52×10^{-3}	7.30×10^{-3}	3.36×10^{-2}	4.04×10^{-2}	
+ SA + BAO + H_0 + SKA2	4.26×10^{-3}	6.34×10^{-3}	2.53×10^{-2}	3.24×10^{-2}	

Table 8: $f_{\text{sky}} = 0.2$, $N_{\text{field}} = 4$, $\Sigma m_\nu = 0.1$ eV, without the residual foregrounds.

	$\sigma(\Omega_m h^2)$	$\sigma(\Omega_b h^2)$	$\sigma(\Omega_\Lambda)$	$\sigma(n_s)$	$\sigma(A_s \times 10^{10})$
Planck	5.35×10^{-3}	2.45×10^{-4}	2.41×10^{-2}	8.61×10^{-3}	2.83×10^{-1}
+ PB-2 (0.2)	3.63×10^{-3}	1.50×10^{-4}	1.40×10^{-2}	5.36×10^{-3}	2.38×10^{-1}
+ PB-2 + BAO + H_0	3.07×10^{-3}	1.19×10^{-4}	8.32×10^{-3}	4.13×10^{-3}	2.25×10^{-1}
+ PB-2 + BAO + H_0 + SKA1	9.23×10^{-4}	1.15×10^{-4}	4.36×10^{-3}	3.83×10^{-3}	1.99×10^{-1}
+ PB-2 + BAO + H_0 + SKA2	5.69×10^{-4}	1.07×10^{-4}	2.66×10^{-3}	2.56×10^{-3}	1.85×10^{-1}
+ SA (0.2)	3.32×10^{-3}	1.42×10^{-4}	1.30×10^{-2}	5.04×10^{-3}	2.32×10^{-1}
+ SA + BAO + H_0	2.88×10^{-3}	1.14×10^{-4}	7.87×10^{-3}	3.93×10^{-3}	2.22×10^{-1}
+ SA + BAO + H_0 + SKA1	9.16×10^{-4}	1.10×10^{-4}	4.32×10^{-3}	3.67×10^{-3}	1.97×10^{-1}
+ SA + BAO + H_0 + SKA2	5.67×10^{-4}	1.04×10^{-4}	2.65×10^{-3}	2.50×10^{-3}	1.83×10^{-1}
	$\sigma(\tau)$	$\sigma(Y_p)$	$\sigma(\Sigma m_\nu)$	$\sigma(N_\nu)$	
Planck	4.78×10^{-3}	1.69×10^{-2}	1.54×10^{-1}	2.98×10^{-1}	
+ PB-2 (0.2)	4.55×10^{-3}	1.10×10^{-2}	8.41×10^{-2}	1.95×10^{-1}	
+ PB-2 + BAO + H_0	4.55×10^{-3}	9.69×10^{-3}	6.62×10^{-2}	1.27×10^{-1}	
+ PB-2 + BAO + H_0 + SKA1	4.51×10^{-3}	7.82×10^{-3}	3.75×10^{-2}	4.13×10^{-2}	
+ PB-2 + BAO + H_0 + SKA2	4.25×10^{-3}	6.68×10^{-3}	2.85×10^{-2}	3.32×10^{-2}	
+ SA (0.2)	4.54×10^{-3}	9.99×10^{-3}	7.58×10^{-2}	1.75×10^{-1}	
+ SA + BAO + H_0	4.54×10^{-3}	9.02×10^{-3}	6.11×10^{-2}	1.18×10^{-1}	
+ SA + BAO + H_0 + SKA1	4.49×10^{-3}	7.29×10^{-3}	3.40×10^{-2}	4.03×10^{-2}	
+ SA + BAO + H_0 + SKA2	4.22×10^{-3}	6.32×10^{-3}	2.54×10^{-2}	3.23×10^{-2}	

Table 9: $f_{\text{sky}} = 0.2$, $N_{\text{field}} = 4$, $\Sigma m_\nu = 0.06$ eV, without the residual foregrounds.

	$\sigma(\Omega_m h^2)$	$\sigma(\Omega_b h^2)$	$\sigma(\Omega_\Lambda)$	$\sigma(n_s)$	$\sigma(A_s \times 10^{10})$
Planck	5.37×10^{-3}	2.49×10^{-4}	2.43×10^{-2}	8.82×10^{-3}	2.86×10^{-1}
+ PB-2 (0.2)	4.22×10^{-3}	1.75×10^{-4}	1.69×10^{-2}	6.20×10^{-3}	2.51×10^{-1}
+ PB-2 + BAO + H_0	3.41×10^{-3}	1.35×10^{-4}	9.18×10^{-3}	4.60×10^{-3}	2.28×10^{-1}
+ PB-2 + BAO + H_0 + SKA1	2.34×10^{-3}	1.34×10^{-4}	6.85×10^{-3}	4.53×10^{-3}	2.13×10^{-1}
+ PB-2 + BAO + H_0 + SKA2	1.60×10^{-3}	1.29×10^{-4}	4.47×10^{-3}	3.91×10^{-3}	2.01×10^{-1}
+ SA (0.2)	3.30×10^{-3}	1.43×10^{-4}	1.31×10^{-2}	5.08×10^{-3}	2.29×10^{-1}
+ SA + BAO + H_0	2.86×10^{-3}	1.14×10^{-4}	7.82×10^{-3}	3.96×10^{-3}	2.19×10^{-1}
+ SA + BAO + H_0 + SKA1	2.14×10^{-3}	1.14×10^{-4}	6.32×10^{-3}	3.90×10^{-3}	2.08×10^{-1}
+ SA + BAO + H_0 + SKA2	1.53×10^{-3}	1.11×10^{-4}	4.32×10^{-3}	3.47×10^{-3}	1.96×10^{-1}
	$\sigma(\tau)$	$\sigma(Y_p)$	$\sigma(\Sigma m_\nu)$	$\sigma(N_\nu)$	
Planck	4.84×10^{-3}	1.71×10^{-2}	1.52×10^{-1}	3.03×10^{-1}	
+ PB-2 (0.2)	4.58×10^{-3}	1.28×10^{-2}	1.06×10^{-1}	2.32×10^{-1}	
+ PB-2 + BAO + H_0	4.57×10^{-3}	1.11×10^{-2}	7.75×10^{-2}	1.44×10^{-1}	
+ PB-2 + BAO + H_0 + SKA1	4.56×10^{-3}	9.95×10^{-3}	6.14×10^{-2}	1.00×10^{-1}	
+ PB-2 + BAO + H_0 + SKA2	4.47×10^{-3}	9.06×10^{-3}	4.71×10^{-2}	7.65×10^{-2}	
+ SA (0.2)	4.49×10^{-3}	1.01×10^{-2}	7.57×10^{-2}	1.75×10^{-1}	
+ SA + BAO + H_0	4.49×10^{-3}	9.11×10^{-3}	6.08×10^{-2}	1.18×10^{-1}	
+ SA + BAO + H_0 + SKA1	4.49×10^{-3}	8.41×10^{-3}	4.93×10^{-2}	8.96×10^{-2}	
+ SA + BAO + H_0 + SKA2	4.40×10^{-3}	7.80×10^{-3}	3.65×10^{-2}	7.10×10^{-2}	

Table 10: $f_{\text{sky}} = 0.2$, $N_{\text{field}} = 4$, $\Sigma m_\nu = 0.1$ eV, with the residual foregrounds.

	$\sigma(\Omega_m h^2)$	$\sigma(\Omega_b h^2)$	$\sigma(\Omega_\Lambda)$	$\sigma(n_s)$	$\sigma(A_s \times 10^{10})$
Planck	5.42×10^{-3}	2.50×10^{-4}	2.46×10^{-2}	8.82×10^{-3}	2.86×10^{-1}
+ PB-2 (0.2)	4.26×10^{-3}	1.75×10^{-4}	1.70×10^{-2}	6.19×10^{-3}	2.51×10^{-1}
+ PB-2 + BAO + H_0	3.45×10^{-3}	1.35×10^{-4}	9.29×10^{-3}	4.60×10^{-3}	2.28×10^{-1}
+ PB-2 + BAO + H_0 + SKA1	2.35×10^{-3}	1.34×10^{-4}	6.87×10^{-3}	4.53×10^{-3}	2.13×10^{-1}
+ PB-2 + BAO + H_0 + SKA2	1.59×10^{-3}	1.29×10^{-4}	4.45×10^{-3}	3.89×10^{-3}	2.00×10^{-1}
+ SA (0.2)	3.35×10^{-3}	1.43×10^{-4}	1.31×10^{-2}	5.08×10^{-3}	2.30×10^{-1}
+ SA + BAO + H_0	2.90×10^{-3}	1.14×10^{-4}	7.91×10^{-3}	3.95×10^{-3}	2.19×10^{-1}
+ SA + BAO + H_0 + SKA1	2.15×10^{-3}	1.14×10^{-4}	6.34×10^{-3}	3.90×10^{-3}	2.08×10^{-1}
+ SA + BAO + H_0 + SKA2	1.52×10^{-3}	1.11×10^{-4}	4.30×10^{-3}	3.45×10^{-3}	1.96×10^{-1}
	$\sigma(\tau)$	$\sigma(Y_p)$	$\sigma(\Sigma m_\nu)$	$\sigma(N_\nu)$	
Planck	4.82×10^{-3}	1.72×10^{-2}	1.56×10^{-1}	3.03×10^{-1}	
+ PB-2 (0.2)	4.55×10^{-3}	1.28×10^{-2}	1.08×10^{-1}	2.33×10^{-1}	
+ PB-2 + BAO + H_0	4.55×10^{-3}	1.11×10^{-2}	7.91×10^{-2}	1.45×10^{-1}	
+ PB-2 + BAO + H_0 + SKA1	4.54×10^{-3}	9.93×10^{-3}	6.23×10^{-2}	1.00×10^{-1}	
+ PB-2 + BAO + H_0 + SKA2	4.45×10^{-3}	9.02×10^{-3}	4.74×10^{-2}	7.60×10^{-2}	
+ SA (0.2)	4.47×10^{-3}	1.01×10^{-2}	7.64×10^{-2}	1.77×10^{-1}	
+ SA + BAO + H_0	4.47×10^{-3}	9.10×10^{-3}	6.14×10^{-2}	1.19×10^{-1}	
+ SA + BAO + H_0 + SKA1	4.46×10^{-3}	8.38×10^{-3}	4.95×10^{-2}	8.94×10^{-2}	
+ SA + BAO + H_0 + SKA2	4.37×10^{-3}	7.77×10^{-3}	3.65×10^{-2}	7.06×10^{-2}	

Table 11: $f_{\text{sky}} = 0.2$, $N_{\text{field}} = 4$, $\Sigma m_\nu = 0.06$ eV, with the residual foregrounds.

	$\sigma(\Omega_m h^2)$	$\sigma(\Omega_b h^2)$	$\sigma(\Omega_\Lambda)$	$\sigma(n_s)$	$\sigma(A_s \times 10^{10})$
Planck	5.31×10^{-3}	2.44×10^{-4}	2.38×10^{-2}	8.61×10^{-3}	2.83×10^{-1}
+ PB-2 (0.65)	2.98×10^{-3}	1.17×10^{-4}	1.13×10^{-2}	4.21×10^{-3}	2.23×10^{-1}
+ PB-2 + BAO + H_0	2.62×10^{-3}	9.60×10^{-5}	7.20×10^{-3}	3.44×10^{-3}	2.17×10^{-1}
+ PB-2 + BAO + H_0 + SKA1	8.99×10^{-4}	9.36×10^{-5}	4.25×10^{-3}	3.25×10^{-3}	1.93×10^{-1}
+ PB-2 + BAO + H_0 + SKA2	5.60×10^{-4}	8.88×10^{-5}	2.65×10^{-3}	2.36×10^{-3}	1.80×10^{-1}
+ SA (0.65)	2.61×10^{-3}	1.05×10^{-4}	1.01×10^{-2}	3.82×10^{-3}	2.16×10^{-1}
+ SA + BAO + H_0	2.37×10^{-3}	8.83×10^{-5}	6.60×10^{-3}	3.20×10^{-3}	2.12×10^{-1}
+ SA + BAO + H_0 + SKA1	8.85×10^{-4}	8.63×10^{-5}	4.17×10^{-3}	3.04×10^{-3}	1.91×10^{-1}
+ SA + BAO + H_0 + SKA2	5.56×10^{-4}	8.25×10^{-5}	2.63×10^{-3}	2.26×10^{-3}	1.77×10^{-1}
	$\sigma(\tau)$	$\sigma(Y_p)$	$\sigma(\Sigma m_\nu)$	$\sigma(N_\nu)$	
Planck	4.80×10^{-3}	1.69×10^{-2}	1.50×10^{-1}	2.98×10^{-1}	
+ PB-2 (0.65)	4.49×10^{-3}	8.86×10^{-3}	7.13×10^{-2}	1.58×10^{-1}	
+ PB-2 + BAO + H_0	4.47×10^{-3}	7.92×10^{-3}	5.79×10^{-2}	1.10×10^{-1}	
+ PB-2 + BAO + H_0 + SKA1	4.43×10^{-3}	6.45×10^{-3}	3.57×10^{-2}	3.93×10^{-2}	
+ PB-2 + BAO + H_0 + SKA2	4.19×10^{-3}	5.71×10^{-3}	2.74×10^{-2}	3.10×10^{-2}	
+ SA (0.65)	4.46×10^{-3}	7.81×10^{-3}	6.23×10^{-2}	1.35×10^{-1}	
+ SA + BAO + H_0	4.44×10^{-3}	7.12×10^{-3}	5.18×10^{-2}	9.87×10^{-2}	
+ SA + BAO + H_0 + SKA1	4.40×10^{-3}	5.88×10^{-3}	3.23×10^{-2}	3.81×10^{-2}	
+ SA + BAO + H_0 + SKA2	4.15×10^{-3}	5.27×10^{-3}	2.44×10^{-2}	3.00×10^{-2}	

Table 12: $f_{\text{sky}} = 0.65$, $N_{\text{field}} = 4$, $\Sigma m_\nu = 0.1$ eV, without the residual foregrounds.

	$\sigma(\Omega_m h^2)$	$\sigma(\Omega_b h^2)$	$\sigma(\Omega_\Lambda)$	$\sigma(n_s)$	$\sigma(A_s \times 10^{10})$
Planck	5.35×10^{-3}	2.45×10^{-4}	2.41×10^{-2}	8.61×10^{-3}	2.83×10^{-1}
+ PB-2 (0.65)	3.02×10^{-3}	1.17×10^{-4}	1.14×10^{-2}	4.21×10^{-3}	2.23×10^{-1}
+ PB-2 + BAO + H_0	2.65×10^{-3}	9.60×10^{-5}	7.28×10^{-3}	3.44×10^{-3}	2.17×10^{-1}
+ PB-2 + BAO + H_0 + SKA1	9.05×10^{-4}	9.36×10^{-5}	4.26×10^{-3}	3.25×10^{-3}	1.92×10^{-1}
+ PB-2 + BAO + H_0 + SKA2	5.63×10^{-4}	8.87×10^{-5}	2.64×10^{-3}	2.34×10^{-3}	1.80×10^{-1}
+ SA (0.65)	2.65×10^{-3}	1.05×10^{-4}	1.01×10^{-2}	3.82×10^{-3}	2.17×10^{-1}
+ SA + BAO + H_0	2.40×10^{-3}	8.83×10^{-5}	6.67×10^{-3}	3.20×10^{-3}	2.12×10^{-1}
+ SA + BAO + H_0 + SKA1	8.90×10^{-4}	8.62×10^{-5}	4.18×10^{-3}	3.04×10^{-3}	1.90×10^{-1}
+ SA + BAO + H_0 + SKA2	5.58×10^{-4}	8.24×10^{-5}	2.62×10^{-3}	2.25×10^{-3}	1.77×10^{-1}
	$\sigma(\tau)$	$\sigma(Y_p)$	$\sigma(\Sigma m_\nu)$	$\sigma(N_\nu)$	
Planck	4.78×10^{-3}	1.69×10^{-2}	1.54×10^{-1}	2.98×10^{-1}	
+ PB-2 (0.65)	4.46×10^{-3}	8.88×10^{-3}	7.27×10^{-2}	1.58×10^{-1}	
+ PB-2 + BAO + H_0	4.44×10^{-3}	7.91×10^{-3}	5.89×10^{-2}	1.10×10^{-1}	
+ PB-2 + BAO + H_0 + SKA1	4.40×10^{-3}	6.45×10^{-3}	3.63×10^{-2}	3.93×10^{-2}	
+ PB-2 + BAO + H_0 + SKA2	4.16×10^{-3}	5.70×10^{-3}	2.76×10^{-2}	3.10×10^{-2}	
+ SA (0.65)	4.43×10^{-3}	7.83×10^{-3}	6.31×10^{-2}	1.37×10^{-1}	
+ SA + BAO + H_0	4.41×10^{-3}	7.11×10^{-3}	5.25×10^{-2}	9.93×10^{-2}	
+ SA + BAO + H_0 + SKA1	4.37×10^{-3}	5.87×10^{-3}	3.28×10^{-2}	3.81×10^{-2}	
+ SA + BAO + H_0 + SKA2	4.12×10^{-3}	5.26×10^{-3}	2.46×10^{-2}	3.00×10^{-2}	

Table 13: $f_{\text{sky}} = 0.65$, $N_{\text{field}} = 4$, $\Sigma m_\nu = 0.06$ eV, without the residual foregrounds.

	$\sigma(\Omega_m h^2)$	$\sigma(\Omega_b h^2)$	$\sigma(\Omega_\Lambda)$	$\sigma(n_s)$	$\sigma(A_s \times 10^{10})$
Planck	5.37×10^{-3}	2.49×10^{-4}	2.43×10^{-2}	8.82×10^{-3}	2.86×10^{-1}
+ PB-2 (0.65)	3.46×10^{-3}	1.36×10^{-4}	1.32×10^{-2}	4.82×10^{-3}	2.34×10^{-1}
+ PB-2 + BAO + H_0	2.94×10^{-3}	1.09×10^{-4}	7.99×10^{-3}	3.81×10^{-3}	2.23×10^{-1}
+ PB-2 + BAO + H_0 + SKA1	2.17×10^{-3}	1.09×10^{-4}	6.38×10^{-3}	3.77×10^{-3}	2.11×10^{-1}
+ PB-2 + BAO + H_0 + SKA2	1.54×10^{-3}	1.06×10^{-4}	4.34×10^{-3}	3.37×10^{-3}	1.99×10^{-1}
+ SA (0.65)	2.65×10^{-3}	1.06×10^{-4}	1.02×10^{-2}	3.86×10^{-3}	2.15×10^{-1}
+ SA + BAO + H_0	2.39×10^{-3}	8.90×10^{-5}	6.66×10^{-3}	3.22×10^{-3}	2.11×10^{-1}
+ SA + BAO + H_0 + SKA1	1.92×10^{-3}	8.87×10^{-5}	5.74×10^{-3}	3.19×10^{-3}	2.02×10^{-1}
+ SA + BAO + H_0 + SKA2	1.44×10^{-3}	8.73×10^{-5}	4.13×10^{-3}	2.93×10^{-3}	1.91×10^{-1}
	$\sigma(\tau)$	$\sigma(Y_p)$	$\sigma(\Sigma m_\nu)$	$\sigma(N_\nu)$	
Planck	4.84×10^{-3}	1.71×10^{-2}	1.52×10^{-1}	3.03×10^{-1}	
+ PB-2 (0.65)	4.56×10^{-3}	1.02×10^{-2}	8.51×10^{-2}	1.86×10^{-1}	
+ PB-2 + BAO + H_0	4.55×10^{-3}	8.97×10^{-3}	6.63×10^{-2}	1.24×10^{-1}	
+ PB-2 + BAO + H_0 + SKA1	4.55×10^{-3}	8.18×10^{-3}	5.47×10^{-2}	9.23×10^{-2}	
+ PB-2 + BAO + H_0 + SKA2	4.46×10^{-3}	7.58×10^{-3}	4.20×10^{-2}	7.23×10^{-2}	
+ SA (0.65)	4.41×10^{-3}	7.93×10^{-3}	6.30×10^{-2}	1.38×10^{-1}	
+ SA + BAO + H_0	4.39×10^{-3}	7.21×10^{-3}	5.22×10^{-2}	9.98×10^{-2}	
+ SA + BAO + H_0 + SKA1	4.38×10^{-3}	6.76×10^{-3}	4.50×10^{-2}	8.06×10^{-2}	
+ SA + BAO + H_0 + SKA2	4.30×10^{-3}	6.39×10^{-3}	3.47×10^{-2}	6.63×10^{-2}	

Table 14: $f_{\text{sky}} = 0.65$, $N_{\text{field}} = 4$, $\Sigma m_\nu = 0.1$ eV, with the residual foregrounds.

	$\sigma(\Omega_m h^2)$	$\sigma(\Omega_b h^2)$	$\sigma(\Omega_\Lambda)$	$\sigma(n_s)$	$\sigma(A_s \times 10^{10})$
Planck	5.42×10^{-3}	2.50×10^{-4}	2.46×10^{-2}	8.82×10^{-3}	2.86×10^{-1}
+ PB-2 (0.65)	3.49×10^{-3}	1.36×10^{-4}	1.33×10^{-2}	4.81×10^{-3}	2.34×10^{-1}
+ PB-2 + BAO + H_0	2.98×10^{-3}	1.09×10^{-4}	8.09×10^{-3}	3.81×10^{-3}	2.23×10^{-1}
+ PB-2 + BAO + H_0 + SKA1	2.18×10^{-3}	1.09×10^{-4}	6.41×10^{-3}	3.77×10^{-3}	2.11×10^{-1}
+ PB-2 + BAO + H_0 + SKA2	1.54×10^{-3}	1.06×10^{-4}	4.32×10^{-3}	3.36×10^{-3}	1.98×10^{-1}
+ SA (0.65)	2.69×10^{-3}	1.06×10^{-4}	1.02×10^{-2}	3.86×10^{-3}	2.15×10^{-1}
+ SA + BAO + H_0	2.42×10^{-3}	8.89×10^{-5}	6.73×10^{-3}	3.22×10^{-3}	2.11×10^{-1}
+ SA + BAO + H_0 + SKA1	1.93×10^{-3}	8.86×10^{-5}	5.76×10^{-3}	3.19×10^{-3}	2.02×10^{-1}
+ SA + BAO + H_0 + SKA2	1.44×10^{-3}	8.72×10^{-5}	4.12×10^{-3}	2.92×10^{-3}	1.90×10^{-1}
	$\sigma(\tau)$	$\sigma(Y_p)$	$\sigma(\Sigma m_\nu)$	$\sigma(N_\nu)$	
Planck	4.82×10^{-3}	1.72×10^{-2}	1.56×10^{-1}	3.03×10^{-1}	
+ PB-2 (0.65)	4.53×10^{-3}	1.02×10^{-2}	8.72×10^{-2}	1.87×10^{-1}	
+ PB-2 + BAO + H_0	4.53×10^{-3}	8.97×10^{-3}	6.77×10^{-2}	1.24×10^{-1}	
+ PB-2 + BAO + H_0 + SKA1	4.52×10^{-3}	8.17×10^{-3}	5.55×10^{-2}	9.21×10^{-2}	
+ PB-2 + BAO + H_0 + SKA2	4.43×10^{-3}	7.55×10^{-3}	4.24×10^{-2}	7.19×10^{-2}	
+ SA (0.65)	4.38×10^{-3}	7.95×10^{-3}	6.38×10^{-2}	1.39×10^{-1}	
+ SA + BAO + H_0	4.37×10^{-3}	7.20×10^{-3}	5.30×10^{-2}	1.00×10^{-1}	
+ SA + BAO + H_0 + SKA1	4.36×10^{-3}	6.75×10^{-3}	4.54×10^{-2}	8.06×10^{-2}	
+ SA + BAO + H_0 + SKA2	4.27×10^{-3}	6.36×10^{-3}	3.49×10^{-2}	6.61×10^{-2}	

Table 15: $f_{\text{sky}} = 0.65$, $N_{\text{field}} = 4$, $\Sigma m_\nu = 0.06$ eV, with the residual foregrounds.

	$\sigma(\Omega_m h^2)$	$\sigma(\Omega_b h^2)$	$\sigma(\Omega_\Lambda)$	$\sigma(n_s)$	$\sigma(A_s \times 10^{10})$
Planck + PB-2(0.016) + BAO + H_0	3.92×10^{-3}	1.70×10^{-4}	1.05×10^{-2}	5.75×10^{-3}	2.34×10^{-1}
+ SKA1 ($N_{\text{field}} = 4$)	9.47×10^{-4}	1.55×10^{-4}	4.51×10^{-3}	5.12×10^{-3}	2.09×10^{-1}
+ SKA1 ($N_{\text{field}} = 8$)	7.23×10^{-4}	1.46×10^{-4}	4.12×10^{-3}	4.66×10^{-3}	2.06×10^{-1}
+ SKA2 ($N_{\text{field}} = 4$)	5.79×10^{-4}	1.37×10^{-4}	2.72×10^{-3}	2.99×10^{-3}	1.96×10^{-1}
+ SKA2 ($N_{\text{field}} = 8$)	4.20×10^{-4}	1.26×10^{-4}	2.12×10^{-3}	2.30×10^{-3}	1.91×10^{-1}
Planck + SA(0.016) + BAO + H_0	3.57×10^{-3}	1.54×10^{-4}	9.61×10^{-3}	5.23×10^{-3}	2.29×10^{-1}
+ SKA1 ($N_{\text{field}} = 4$)	9.37×10^{-4}	1.45×10^{-4}	4.44×10^{-3}	4.71×10^{-3}	2.06×10^{-1}
+ SKA1 ($N_{\text{field}} = 8$)	7.13×10^{-4}	1.38×10^{-4}	4.04×10^{-3}	4.32×10^{-3}	2.02×10^{-1}
+ SKA2 ($N_{\text{field}} = 4$)	5.75×10^{-4}	1.31×10^{-4}	2.70×10^{-3}	2.86×10^{-3}	1.90×10^{-1}
+ SKA2 ($N_{\text{field}} = 8$)	4.17×10^{-4}	1.22×10^{-4}	2.10×10^{-3}	2.23×10^{-3}	1.82×10^{-1}
	$\sigma(\tau)$	$\sigma(Y_p)$	$\sigma(\Sigma m_\nu)$	$\sigma(N_\nu)$	
Planck + PB-2(0.016) + BAO + H_0	4.63×10^{-3}	1.40×10^{-2}	9.37×10^{-2}	1.68×10^{-1}	
+ SKA1 ($N_{\text{field}} = 4$)	4.62×10^{-3}	1.05×10^{-2}	5.55×10^{-2}	4.72×10^{-2}	
+ SKA1 ($N_{\text{field}} = 8$)	4.57×10^{-3}	9.76×10^{-3}	5.21×10^{-2}	3.91×10^{-2}	
+ SKA2 ($N_{\text{field}} = 4$)	4.39×10^{-3}	8.19×10^{-3}	4.11×10^{-2}	3.84×10^{-2}	
+ SKA2 ($N_{\text{field}} = 8$)	4.29×10^{-3}	7.46×10^{-3}	3.42×10^{-2}	3.29×10^{-2}	
Planck + SA(0.016) + BAO + H_0	4.60×10^{-3}	1.26×10^{-2}	7.79×10^{-2}	1.51×10^{-1}	
+ SKA1 ($N_{\text{field}} = 4$)	4.60×10^{-3}	9.55×10^{-3}	4.09×10^{-2}	4.45×10^{-2}	
+ SKA1 ($N_{\text{field}} = 8$)	4.55×10^{-3}	8.95×10^{-3}	3.86×10^{-2}	3.65×10^{-2}	
+ SKA2 ($N_{\text{field}} = 4$)	4.33×10^{-3}	7.70×10^{-3}	3.10×10^{-2}	3.62×10^{-2}	
+ SKA2 ($N_{\text{field}} = 8$)	4.17×10^{-3}	7.03×10^{-3}	2.71×10^{-2}	3.09×10^{-2}	

Table 16: $f_{\text{sky}} = 0.016$, $\Sigma m_\nu = 0.1$ eV, with the residual foregrounds of CMB, without those of 21 cm line.

	$\sigma(\Omega_m h^2)$	$\sigma(\Omega_b h^2)$	$\sigma(\Omega_\Lambda)$	$\sigma(n_s)$	$\sigma(A_s \times 10^{10})$
Planck + PB-2(0.016) + BAO + H_0	3.97×10^{-3}	1.70×10^{-4}	1.06×10^{-2}	5.75×10^{-3}	2.34×10^{-1}
+ SKA1 ($N_{\text{field}} = 4$)	9.54×10^{-4}	1.55×10^{-4}	4.52×10^{-3}	5.11×10^{-3}	2.09×10^{-1}
+ SKA1 ($N_{\text{field}} = 8$)	7.29×10^{-4}	1.46×10^{-4}	4.13×10^{-3}	4.65×10^{-3}	2.06×10^{-1}
+ SKA2 ($N_{\text{field}} = 4$)	5.82×10^{-4}	1.36×10^{-4}	2.71×10^{-3}	2.95×10^{-3}	1.95×10^{-1}
+ SKA2 ($N_{\text{field}} = 8$)	4.21×10^{-4}	1.26×10^{-4}	2.10×10^{-3}	2.27×10^{-3}	1.91×10^{-1}
Planck + SA(0.016) + BAO + H_0	3.61×10^{-3}	1.54×10^{-4}	9.71×10^{-3}	5.23×10^{-3}	2.29×10^{-1}
+ SKA1 ($N_{\text{field}} = 4$)	9.41×10^{-4}	1.45×10^{-4}	4.45×10^{-3}	4.70×10^{-3}	2.06×10^{-1}
+ SKA1 ($N_{\text{field}} = 8$)	7.17×10^{-4}	1.38×10^{-4}	4.05×10^{-3}	4.30×10^{-3}	2.02×10^{-1}
+ SKA2 ($N_{\text{field}} = 4$)	5.77×10^{-4}	1.30×10^{-4}	2.68×10^{-3}	2.84×10^{-3}	1.89×10^{-1}
+ SKA2 ($N_{\text{field}} = 8$)	4.18×10^{-4}	1.22×10^{-4}	2.09×10^{-3}	2.21×10^{-3}	1.82×10^{-1}
	$\sigma(\tau)$	$\sigma(Y_p)$	$\sigma(\Sigma m_\nu)$	$\sigma(N_\nu)$	
Planck + PB-2(0.016) + BAO + H_0	4.60×10^{-3}	1.40×10^{-2}	9.56×10^{-2}	1.69×10^{-1}	
+ SKA1 ($N_{\text{field}} = 4$)	4.59×10^{-3}	1.05×10^{-2}	5.63×10^{-2}	4.72×10^{-2}	
+ SKA1 ($N_{\text{field}} = 8$)	4.54×10^{-3}	9.74×10^{-3}	5.28×10^{-2}	3.90×10^{-2}	
+ SKA2 ($N_{\text{field}} = 4$)	4.36×10^{-3}	8.16×10^{-3}	4.09×10^{-2}	3.83×10^{-2}	
+ SKA2 ($N_{\text{field}} = 8$)	4.26×10^{-3}	7.43×10^{-3}	3.37×10^{-2}	3.27×10^{-2}	
Planck + SA(0.016) + BAO + H_0	4.57×10^{-3}	1.26×10^{-2}	7.81×10^{-2}	1.51×10^{-1}	
+ SKA1 ($N_{\text{field}} = 4$)	4.57×10^{-3}	9.54×10^{-3}	4.13×10^{-2}	4.44×10^{-2}	
+ SKA1 ($N_{\text{field}} = 8$)	4.53×10^{-3}	8.94×10^{-3}	3.90×10^{-2}	3.64×10^{-2}	
+ SKA2 ($N_{\text{field}} = 4$)	4.30×10^{-3}	7.66×10^{-3}	3.10×10^{-2}	3.62×10^{-2}	
+ SKA2 ($N_{\text{field}} = 8$)	4.15×10^{-3}	7.00×10^{-3}	2.69×10^{-2}	3.08×10^{-2}	

Table 17: $f_{\text{sky}} = 0.016$, $\Sigma m_\nu = 0.06$ eV, with the residual foregrounds of CMB, without those of 21 cm line.

	$\sigma(\Omega_m h^2)$	$\sigma(\Omega_b h^2)$	$\sigma(\Omega_\Lambda)$	$\sigma(n_s)$	$\sigma(A_s \times 10^{10})$
Planck + PB-2(0.2) + BAO + H_0	3.41×10^{-3}	1.35×10^{-4}	9.18×10^{-3}	4.60×10^{-3}	2.28×10^{-1}
+ SKA1 ($N_{\text{field}} = 4$)	9.32×10^{-4}	1.28×10^{-4}	4.43×10^{-3}	4.24×10^{-3}	2.03×10^{-1}
+ SKA1 ($N_{\text{field}} = 8$)	7.11×10^{-4}	1.23×10^{-4}	4.05×10^{-3}	3.95×10^{-3}	2.01×10^{-1}
+ SKA2 ($N_{\text{field}} = 4$)	5.72×10^{-4}	1.18×10^{-4}	2.70×10^{-3}	2.74×10^{-3}	1.91×10^{-1}
+ SKA2 ($N_{\text{field}} = 8$)	4.14×10^{-4}	1.10×10^{-4}	2.11×10^{-3}	2.17×10^{-3}	1.85×10^{-1}
Planck + SA(0.2) + BAO + H_0	2.86×10^{-3}	1.14×10^{-4}	7.82×10^{-3}	3.96×10^{-3}	2.19×10^{-1}
+ SKA1 ($N_{\text{field}} = 4$)	9.11×10^{-4}	1.11×10^{-4}	4.31×10^{-3}	3.69×10^{-3}	1.97×10^{-1}
+ SKA1 ($N_{\text{field}} = 8$)	6.96×10^{-4}	1.08×10^{-4}	3.95×10^{-3}	3.48×10^{-3}	1.95×10^{-1}
+ SKA2 ($N_{\text{field}} = 4$)	5.65×10^{-4}	1.04×10^{-4}	2.66×10^{-3}	2.53×10^{-3}	1.83×10^{-1}
+ SKA2 ($N_{\text{field}} = 8$)	4.09×10^{-4}	9.96×10^{-5}	2.08×10^{-3}	2.03×10^{-3}	1.74×10^{-1}
	$\sigma(\tau)$	$\sigma(Y_p)$	$\sigma(\Sigma m_\nu)$	$\sigma(N_\nu)$	
Planck + PB-2(0.2) + BAO + H_0	4.57×10^{-3}	1.11×10^{-2}	7.75×10^{-2}	1.44×10^{-1}	
+ SKA1 ($N_{\text{field}} = 4$)	4.59×10^{-3}	8.64×10^{-3}	4.56×10^{-2}	4.36×10^{-2}	
+ SKA1 ($N_{\text{field}} = 8$)	4.55×10^{-3}	8.20×10^{-3}	4.32×10^{-2}	3.56×10^{-2}	
+ SKA2 ($N_{\text{field}} = 4$)	4.35×10^{-3}	7.19×10^{-3}	3.51×10^{-2}	3.52×10^{-2}	
+ SKA2 ($N_{\text{field}} = 8$)	4.22×10^{-3}	6.63×10^{-3}	3.01×10^{-2}	2.98×10^{-2}	
Planck + SA(0.2) + BAO + H_0	4.49×10^{-3}	9.11×10^{-3}	6.08×10^{-2}	1.18×10^{-1}	
+ SKA1 ($N_{\text{field}} = 4$)	4.52×10^{-3}	7.38×10^{-3}	3.39×10^{-2}	4.05×10^{-2}	
+ SKA1 ($N_{\text{field}} = 8$)	4.48×10^{-3}	7.07×10^{-3}	3.18×10^{-2}	3.26×10^{-2}	
+ SKA2 ($N_{\text{field}} = 4$)	4.25×10^{-3}	6.39×10^{-3}	2.56×10^{-2}	3.24×10^{-2}	
+ SKA2 ($N_{\text{field}} = 8$)	4.07×10^{-3}	5.93×10^{-3}	2.25×10^{-2}	2.71×10^{-2}	

Table 18: $f_{\text{sky}} = 0.2$, $\Sigma m_\nu = 0.1$ eV, with the residual foregrounds of CMB, without those of 21 cm line.

	$\sigma(\Omega_m h^2)$	$\sigma(\Omega_b h^2)$	$\sigma(\Omega_\Lambda)$	$\sigma(n_s)$	$\sigma(A_s \times 10^{10})$
Planck + PB-2(0.2) + BAO + H_0	3.45×10^{-3}	1.35×10^{-4}	9.29×10^{-3}	4.60×10^{-3}	2.28×10^{-1}
+ SKA1 ($N_{\text{field}} = 4$)	9.38×10^{-4}	1.28×10^{-4}	4.44×10^{-3}	4.23×10^{-3}	2.03×10^{-1}
+ SKA1 ($N_{\text{field}} = 8$)	7.16×10^{-4}	1.23×10^{-4}	4.06×10^{-3}	3.94×10^{-3}	2.00×10^{-1}
+ SKA2 ($N_{\text{field}} = 4$)	5.74×10^{-4}	1.18×10^{-4}	2.69×10^{-3}	2.71×10^{-3}	1.90×10^{-1}
+ SKA2 ($N_{\text{field}} = 8$)	4.15×10^{-4}	1.10×10^{-4}	2.09×10^{-3}	2.14×10^{-3}	1.84×10^{-1}
Planck + SA(0.2) + BAO + H_0	2.90×10^{-3}	1.14×10^{-4}	7.91×10^{-3}	3.95×10^{-3}	2.19×10^{-1}
+ SKA1 ($N_{\text{field}} = 4$)	9.16×10^{-4}	1.11×10^{-4}	4.32×10^{-3}	3.69×10^{-3}	1.97×10^{-1}
+ SKA1 ($N_{\text{field}} = 8$)	7.00×10^{-4}	1.08×10^{-4}	3.95×10^{-3}	3.47×10^{-3}	1.94×10^{-1}
+ SKA2 ($N_{\text{field}} = 4$)	5.67×10^{-4}	1.04×10^{-4}	2.65×10^{-3}	2.51×10^{-3}	1.83×10^{-1}
+ SKA2 ($N_{\text{field}} = 8$)	4.10×10^{-4}	9.96×10^{-5}	2.07×10^{-3}	2.01×10^{-3}	1.74×10^{-1}
	$\sigma(\tau)$	$\sigma(Y_p)$	$\sigma(\Sigma m_\nu)$	$\sigma(N_\nu)$	
Planck + PB-2(0.2) + BAO + H_0	4.55×10^{-3}	1.11×10^{-2}	7.91×10^{-2}	1.45×10^{-1}	
+ SKA1 ($N_{\text{field}} = 4$)	4.56×10^{-3}	8.63×10^{-3}	4.64×10^{-2}	4.36×10^{-2}	
+ SKA1 ($N_{\text{field}} = 8$)	4.52×10^{-3}	8.19×10^{-3}	4.39×10^{-2}	3.55×10^{-2}	
+ SKA2 ($N_{\text{field}} = 4$)	4.32×10^{-3}	7.17×10^{-3}	3.51×10^{-2}	3.52×10^{-2}	
+ SKA2 ($N_{\text{field}} = 8$)	4.19×10^{-3}	6.60×10^{-3}	2.99×10^{-2}	2.97×10^{-2}	
Planck + SA(0.2) + BAO + H_0	4.47×10^{-3}	9.10×10^{-3}	6.14×10^{-2}	1.19×10^{-1}	
+ SKA1 ($N_{\text{field}} = 4$)	4.49×10^{-3}	7.37×10^{-3}	3.43×10^{-2}	4.04×10^{-2}	
+ SKA1 ($N_{\text{field}} = 8$)	4.45×10^{-3}	7.05×10^{-3}	3.21×10^{-2}	3.25×10^{-2}	
+ SKA2 ($N_{\text{field}} = 4$)	4.22×10^{-3}	6.37×10^{-3}	2.57×10^{-2}	3.24×10^{-2}	
+ SKA2 ($N_{\text{field}} = 8$)	4.03×10^{-3}	5.91×10^{-3}	2.26×10^{-2}	2.71×10^{-2}	

Table 19: $f_{\text{sky}} = 0.2$, $\Sigma m_\nu = 0.06$ eV, with the residual foregrounds of CMB, without those of 21 cm line.

	$\sigma(\Omega_m h^2)$	$\sigma(\Omega_b h^2)$	$\sigma(\Omega_\Lambda)$	$\sigma(n_s)$	$\sigma(A_s \times 10^{10})$
Planck + PB-2(0.65) + BAO + H_0	2.94×10^{-3}	1.09×10^{-4}	7.99×10^{-3}	3.81×10^{-3}	2.23×10^{-1}
+ SKA1 ($N_{\text{field}} = 4$)	9.14×10^{-4}	1.06×10^{-4}	4.34×10^{-3}	3.58×10^{-3}	2.00×10^{-1}
+ SKA1 ($N_{\text{field}} = 8$)	7.00×10^{-4}	1.03×10^{-4}	3.98×10^{-3}	3.40×10^{-3}	1.98×10^{-1}
+ SKA2 ($N_{\text{field}} = 4$)	5.65×10^{-4}	9.88×10^{-5}	2.68×10^{-3}	2.50×10^{-3}	1.88×10^{-1}
+ SKA2 ($N_{\text{field}} = 8$)	4.09×10^{-4}	9.38×10^{-5}	2.10×10^{-3}	2.03×10^{-3}	1.81×10^{-1}
Planck + SA(0.65) + BAO + H_0	2.39×10^{-3}	8.90×10^{-5}	6.66×10^{-3}	3.22×10^{-3}	2.11×10^{-1}
+ SKA1 ($N_{\text{field}} = 4$)	8.86×10^{-4}	8.70×10^{-5}	4.17×10^{-3}	3.07×10^{-3}	1.91×10^{-1}
+ SKA1 ($N_{\text{field}} = 8$)	6.82×10^{-4}	8.53×10^{-5}	3.85×10^{-3}	2.94×10^{-3}	1.89×10^{-1}
+ SKA2 ($N_{\text{field}} = 4$)	5.57×10^{-4}	8.30×10^{-5}	2.63×10^{-3}	2.27×10^{-3}	1.78×10^{-1}
+ SKA2 ($N_{\text{field}} = 8$)	4.04×10^{-4}	8.00×10^{-5}	2.07×10^{-3}	1.87×10^{-3}	1.69×10^{-1}
	$\sigma(\tau)$	$\sigma(Y_p)$	$\sigma(\Sigma m_\nu)$	$\sigma(N_\nu)$	
Planck + PB-2(0.65) + BAO + H_0	4.55×10^{-3}	8.97×10^{-3}	6.63×10^{-2}	1.24×10^{-1}	
+ SKA1 ($N_{\text{field}} = 4$)	4.58×10^{-3}	7.11×10^{-3}	4.03×10^{-2}	4.09×10^{-2}	
+ SKA1 ($N_{\text{field}} = 8$)	4.54×10^{-3}	6.83×10^{-3}	3.82×10^{-2}	3.27×10^{-2}	
+ SKA2 ($N_{\text{field}} = 4$)	4.33×10^{-3}	6.18×10^{-3}	3.11×10^{-2}	3.24×10^{-2}	
+ SKA2 ($N_{\text{field}} = 8$)	4.17×10^{-3}	5.73×10^{-3}	2.71×10^{-2}	2.69×10^{-2}	
Planck + SA(0.65) + BAO + H_0	4.39×10^{-3}	7.21×10^{-3}	5.22×10^{-2}	9.98×10^{-2}	
+ SKA1 ($N_{\text{field}} = 4$)	4.41×10^{-3}	5.95×10^{-3}	3.27×10^{-2}	3.82×10^{-2}	
+ SKA1 ($N_{\text{field}} = 8$)	4.38×10^{-3}	5.75×10^{-3}	3.06×10^{-2}	3.03×10^{-2}	
+ SKA2 ($N_{\text{field}} = 4$)	4.16×10^{-3}	5.33×10^{-3}	2.47×10^{-2}	3.01×10^{-2}	
+ SKA2 ($N_{\text{field}} = 8$)	3.98×10^{-3}	4.98×10^{-3}	2.17×10^{-2}	2.46×10^{-2}	

Table 20: $f_{\text{sky}} = 0.65$, $\Sigma m_\nu = 0.1$ eV, with the residual foregrounds of CMB, without those of 21 cm line.

	$\sigma(\Omega_m h^2)$	$\sigma(\Omega_b h^2)$	$\sigma(\Omega_\Lambda)$	$\sigma(n_s)$	$\sigma(A_s \times 10^{10})$
Planck + PB-2(0.65) + BAO + H_0	2.98×10^{-3}	1.09×10^{-4}	8.09×10^{-3}	3.81×10^{-3}	2.23×10^{-1}
+ SKA1 ($N_{\text{field}} = 4$)	9.21×10^{-4}	1.06×10^{-4}	4.35×10^{-3}	3.58×10^{-3}	2.00×10^{-1}
+ SKA1 ($N_{\text{field}} = 8$)	7.05×10^{-4}	1.03×10^{-4}	3.99×10^{-3}	3.39×10^{-3}	1.97×10^{-1}
+ SKA2 ($N_{\text{field}} = 4$)	5.68×10^{-4}	9.87×10^{-5}	2.66×10^{-3}	2.49×10^{-3}	1.87×10^{-1}
+ SKA2 ($N_{\text{field}} = 8$)	4.11×10^{-4}	9.37×10^{-5}	2.08×10^{-3}	2.01×10^{-3}	1.80×10^{-1}
Planck + SA(0.65) + BAO + H_0	2.42×10^{-3}	8.89×10^{-5}	6.73×10^{-3}	3.22×10^{-3}	2.11×10^{-1}
+ SKA1 ($N_{\text{field}} = 4$)	8.92×10^{-4}	8.69×10^{-5}	4.19×10^{-3}	3.06×10^{-3}	1.91×10^{-1}
+ SKA1 ($N_{\text{field}} = 8$)	6.87×10^{-4}	8.53×10^{-5}	3.85×10^{-3}	2.93×10^{-3}	1.88×10^{-1}
+ SKA2 ($N_{\text{field}} = 4$)	5.59×10^{-4}	8.30×10^{-5}	2.62×10^{-3}	2.26×10^{-3}	1.77×10^{-1}
+ SKA2 ($N_{\text{field}} = 8$)	4.05×10^{-4}	8.00×10^{-5}	2.06×10^{-3}	1.86×10^{-3}	1.69×10^{-1}
	$\sigma(\tau)$	$\sigma(Y_p)$	$\sigma(\Sigma m_\nu)$	$\sigma(N_\nu)$	
Planck + PB-2(0.65) + BAO + H_0	4.53×10^{-3}	8.97×10^{-3}	6.77×10^{-2}	1.24×10^{-1}	
+ SKA1 ($N_{\text{field}} = 4$)	4.55×10^{-3}	7.11×10^{-3}	4.11×10^{-2}	4.09×10^{-2}	
+ SKA1 ($N_{\text{field}} = 8$)	4.51×10^{-3}	6.82×10^{-3}	3.88×10^{-2}	3.27×10^{-2}	
+ SKA2 ($N_{\text{field}} = 4$)	4.30×10^{-3}	6.16×10^{-3}	3.13×10^{-2}	3.24×10^{-2}	
+ SKA2 ($N_{\text{field}} = 8$)	4.14×10^{-3}	5.72×10^{-3}	2.71×10^{-2}	2.69×10^{-2}	
Planck + SA(0.65) + BAO + H_0	4.37×10^{-3}	7.20×10^{-3}	5.30×10^{-2}	1.00×10^{-1}	
+ SKA1 ($N_{\text{field}} = 4$)	4.38×10^{-3}	5.94×10^{-3}	3.31×10^{-2}	3.82×10^{-2}	
+ SKA1 ($N_{\text{field}} = 8$)	4.35×10^{-3}	5.74×10^{-3}	3.11×10^{-2}	3.03×10^{-2}	
+ SKA2 ($N_{\text{field}} = 4$)	4.13×10^{-3}	5.31×10^{-3}	2.49×10^{-2}	3.01×10^{-2}	
+ SKA2 ($N_{\text{field}} = 8$)	3.94×10^{-3}	4.96×10^{-3}	2.18×10^{-2}	2.46×10^{-2}	

Table 21: $f_{\text{sky}} = 0.65$, $\Sigma m_\nu = 0.06$ eV, with the residual foregrounds of CMB, without those of 21 cm line.

	$\sigma(\Omega_m h^2)$	$\sigma(\Omega_b h^2)$	$\sigma(\Omega_\Lambda)$	$\sigma(n_s)$	$\sigma(A_s \times 10^{10})$
Planck	5.37×10^{-3}	2.49×10^{-4}	2.43×10^{-2}	8.82×10^{-3}	2.86×10^{-1}
+ PB-2 (0.2)	4.22×10^{-3}	1.75×10^{-4}	1.69×10^{-2}	6.20×10^{-3}	2.51×10^{-1}
+ PB-2 + BAO + H_0	3.41×10^{-3}	1.35×10^{-4}	9.18×10^{-3}	4.60×10^{-3}	2.28×10^{-1}
+ SA (1) (0.2)	4.15×10^{-3}	1.72×10^{-4}	1.65×10^{-2}	6.08×10^{-3}	2.49×10^{-1}
+ SA (2) (0.2)	3.30×10^{-3}	1.43×10^{-4}	1.31×10^{-2}	5.08×10^{-3}	2.29×10^{-1}
+ SA (1) + BAO + H_0	3.37×10^{-3}	1.33×10^{-4}	9.07×10^{-3}	4.53×10^{-3}	2.27×10^{-1}
+ SA (2) + BAO + H_0	2.86×10^{-3}	1.14×10^{-4}	7.82×10^{-3}	3.96×10^{-3}	2.19×10^{-1}
	$\sigma(\tau)$	$\sigma(Y_p)$	$\sigma(\Sigma m_\nu)$	$\sigma(N_\nu)$	
Planck	4.84×10^{-3}	1.71×10^{-2}	1.52×10^{-1}	3.03×10^{-1}	
+ PB-2 (0.2)	4.58×10^{-3}	1.28×10^{-2}	1.06×10^{-1}	2.32×10^{-1}	
+ PB-2 + BAO + H_0	4.57×10^{-3}	1.11×10^{-2}	7.75×10^{-2}	1.44×10^{-1}	
+ SA (1) (0.2)	4.57×10^{-3}	1.26×10^{-2}	1.03×10^{-1}	2.28×10^{-1}	
+ SA (2) (0.2)	4.49×10^{-3}	1.01×10^{-2}	7.57×10^{-2}	1.75×10^{-1}	
+ SA (1) + BAO + H_0	4.57×10^{-3}	1.09×10^{-2}	7.60×10^{-2}	1.42×10^{-1}	
+ SA (2) + BAO + H_0	4.49×10^{-3}	9.11×10^{-3}	6.08×10^{-2}	1.18×10^{-1}	

Table 22: $f_{\text{sky}} = 0.2$, $\Sigma m_\nu = 0.1$ eV, with the residual foregrounds. SA (1) and SA (2) mean that the 220GHz band is used for CMB observation or foreground removal, respectively (see Fig.9).

	$\sigma(\Omega_m h^2)$	$\sigma(\Omega_b h^2)$	$\sigma(\Omega_\Lambda)$	$\sigma(n_s)$	$\sigma(A_s \times 10^{10})$
Planck	5.42×10^{-3}	2.50×10^{-4}	2.46×10^{-2}	8.82×10^{-3}	2.86×10^{-1}
+ PB-2 (0.2)	4.26×10^{-3}	1.75×10^{-4}	1.70×10^{-2}	6.19×10^{-3}	2.51×10^{-1}
+ PB-2 + BAO + H_0	3.45×10^{-3}	1.35×10^{-4}	9.29×10^{-3}	4.60×10^{-3}	2.28×10^{-1}
+ SA (1) (0.2)	4.19×10^{-3}	1.72×10^{-4}	1.66×10^{-2}	6.07×10^{-3}	2.49×10^{-1}
+ SA (2) (0.2)	3.35×10^{-3}	1.43×10^{-4}	1.31×10^{-2}	5.08×10^{-3}	2.30×10^{-1}
+ SA (1) + BAO + H_0	3.41×10^{-3}	1.33×10^{-4}	9.18×10^{-3}	4.53×10^{-3}	2.27×10^{-1}
+ SA (2) + BAO + H_0	2.90×10^{-3}	1.14×10^{-4}	7.91×10^{-3}	3.95×10^{-3}	2.19×10^{-1}
	$\sigma(\tau)$	$\sigma(Y_p)$	$\sigma(\Sigma m_\nu)$	$\sigma(N_\nu)$	
Planck	4.82×10^{-3}	1.72×10^{-2}	1.56×10^{-1}	3.03×10^{-1}	
+ PB-2 (0.2)	4.55×10^{-3}	1.28×10^{-2}	1.08×10^{-1}	2.33×10^{-1}	
+ PB-2 + BAO + H_0	4.55×10^{-3}	1.11×10^{-2}	7.91×10^{-2}	1.45×10^{-1}	
+ SA (1) (0.2)	4.55×10^{-3}	1.26×10^{-2}	1.05×10^{-1}	2.29×10^{-1}	
+ SA (2) (0.2)	4.47×10^{-3}	1.01×10^{-2}	7.64×10^{-2}	1.77×10^{-1}	
+ SA (1) + BAO + H_0	4.54×10^{-3}	1.09×10^{-2}	7.75×10^{-2}	1.42×10^{-1}	
+ SA (2) + BAO + H_0	4.47×10^{-3}	9.10×10^{-3}	6.14×10^{-2}	1.19×10^{-1}	

Table 23: $f_{\text{sky}} = 0.2$, $\Sigma m_\nu = 0.06$ eV, with the residual foregrounds.

by the combinations of them, we will be able to determine the neutrino mass hierarchy to be inverted or normal for $\Sigma m_\nu \sim 0.06$ eV or $\Sigma m_\nu \sim 0.1$ eV at 95 % C.L., respectively. In particular, the detectability becomes larger as the sky coverage of Simons Array and the number of observed field of SKA become larger. This improvement on the observed field of SKA is more effective than that of the large integrated time per one field. Those results should be reasonable because a precise discrimination of the mass hierarchy itself may have no meaning if the masses are highly degenerate, i.e., if 0.1 eV $\ll \Sigma m_\nu$.

Once a clear signature $\Sigma m_\nu \ll 0.1$ eV were determined by observations or experiments, it should be obvious that the hierarchy must be normal without any ambiguities. On the other hand, if the hierarchy were inverted, we could not determine it by using information of only Σm_ν . However, it is remarkable that our method is quite useful because we can discriminate the hierarchy from the other even if the fiducial values were $\Sigma m_\nu \gtrsim 0.1$ eV for both the normal and inverted cases. This is clearly shown in these figures. In case that a fiducial value of Σm_ν is taken to be the lowest values in neutrino oscillation experiments, these figures indicate that by Planck + Simons Array + BAO + SKA phase 2, we can discriminate the inverted (normal) mass hierarchy from the normal (inverted) one. By using Omniscope, we can discriminate any mass hierarchies up to $\Sigma m_\nu \sim 0.1$ eV [52].

6 Conclusions

In this paper, we have studied how well we can constrain the total neutrino mass Σm_ν , the effective number of neutrino species N_ν and the neutrino mass hierarchy by using 21 cm line (SKA) and CMB (Planck + POLARBEAR-2 or Simons Array) observations. It is essential to combine the 21 cm line observation with the precise CMB polarization observation to break various degeneracies in cosmological parameters when we perform multiple-parameter fittings.

About the constraints on the Σm_ν - N_ν plane, we have found that there is a significant improvement in the sensitivity to Σm_ν and N_ν by adding the information of BAO observation to that of CMB. However, for a fiducial value $\Sigma m_\nu = 0.1$ eV, it is impossible to detect the nonzero neutrino mass at 2σ level even by using the combination of Simons Array and DESI. On the other hand, by adding the information of 21 cm observation (SKA) to that of CMB, we have found that there is a substantial improvement. By using Planck + Simons Array + BAO (DESI) + SKA phase 1, we can detect the nonzero neutrino mass if the value satisfies $\Sigma m_\nu \geq 0.1$ eV (but it is necessary to remove foregrounds with high degree of accuracy). For a fiducial value $\Sigma m_\nu = 0.06$ eV, which corresponds to the lowest value in the normal hierarchy of the neutrino total mass, we need the sensitivity of SKA phase 2 with relatively large sky coverage and very strong foreground removal in order to detect the nonzero neutrino mass at 2σ level.

As for the determination of the neutrino mass hierarchy, we have used the parameter $r_\nu = (m_3 - m_1)/\Sigma m_\nu$, and studied how to discriminate a true mass hierarchy from the other by constraining r_ν . As was clearly shown in Fig. 10-13, by adopting the combination

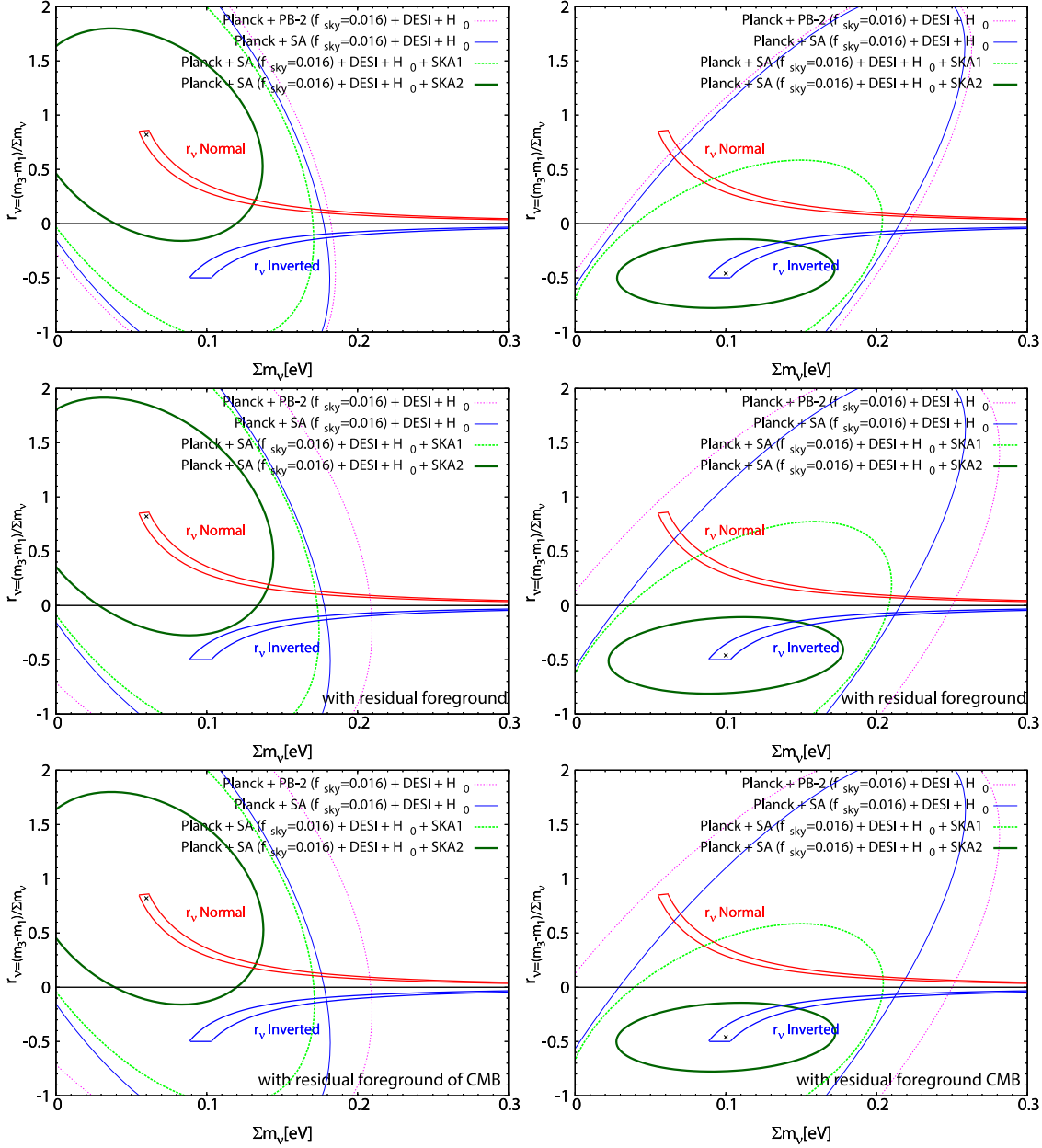


Figure 10: Contours of 95% C.L. forecasts in Σm_ν - r_ν plane. We plot the cases of Planck + BAO(DESI) + Hubble prior combined with POLARBEAR-2 (PB-2) ($f_{\text{sky}} = 0.016$) (dotted line) or Simons Array (SA) ($f_{\text{sky}} = 0.016$) (outer thin solid line), Planck + BAO(DESI) + Hubble prior + Simons Array combined with SKA phase 1 ($N_{\text{field}} = 4$) (inner thick dashed line) or phase 2 ($N_{\text{field}} = 4$) (inner thick solid line), respectively. Allowed parameters on r_ν by neutrino oscillation experiments are also plotted as two bands for the inverted and the normal hierarchies, respectively (the name of each hierarchy is written in the close vicinity of the line). The lowest two panels are forecasts when the foreground of 21 cm line is completely removed (i.e. only the residual foreground of CMB exists).

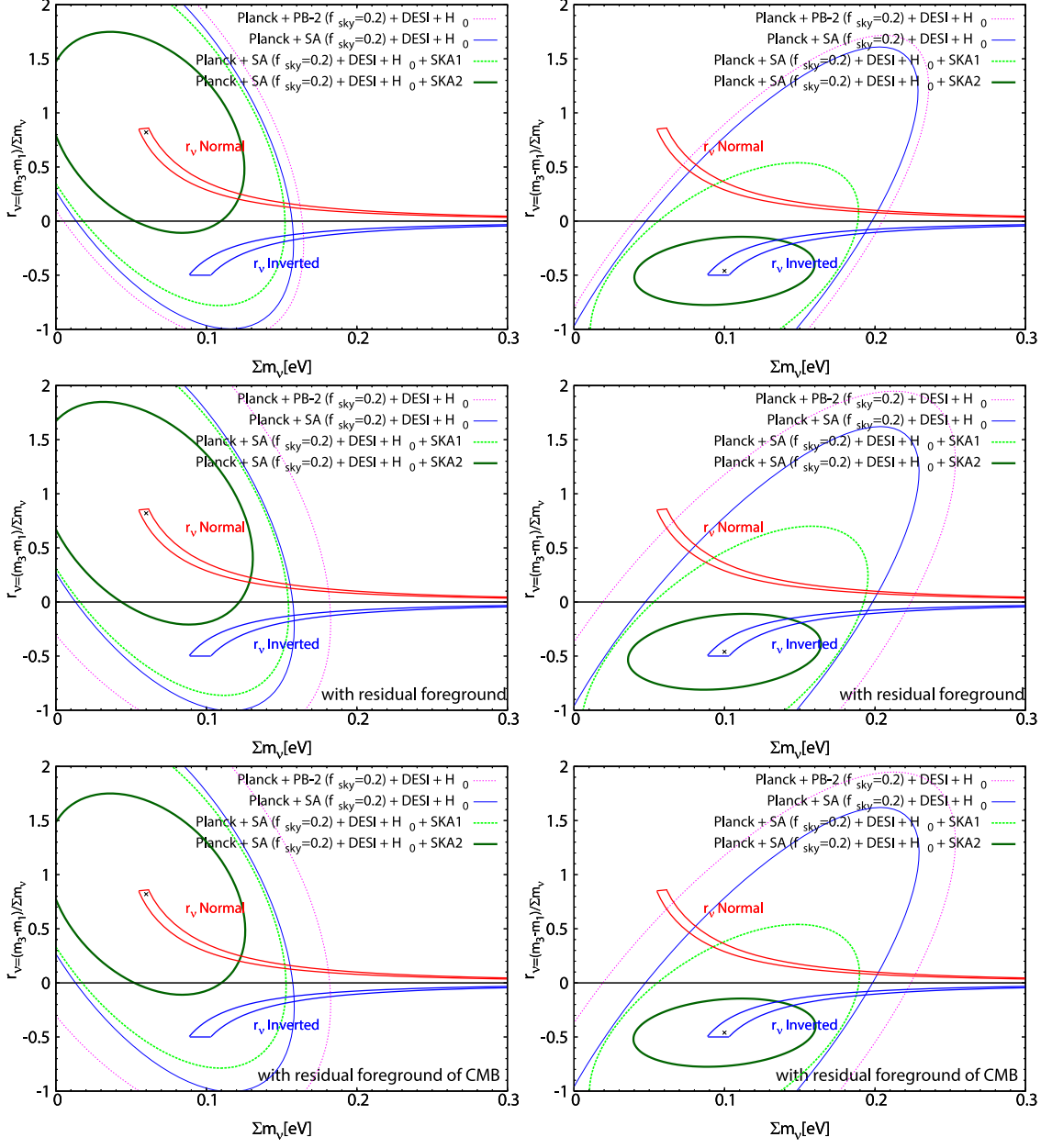


Figure 11: Same as Fig.10, but the sky coverages of POLARBEAR-2 and Simons Array are $f_{\text{sky}} = 0.2$.

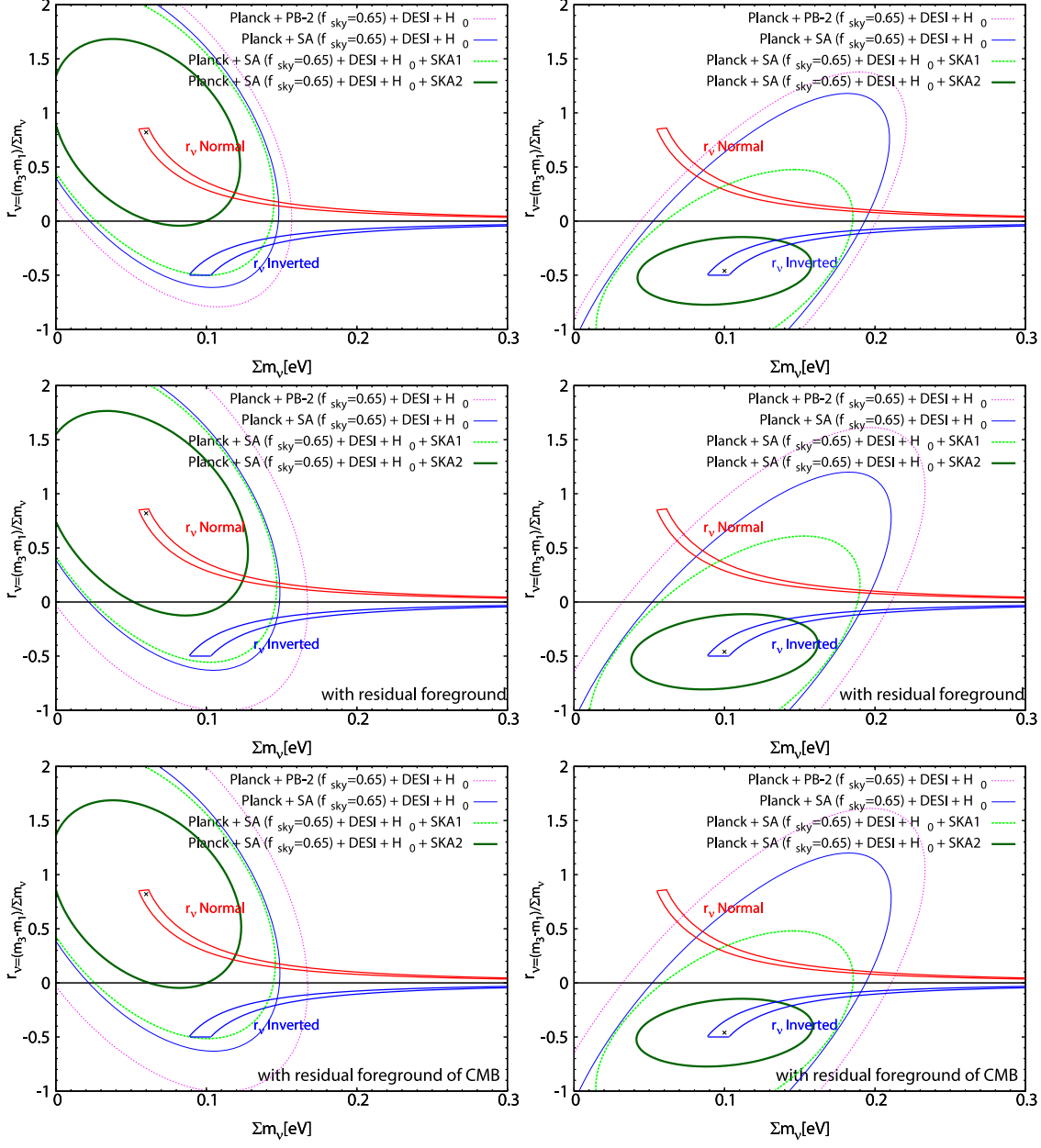


Figure 12: Same as Fig.10, but the sky coverages of POLARBEAR-2 and Simons Array are $f_{\text{sky}} = 0.65$.

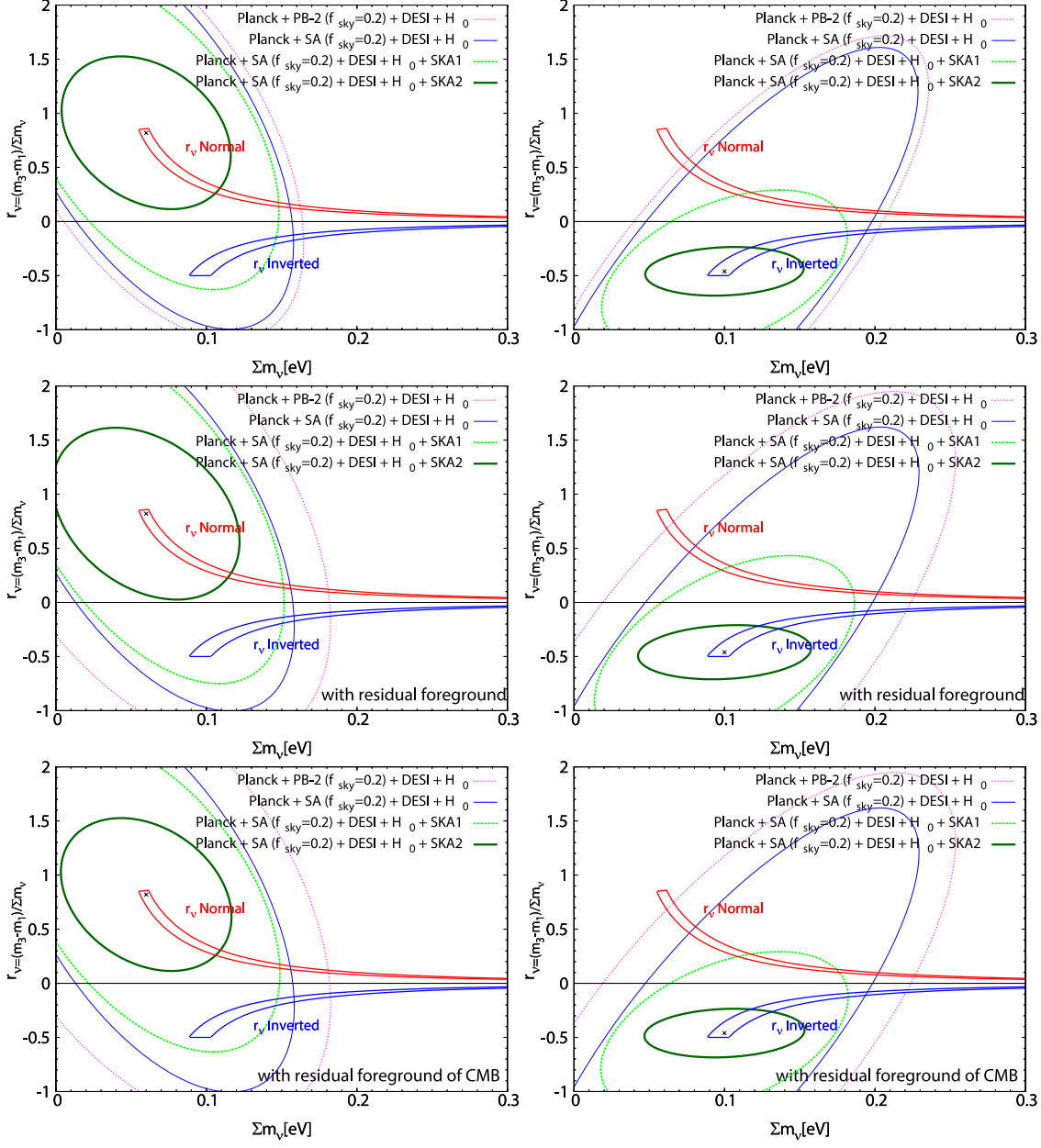


Figure 13: Same as Fig.11, but the observed fields of SKA are twice as large as that of Fig.11 (i.e. $N_{\text{field}} = 8$).

	$\sigma(\Omega_m h^2)$	$\sigma(\Omega_b h^2)$	$\sigma(\Omega_\Lambda)$	$\sigma(n_s)$	$\sigma(A_s \times 10^{10})$
Planck + PB-2(0.016) + BAO + H_0	7.90×10^{-4}	1.52×10^{-4}	4.68×10^{-3}	5.35×10^{-3}	2.12×10^{-1}
+ SKA1 ($N_{\text{field}} = 4$)	6.71×10^{-4}	1.32×10^{-4}	4.32×10^{-3}	4.69×10^{-3}	2.07×10^{-1}
+ SKA1 ($N_{\text{field}} = 8$)	6.02×10^{-4}	1.20×10^{-4}	4.06×10^{-3}	4.27×10^{-3}	2.03×10^{-1}
+ SKA2 ($N_{\text{field}} = 4$)	4.28×10^{-4}	1.12×10^{-4}	2.68×10^{-3}	2.75×10^{-3}	1.91×10^{-1}
+ SKA2 ($N_{\text{field}} = 8$)	3.36×10^{-4}	9.59×10^{-5}	2.09×10^{-3}	2.13×10^{-3}	1.84×10^{-1}
Planck + SA(0.016) + BAO + H_0	7.76×10^{-4}	1.51×10^{-4}	4.66×10^{-3}	5.21×10^{-3}	2.11×10^{-1}
+ SKA1 ($N_{\text{field}} = 4$)	6.65×10^{-4}	1.30×10^{-4}	4.31×10^{-3}	4.58×10^{-3}	2.06×10^{-1}
+ SKA1 ($N_{\text{field}} = 8$)	5.98×10^{-4}	1.18×10^{-4}	4.05×10^{-3}	4.18×10^{-3}	2.02×10^{-1}
+ SKA2 ($N_{\text{field}} = 4$)	4.26×10^{-4}	1.10×10^{-4}	2.68×10^{-3}	2.72×10^{-3}	1.90×10^{-1}
+ SKA2 ($N_{\text{field}} = 8$)	3.34×10^{-4}	9.44×10^{-5}	2.09×10^{-3}	2.11×10^{-3}	1.82×10^{-1}
	$\sigma(\tau)$	$\sigma(Y_p)$	$\sigma(\Sigma m_\nu)$	$\sigma(r_\nu)$	
Planck + PB-2(0.016) + BAO + H_0	4.66×10^{-3}	9.46×10^{-3}	5.06×10^{-2}	9.34×10^{-1}	
+ SKA1 ($N_{\text{field}} = 4$)	4.58×10^{-3}	8.04×10^{-3}	4.66×10^{-2}	7.72×10^{-1}	
+ SKA1 ($N_{\text{field}} = 8$)	4.52×10^{-3}	7.27×10^{-3}	4.41×10^{-2}	6.74×10^{-1}	
+ SKA2 ($N_{\text{field}} = 4$)	4.31×10^{-3}	5.66×10^{-3}	3.27×10^{-2}	3.96×10^{-1}	
+ SKA2 ($N_{\text{field}} = 8$)	4.16×10^{-3}	4.86×10^{-3}	2.77×10^{-2}	2.94×10^{-1}	
Planck + SA(0.016) + BAO + H_0	4.65×10^{-3}	8.99×10^{-3}	4.88×10^{-2}	9.26×10^{-1}	
+ SKA1 ($N_{\text{field}} = 4$)	4.58×10^{-3}	7.68×10^{-3}	4.48×10^{-2}	7.68×10^{-1}	
+ SKA1 ($N_{\text{field}} = 8$)	4.52×10^{-3}	6.94×10^{-3}	4.23×10^{-2}	6.71×10^{-1}	
+ SKA2 ($N_{\text{field}} = 4$)	4.29×10^{-3}	5.48×10^{-3}	3.11×10^{-2}	3.95×10^{-1}	
+ SKA2 ($N_{\text{field}} = 8$)	4.12×10^{-3}	4.69×10^{-3}	2.64×10^{-2}	2.94×10^{-1}	

Table 24: $f_{\text{sky}} = 0.016$, normal hierarchy, without the residual foregrounds.

	$\sigma(\Omega_m h^2)$	$\sigma(\Omega_b h^2)$	$\sigma(\Omega_\Lambda)$	$\sigma(n_s)$	$\sigma(A_s \times 10^{10})$
Planck + PB-2(0.016) + BAO + H_0	8.64×10^{-4}	1.52×10^{-4}	4.77×10^{-3}	5.36×10^{-3}	2.12×10^{-1}
+ SKA1 ($N_{\text{field}} = 4$)	6.59×10^{-4}	1.32×10^{-4}	4.28×10^{-3}	4.69×10^{-3}	2.07×10^{-1}
+ SKA1 ($N_{\text{field}} = 8$)	5.83×10^{-4}	1.19×10^{-4}	4.02×10^{-3}	4.28×10^{-3}	2.04×10^{-1}
+ SKA2 ($N_{\text{field}} = 4$)	4.22×10^{-4}	1.12×10^{-4}	2.68×10^{-3}	2.79×10^{-3}	1.92×10^{-1}
+ SKA2 ($N_{\text{field}} = 8$)	3.31×10^{-4}	9.59×10^{-5}	2.10×10^{-3}	2.17×10^{-3}	1.85×10^{-1}
Planck + SA(0.016) + BAO + H_0	8.51×10^{-4}	1.51×10^{-4}	4.75×10^{-3}	5.22×10^{-3}	2.11×10^{-1}
+ SKA1 ($N_{\text{field}} = 4$)	6.54×10^{-4}	1.30×10^{-4}	4.27×10^{-3}	4.58×10^{-3}	2.06×10^{-1}
+ SKA1 ($N_{\text{field}} = 8$)	5.80×10^{-4}	1.17×10^{-4}	4.00×10^{-3}	4.18×10^{-3}	2.03×10^{-1}
+ SKA2 ($N_{\text{field}} = 4$)	4.20×10^{-4}	1.10×10^{-4}	2.68×10^{-3}	2.75×10^{-3}	1.91×10^{-1}
+ SKA2 ($N_{\text{field}} = 8$)	3.29×10^{-4}	9.42×10^{-5}	2.10×10^{-3}	2.14×10^{-3}	1.83×10^{-1}
	$\sigma(\tau)$	$\sigma(Y_p)$	$\sigma(\Sigma m_\nu)$	$\sigma(r_\nu)$	
Planck + PB-2(0.016) + BAO + H_0	4.66×10^{-3}	9.46×10^{-3}	6.54×10^{-2}	1.06	
+ SKA1 ($N_{\text{field}} = 4$)	4.58×10^{-3}	8.05×10^{-3}	4.40×10^{-2}	4.22×10^{-1}	
+ SKA1 ($N_{\text{field}} = 8$)	4.53×10^{-3}	7.28×10^{-3}	4.08×10^{-2}	3.11×10^{-1}	
+ SKA2 ($N_{\text{field}} = 4$)	4.32×10^{-3}	5.69×10^{-3}	3.10×10^{-2}	1.28×10^{-1}	
+ SKA2 ($N_{\text{field}} = 8$)	4.17×10^{-3}	4.89×10^{-3}	2.68×10^{-2}	9.09×10^{-2}	
Planck + SA(0.016) + BAO + H_0	4.65×10^{-3}	8.99×10^{-3}	6.37×10^{-2}	1.05	
+ SKA1 ($N_{\text{field}} = 4$)	4.58×10^{-3}	7.68×10^{-3}	4.18×10^{-2}	4.22×10^{-1}	
+ SKA1 ($N_{\text{field}} = 8$)	4.52×10^{-3}	6.95×10^{-3}	3.86×10^{-2}	3.11×10^{-1}	
+ SKA2 ($N_{\text{field}} = 4$)	4.31×10^{-3}	5.51×10^{-3}	2.91×10^{-2}	1.28×10^{-1}	
+ SKA2 ($N_{\text{field}} = 8$)	4.14×10^{-3}	4.72×10^{-3}	2.53×10^{-2}	9.09×10^{-2}	

Table 25: $f_{\text{sky}} = 0.016$, inverted hierarchy, without the residual foregrounds.

	$\sigma(\Omega_m h^2)$	$\sigma(\Omega_b h^2)$	$\sigma(\Omega_\Lambda)$	$\sigma(n_s)$	$\sigma(A_s \times 10^{10})$
Planck + PB-2(0.016) + BAO + H_0	8.28×10^{-4}	1.65×10^{-4}	4.72×10^{-3}	5.74×10^{-3}	2.12×10^{-1}
+ SKA1 ($N_{\text{field}} = 4$)	7.41×10^{-4}	1.54×10^{-4}	4.47×10^{-3}	5.33×10^{-3}	2.08×10^{-1}
+ SKA1 ($N_{\text{field}} = 8$)	6.81×10^{-4}	1.46×10^{-4}	4.28×10^{-3}	5.01×10^{-3}	2.06×10^{-1}
+ SKA2 ($N_{\text{field}} = 4$)	5.13×10^{-4}	1.34×10^{-4}	3.01×10^{-3}	3.38×10^{-3}	1.96×10^{-1}
+ SKA2 ($N_{\text{field}} = 8$)	4.15×10^{-4}	1.20×10^{-4}	2.41×10^{-3}	2.67×10^{-3}	1.91×10^{-1}
Planck + SA(0.016) + BAO + H_0	7.78×10^{-4}	1.51×10^{-4}	4.67×10^{-3}	5.22×10^{-3}	2.08×10^{-1}
+ SKA1 ($N_{\text{field}} = 4$)	7.12×10^{-4}	1.40×10^{-4}	4.44×10^{-3}	4.85×10^{-3}	2.05×10^{-1}
+ SKA1 ($N_{\text{field}} = 8$)	6.61×10^{-4}	1.32×10^{-4}	4.24×10^{-3}	4.56×10^{-3}	2.03×10^{-1}
+ SKA2 ($N_{\text{field}} = 4$)	4.97×10^{-4}	1.23×10^{-4}	3.00×10^{-3}	3.19×10^{-3}	1.92×10^{-1}
+ SKA2 ($N_{\text{field}} = 8$)	4.04×10^{-4}	1.11×10^{-4}	2.39×10^{-3}	2.53×10^{-3}	1.85×10^{-1}
	$\sigma(\tau)$	$\sigma(Y_p)$	$\sigma(\Sigma m_\nu)$	$\sigma(r_\nu)$	
Planck + PB-2(0.016) + BAO + H_0	4.59×10^{-3}	1.02×10^{-2}	6.03×10^{-2}	9.58×10^{-1}	
+ SKA1 ($N_{\text{field}} = 4$)	4.55×10^{-3}	9.27×10^{-3}	5.75×10^{-2}	8.42×10^{-1}	
+ SKA1 ($N_{\text{field}} = 8$)	4.52×10^{-3}	8.65×10^{-3}	5.53×10^{-2}	7.60×10^{-1}	
+ SKA2 ($N_{\text{field}} = 4$)	4.36×10^{-3}	6.71×10^{-3}	4.37×10^{-2}	4.46×10^{-1}	
+ SKA2 ($N_{\text{field}} = 8$)	4.26×10^{-3}	5.79×10^{-3}	3.74×10^{-2}	3.35×10^{-1}	
Planck + SA(0.016) + BAO + H_0	4.57×10^{-3}	9.05×10^{-3}	4.89×10^{-2}	9.28×10^{-1}	
+ SKA1 ($N_{\text{field}} = 4$)	4.54×10^{-3}	8.28×10^{-3}	4.64×10^{-2}	8.20×10^{-1}	
+ SKA1 ($N_{\text{field}} = 8$)	4.50×10^{-3}	7.73×10^{-3}	4.45×10^{-2}	7.43×10^{-1}	
+ SKA2 ($N_{\text{field}} = 4$)	4.32×10^{-3}	6.25×10^{-3}	3.39×10^{-2}	4.42×10^{-1}	
+ SKA2 ($N_{\text{field}} = 8$)	4.19×10^{-3}	5.40×10^{-3}	2.97×10^{-2}	3.32×10^{-1}	

Table 26: $f_{\text{sky}} = 0.016$, normal hierarchy, with the residual foregrounds.

	$\sigma(\Omega_m h^2)$	$\sigma(\Omega_b h^2)$	$\sigma(\Omega_\Lambda)$	$\sigma(n_s)$	$\sigma(A_s \times 10^{10})$
Planck + PB-2(0.016) + BAO + H_0	9.04×10^{-4}	1.65×10^{-4}	4.80×10^{-3}	5.75×10^{-3}	2.12×10^{-1}
+ SKA1 ($N_{\text{field}} = 4$)	7.35×10^{-4}	1.54×10^{-4}	4.45×10^{-3}	5.34×10^{-3}	2.09×10^{-1}
+ SKA1 ($N_{\text{field}} = 8$)	6.66×10^{-4}	1.46×10^{-4}	4.24×10^{-3}	5.04×10^{-3}	2.06×10^{-1}
+ SKA2 ($N_{\text{field}} = 4$)	5.06×10^{-4}	1.35×10^{-4}	3.02×10^{-3}	3.44×10^{-3}	1.97×10^{-1}
+ SKA2 ($N_{\text{field}} = 8$)	4.10×10^{-4}	1.21×10^{-4}	2.42×10^{-3}	2.73×10^{-3}	1.92×10^{-1}
Planck + SA(0.016) + BAO + H_0	8.53×10^{-4}	1.51×10^{-4}	4.75×10^{-3}	5.23×10^{-3}	2.08×10^{-1}
+ SKA1 ($N_{\text{field}} = 4$)	7.08×10^{-4}	1.39×10^{-4}	4.41×10^{-3}	4.85×10^{-3}	2.05×10^{-1}
+ SKA1 ($N_{\text{field}} = 8$)	6.48×10^{-4}	1.31×10^{-4}	4.21×10^{-3}	4.57×10^{-3}	2.03×10^{-1}
+ SKA2 ($N_{\text{field}} = 4$)	4.90×10^{-4}	1.24×10^{-4}	3.00×10^{-3}	3.23×10^{-3}	1.93×10^{-1}
+ SKA2 ($N_{\text{field}} = 8$)	3.99×10^{-4}	1.11×10^{-4}	2.40×10^{-3}	2.58×10^{-3}	1.86×10^{-1}
	$\sigma(\tau)$	$\sigma(Y_p)$	$\sigma(\Sigma m_\nu)$	$\sigma(r_\nu)$	
Planck + PB-2(0.016) + BAO + H_0	4.59×10^{-3}	1.02×10^{-2}	7.30×10^{-2}	1.09	
+ SKA1 ($N_{\text{field}} = 4$)	4.55×10^{-3}	9.30×10^{-3}	5.62×10^{-2}	5.01×10^{-1}	
+ SKA1 ($N_{\text{field}} = 8$)	4.52×10^{-3}	8.69×10^{-3}	5.30×10^{-2}	3.75×10^{-1}	
+ SKA2 ($N_{\text{field}} = 4$)	4.37×10^{-3}	6.78×10^{-3}	4.26×10^{-2}	1.43×10^{-1}	
+ SKA2 ($N_{\text{field}} = 8$)	4.27×10^{-3}	5.85×10^{-3}	3.72×10^{-2}	1.01×10^{-1}	
Planck + SA(0.016) + BAO + H_0	4.57×10^{-3}	9.05×10^{-3}	6.39×10^{-2}	1.05	
+ SKA1 ($N_{\text{field}} = 4$)	4.54×10^{-3}	8.29×10^{-3}	4.44×10^{-2}	4.97×10^{-1}	
+ SKA1 ($N_{\text{field}} = 8$)	4.51×10^{-3}	7.75×10^{-3}	4.08×10^{-2}	3.73×10^{-1}	
+ SKA2 ($N_{\text{field}} = 4$)	4.34×10^{-3}	6.30×10^{-3}	3.14×10^{-2}	1.42×10^{-1}	
+ SKA2 ($N_{\text{field}} = 8$)	4.21×10^{-3}	5.45×10^{-3}	2.82×10^{-2}	1.01×10^{-1}	

Table 27: $f_{\text{sky}} = 0.016$, inverted hierarchy, with the residual foregrounds.

	$\sigma(\Omega_m h^2)$	$\sigma(\Omega_b h^2)$	$\sigma(\Omega_\Lambda)$	$\sigma(n_s)$	$\sigma(A_s \times 10^{10})$
Planck + PB-2(0.2) + BAO + H_0	7.17×10^{-4}	1.18×10^{-4}	4.56×10^{-3}	4.13×10^{-3}	1.99×10^{-1}
+ SKA1 ($N_{\text{field}} = 4$)	6.31×10^{-4}	1.07×10^{-4}	4.24×10^{-3}	3.78×10^{-3}	1.97×10^{-1}
+ SKA1 ($N_{\text{field}} = 8$)	5.75×10^{-4}	1.00×10^{-4}	3.99×10^{-3}	3.53×10^{-3}	1.95×10^{-1}
+ SKA2 ($N_{\text{field}} = 4$)	4.07×10^{-4}	9.58×10^{-5}	2.66×10^{-3}	2.49×10^{-3}	1.84×10^{-1}
+ SKA2 ($N_{\text{field}} = 8$)	3.20×10^{-4}	8.49×10^{-5}	2.08×10^{-3}	1.98×10^{-3}	1.76×10^{-1}
Planck + SA(0.2) + BAO + H_0	6.96×10^{-4}	1.14×10^{-4}	4.52×10^{-3}	3.94×10^{-3}	1.97×10^{-1}
+ SKA1 ($N_{\text{field}} = 4$)	6.20×10^{-4}	1.04×10^{-4}	4.21×10^{-3}	3.63×10^{-3}	1.95×10^{-1}
+ SKA1 ($N_{\text{field}} = 8$)	5.67×10^{-4}	9.66×10^{-5}	3.96×10^{-3}	3.40×10^{-3}	1.93×10^{-1}
+ SKA2 ($N_{\text{field}} = 4$)	4.02×10^{-4}	9.26×10^{-5}	2.65×10^{-3}	2.43×10^{-3}	1.82×10^{-1}
+ SKA2 ($N_{\text{field}} = 8$)	3.16×10^{-4}	8.20×10^{-5}	2.07×10^{-3}	1.93×10^{-3}	1.73×10^{-1}
	$\sigma(\tau)$	$\sigma(Y_p)$	$\sigma(\Sigma m_\nu)$	$\sigma(r_\nu)$	
Planck + PB-2(0.2) + BAO + H_0	4.55×10^{-3}	7.27×10^{-3}	4.22×10^{-2}	7.70×10^{-1}	
+ SKA1 ($N_{\text{field}} = 4$)	4.48×10^{-3}	6.49×10^{-3}	3.99×10^{-2}	6.72×10^{-1}	
+ SKA1 ($N_{\text{field}} = 8$)	4.43×10^{-3}	6.00×10^{-3}	3.82×10^{-2}	6.04×10^{-1}	
+ SKA2 ($N_{\text{field}} = 4$)	4.22×10^{-3}	4.99×10^{-3}	2.88×10^{-2}	3.80×10^{-1}	
+ SKA2 ($N_{\text{field}} = 8$)	4.04×10^{-3}	4.35×10^{-3}	2.47×10^{-2}	2.87×10^{-1}	
Planck + SA(0.2) + BAO + H_0	4.53×10^{-3}	6.69×10^{-3}	3.95×10^{-2}	7.32×10^{-1}	
+ SKA1 ($N_{\text{field}} = 4$)	4.46×10^{-3}	6.02×10^{-3}	3.73×10^{-2}	6.46×10^{-1}	
+ SKA1 ($N_{\text{field}} = 8$)	4.41×10^{-3}	5.58×10^{-3}	3.56×10^{-2}	5.84×10^{-1}	
+ SKA2 ($N_{\text{field}} = 4$)	4.19×10^{-3}	4.71×10^{-3}	2.63×10^{-2}	3.74×10^{-1}	
+ SKA2 ($N_{\text{field}} = 8$)	3.98×10^{-3}	4.09×10^{-3}	2.26×10^{-2}	2.85×10^{-1}	

Table 28: $f_{\text{sky}} = 0.2$, normal hierarchy, without the residual foregrounds.

	$\sigma(\Omega_m h^2)$	$\sigma(\Omega_b h^2)$	$\sigma(\Omega_\Lambda)$	$\sigma(n_s)$	$\sigma(A_s \times 10^{10})$
Planck + PB-2(0.2) + BAO + H_0	7.68×10^{-4}	1.18×10^{-4}	4.62×10^{-3}	4.14×10^{-3}	1.99×10^{-1}
+ SKA1 ($N_{\text{field}} = 4$)	6.25×10^{-4}	1.07×10^{-4}	4.21×10^{-3}	3.79×10^{-3}	1.97×10^{-1}
+ SKA1 ($N_{\text{field}} = 8$)	5.61×10^{-4}	1.00×10^{-4}	3.95×10^{-3}	3.54×10^{-3}	1.95×10^{-1}
+ SKA2 ($N_{\text{field}} = 4$)	4.01×10^{-4}	9.58×10^{-5}	2.66×10^{-3}	2.52×10^{-3}	1.85×10^{-1}
+ SKA2 ($N_{\text{field}} = 8$)	3.15×10^{-4}	8.48×10^{-5}	2.09×10^{-3}	2.00×10^{-3}	1.77×10^{-1}
Planck + SA(0.2) + BAO + H_0	7.45×10^{-4}	1.14×10^{-4}	4.58×10^{-3}	3.95×10^{-3}	1.97×10^{-1}
+ SKA1 ($N_{\text{field}} = 4$)	6.15×10^{-4}	1.03×10^{-4}	4.18×10^{-3}	3.63×10^{-3}	1.95×10^{-1}
+ SKA1 ($N_{\text{field}} = 8$)	5.55×10^{-4}	9.64×10^{-5}	3.92×10^{-3}	3.41×10^{-3}	1.93×10^{-1}
+ SKA2 ($N_{\text{field}} = 4$)	3.96×10^{-4}	9.25×10^{-5}	2.65×10^{-3}	2.45×10^{-3}	1.83×10^{-1}
+ SKA2 ($N_{\text{field}} = 8$)	3.12×10^{-4}	8.19×10^{-5}	2.08×10^{-3}	1.96×10^{-3}	1.74×10^{-1}
	$\sigma(\tau)$	$\sigma(Y_p)$	$\sigma(\Sigma m_\nu)$	$\sigma(r_\nu)$	
Planck + PB-2(0.2) + BAO + H_0	4.55×10^{-3}	7.27×10^{-3}	5.48×10^{-2}	8.78×10^{-1}	
+ SKA1 ($N_{\text{field}} = 4$)	4.49×10^{-3}	6.50×10^{-3}	3.86×10^{-2}	4.08×10^{-1}	
+ SKA1 ($N_{\text{field}} = 8$)	4.44×10^{-3}	6.01×10^{-3}	3.56×10^{-2}	3.05×10^{-1}	
+ SKA2 ($N_{\text{field}} = 4$)	4.24×10^{-3}	5.02×10^{-3}	2.69×10^{-2}	1.27×10^{-1}	
+ SKA2 ($N_{\text{field}} = 8$)	4.06×10^{-3}	4.37×10^{-3}	2.36×10^{-2}	9.07×10^{-2}	
Planck + SA(0.2) + BAO + H_0	4.53×10^{-3}	6.70×10^{-3}	5.18×10^{-2}	8.34×10^{-1}	
+ SKA1 ($N_{\text{field}} = 4$)	4.47×10^{-3}	6.03×10^{-3}	3.60×10^{-2}	4.03×10^{-1}	
+ SKA1 ($N_{\text{field}} = 8$)	4.42×10^{-3}	5.59×10^{-3}	3.29×10^{-2}	3.03×10^{-1}	
+ SKA2 ($N_{\text{field}} = 4$)	4.21×10^{-3}	4.73×10^{-3}	2.42×10^{-2}	1.27×10^{-1}	
+ SKA2 ($N_{\text{field}} = 8$)	4.01×10^{-3}	4.10×10^{-3}	2.12×10^{-2}	9.06×10^{-2}	

Table 29: $f_{\text{sky}} = 0.2$, inverted hierarchy, without the residual foregrounds.

	$\sigma(\Omega_m h^2)$	$\sigma(\Omega_b h^2)$	$\sigma(\Omega_\Lambda)$	$\sigma(n_s)$	$\sigma(A_s \times 10^{10})$
Planck + PB-2(0.2) + BAO + H_0	7.53×10^{-4}	1.33×10^{-4}	4.61×10^{-3}	4.60×10^{-3}	2.03×10^{-1}
+ SKA1 ($N_{\text{field}} = 4$)	6.92×10^{-4}	1.27×10^{-4}	4.40×10^{-3}	4.36×10^{-3}	2.01×10^{-1}
+ SKA1 ($N_{\text{field}} = 8$)	6.45×10^{-4}	1.22×10^{-4}	4.22×10^{-3}	4.16×10^{-3}	2.00×10^{-1}
+ SKA2 ($N_{\text{field}} = 4$)	4.84×10^{-4}	1.16×10^{-4}	2.99×10^{-3}	3.05×10^{-3}	1.91×10^{-1}
+ SKA2 ($N_{\text{field}} = 8$)	3.93×10^{-4}	1.06×10^{-4}	2.40×10^{-3}	2.47×10^{-3}	1.86×10^{-1}
Planck + SA(0.2) + BAO + H_0	6.98×10^{-4}	1.14×10^{-4}	4.53×10^{-3}	3.96×10^{-3}	1.94×10^{-1}
+ SKA1 ($N_{\text{field}} = 4$)	6.54×10^{-4}	1.09×10^{-4}	4.33×10^{-3}	3.78×10^{-3}	1.93×10^{-1}
+ SKA1 ($N_{\text{field}} = 8$)	6.16×10^{-4}	1.05×10^{-4}	4.15×10^{-3}	3.63×10^{-3}	1.92×10^{-1}
+ SKA2 ($N_{\text{field}} = 4$)	4.62×10^{-4}	1.01×10^{-4}	2.96×10^{-3}	2.79×10^{-3}	1.84×10^{-1}
+ SKA2 ($N_{\text{field}} = 8$)	3.77×10^{-4}	9.37×10^{-5}	2.37×10^{-3}	2.29×10^{-3}	1.77×10^{-1}
	$\sigma(\tau)$	$\sigma(Y_p)$	$\sigma(\Sigma m_\nu)$	$\sigma(r_\nu)$	
Planck + PB-2(0.2) + BAO + H_0	4.55×10^{-3}	8.10×10^{-3}	4.96×10^{-2}	8.54×10^{-1}	
+ SKA1 ($N_{\text{field}} = 4$)	4.52×10^{-3}	7.56×10^{-3}	4.78×10^{-2}	7.69×10^{-1}	
+ SKA1 ($N_{\text{field}} = 8$)	4.49×10^{-3}	7.15×10^{-3}	4.64×10^{-2}	7.05×10^{-1}	
+ SKA2 ($N_{\text{field}} = 4$)	4.33×10^{-3}	5.96×10^{-3}	3.73×10^{-2}	4.34×10^{-1}	
+ SKA2 ($N_{\text{field}} = 8$)	4.21×10^{-3}	5.24×10^{-3}	3.27×10^{-2}	3.29×10^{-1}	
Planck + SA(0.2) + BAO + H_0	4.46×10^{-3}	6.77×10^{-3}	3.97×10^{-2}	7.36×10^{-1}	
+ SKA1 ($N_{\text{field}} = 4$)	4.43×10^{-3}	6.39×10^{-3}	3.82×10^{-2}	6.79×10^{-1}	
+ SKA1 ($N_{\text{field}} = 8$)	4.40×10^{-3}	6.10×10^{-3}	3.70×10^{-2}	6.33×10^{-1}	
+ SKA2 ($N_{\text{field}} = 4$)	4.24×10^{-3}	5.28×10^{-3}	2.86×10^{-2}	4.15×10^{-1}	
+ SKA2 ($N_{\text{field}} = 8$)	4.09×10^{-3}	4.69×10^{-3}	2.50×10^{-2}	3.20×10^{-1}	

Table 30: $f_{\text{sky}} = 0.2$, normal hierarchy, with the residual foregrounds.

	$\sigma(\Omega_m h^2)$	$\sigma(\Omega_b h^2)$	$\sigma(\Omega_\Lambda)$	$\sigma(n_s)$	$\sigma(A_s \times 10^{10})$
Planck + PB-2(0.2) + BAO + H_0	8.15×10^{-4}	1.33×10^{-4}	4.69×10^{-3}	4.61×10^{-3}	2.03×10^{-1}
+ SKA1 ($N_{\text{field}} = 4$)	6.89×10^{-4}	1.27×10^{-4}	4.38×10^{-3}	4.37×10^{-3}	2.01×10^{-1}
+ SKA1 ($N_{\text{field}} = 8$)	6.33×10^{-4}	1.22×10^{-4}	4.19×10^{-3}	4.18×10^{-3}	2.00×10^{-1}
+ SKA2 ($N_{\text{field}} = 4$)	4.77×10^{-4}	1.16×10^{-4}	3.00×10^{-3}	3.09×10^{-3}	1.92×10^{-1}
+ SKA2 ($N_{\text{field}} = 8$)	3.88×10^{-4}	1.06×10^{-4}	2.41×10^{-3}	2.52×10^{-3}	1.87×10^{-1}
Planck + SA(0.2) + BAO + H_0	7.47×10^{-4}	1.14×10^{-4}	4.59×10^{-3}	3.97×10^{-3}	1.95×10^{-1}
+ SKA1 ($N_{\text{field}} = 4$)	6.55×10^{-4}	1.09×10^{-4}	4.31×10^{-3}	3.78×10^{-3}	1.94×10^{-1}
+ SKA1 ($N_{\text{field}} = 8$)	6.09×10^{-4}	1.05×10^{-4}	4.12×10^{-3}	3.64×10^{-3}	1.93×10^{-1}
+ SKA2 ($N_{\text{field}} = 4$)	4.56×10^{-4}	1.01×10^{-4}	2.96×10^{-3}	2.81×10^{-3}	1.85×10^{-1}
+ SKA2 ($N_{\text{field}} = 8$)	3.73×10^{-4}	9.37×10^{-5}	2.38×10^{-3}	2.32×10^{-3}	1.78×10^{-1}
	$\sigma(\tau)$	$\sigma(Y_p)$	$\sigma(\Sigma m_\nu)$	$\sigma(r_\nu)$	
Planck + PB-2(0.2) + BAO + H_0	4.55×10^{-3}	8.11×10^{-3}	6.20×10^{-2}	9.71×10^{-1}	
+ SKA1 ($N_{\text{field}} = 4$)	4.52×10^{-3}	7.57×10^{-3}	4.73×10^{-2}	4.88×10^{-1}	
+ SKA1 ($N_{\text{field}} = 8$)	4.49×10^{-3}	7.18×10^{-3}	4.43×10^{-2}	3.69×10^{-1}	
+ SKA2 ($N_{\text{field}} = 4$)	4.34×10^{-3}	6.00×10^{-3}	3.56×10^{-2}	1.42×10^{-1}	
+ SKA2 ($N_{\text{field}} = 8$)	4.23×10^{-3}	5.28×10^{-3}	3.19×10^{-2}	1.01×10^{-1}	
Planck + SA(0.2) + BAO + H_0	4.47×10^{-3}	6.77×10^{-3}	5.20×10^{-2}	8.39×10^{-1}	
+ SKA1 ($N_{\text{field}} = 4$)	4.43×10^{-3}	6.40×10^{-3}	3.83×10^{-2}	4.68×10^{-1}	
+ SKA1 ($N_{\text{field}} = 8$)	4.41×10^{-3}	6.11×10^{-3}	3.49×10^{-2}	3.60×10^{-1}	
+ SKA2 ($N_{\text{field}} = 4$)	4.26×10^{-3}	5.32×10^{-3}	2.59×10^{-2}	1.41×10^{-1}	
+ SKA2 ($N_{\text{field}} = 8$)	4.12×10^{-3}	4.72×10^{-3}	2.32×10^{-2}	1.01×10^{-1}	

Table 31: $f_{\text{sky}} = 0.2$, inverted hierarchy, with the residual foregrounds.

	$\sigma(\Omega_m h^2)$	$\sigma(\Omega_b h^2)$	$\sigma(\Omega_\Lambda)$	$\sigma(n_s)$	$\sigma(A_s \times 10^{10})$
Planck + PB-2(0.65) + BAO + H_0	6.53×10^{-4}	9.58×10^{-5}	4.40×10^{-3}	3.44×10^{-3}	1.91×10^{-1}
+ SKA1 ($N_{\text{field}} = 4$)	5.91×10^{-4}	9.04×10^{-5}	4.13×10^{-3}	3.23×10^{-3}	1.89×10^{-1}
+ SKA1 ($N_{\text{field}} = 8$)	5.47×10^{-4}	8.61×10^{-5}	3.91×10^{-3}	3.07×10^{-3}	1.88×10^{-1}
+ SKA2 ($N_{\text{field}} = 4$)	3.88×10^{-4}	8.29×10^{-5}	2.64×10^{-3}	2.30×10^{-3}	1.78×10^{-1}
+ SKA2 ($N_{\text{field}} = 8$)	3.08×10^{-4}	7.54×10^{-5}	2.07×10^{-3}	1.87×10^{-3}	1.71×10^{-1}
Planck + SA(0.65) + BAO + H_0	6.30×10^{-4}	8.83×10^{-5}	4.33×10^{-3}	3.20×10^{-3}	1.87×10^{-1}
+ SKA1 ($N_{\text{field}} = 4$)	5.76×10^{-4}	8.37×10^{-5}	4.07×10^{-3}	3.03×10^{-3}	1.86×10^{-1}
+ SKA1 ($N_{\text{field}} = 8$)	5.35×10^{-4}	8.00×10^{-5}	3.85×10^{-3}	2.89×10^{-3}	1.84×10^{-1}
+ SKA2 ($N_{\text{field}} = 4$)	3.81×10^{-4}	7.73×10^{-5}	2.62×10^{-3}	2.21×10^{-3}	1.75×10^{-1}
+ SKA2 ($N_{\text{field}} = 8$)	3.03×10^{-4}	7.08×10^{-5}	2.06×10^{-3}	1.81×10^{-3}	1.66×10^{-1}
	$\sigma(\tau)$	$\sigma(Y_p)$	$\sigma(\Sigma m_\nu)$	$\sigma(r_\nu)$	
Planck + PB-2(0.65) + BAO + H_0	4.43×10^{-3}	5.88×10^{-3}	3.89×10^{-2}	6.50×10^{-1}	
+ SKA1 ($N_{\text{field}} = 4$)	4.37×10^{-3}	5.43×10^{-3}	3.74×10^{-2}	5.88×10^{-1}	
+ SKA1 ($N_{\text{field}} = 8$)	4.33×10^{-3}	5.12×10^{-3}	3.61×10^{-2}	5.41×10^{-1}	
+ SKA2 ($N_{\text{field}} = 4$)	4.13×10^{-3}	4.42×10^{-3}	2.77×10^{-2}	3.62×10^{-1}	
+ SKA2 ($N_{\text{field}} = 8$)	3.95×10^{-3}	3.92×10^{-3}	2.39×10^{-2}	2.79×10^{-1}	
Planck + SA(0.65) + BAO + H_0	4.38×10^{-3}	5.30×10^{-3}	3.55×10^{-2}	5.78×10^{-1}	
+ SKA1 ($N_{\text{field}} = 4$)	4.33×10^{-3}	4.95×10^{-3}	3.42×10^{-2}	5.33×10^{-1}	
+ SKA1 ($N_{\text{field}} = 8$)	4.28×10^{-3}	4.69×10^{-3}	3.31×10^{-2}	4.97×10^{-1}	
+ SKA2 ($N_{\text{field}} = 4$)	4.08×10^{-3}	4.10×10^{-3}	2.52×10^{-2}	3.48×10^{-1}	
+ SKA2 ($N_{\text{field}} = 8$)	3.87×10^{-3}	3.63×10^{-3}	2.18×10^{-2}	2.72×10^{-1}	

Table 32: $f_{\text{sky}} = 0.65$, normal hierarchy, without the residual foregrounds.

	$\sigma(\Omega_m h^2)$	$\sigma(\Omega_b h^2)$	$\sigma(\Omega_\Lambda)$	$\sigma(n_s)$	$\sigma(A_s \times 10^{10})$
Planck + PB-2(0.65) + BAO + H_0	6.94×10^{-4}	9.60×10^{-5}	4.44×10^{-3}	3.44×10^{-3}	1.91×10^{-1}
+ SKA1 ($N_{\text{field}} = 4$)	5.88×10^{-4}	9.04×10^{-5}	4.10×10^{-3}	3.24×10^{-3}	1.89×10^{-1}
+ SKA1 ($N_{\text{field}} = 8$)	5.35×10^{-4}	8.61×10^{-5}	3.88×10^{-3}	3.08×10^{-3}	1.88×10^{-1}
+ SKA2 ($N_{\text{field}} = 4$)	3.82×10^{-4}	8.29×10^{-5}	2.64×10^{-3}	2.32×10^{-3}	1.79×10^{-1}
+ SKA2 ($N_{\text{field}} = 8$)	3.03×10^{-4}	7.54×10^{-5}	2.08×10^{-3}	1.90×10^{-3}	1.72×10^{-1}
Planck + SA(0.65) + BAO + H_0	6.64×10^{-4}	8.84×10^{-5}	4.37×10^{-3}	3.20×10^{-3}	1.88×10^{-1}
+ SKA1 ($N_{\text{field}} = 4$)	5.75×10^{-4}	8.37×10^{-5}	4.04×10^{-3}	3.03×10^{-3}	1.86×10^{-1}
+ SKA1 ($N_{\text{field}} = 8$)	5.27×10^{-4}	8.00×10^{-5}	3.82×10^{-3}	2.90×10^{-3}	1.85×10^{-1}
+ SKA2 ($N_{\text{field}} = 4$)	3.76×10^{-4}	7.73×10^{-5}	2.62×10^{-3}	2.23×10^{-3}	1.76×10^{-1}
+ SKA2 ($N_{\text{field}} = 8$)	2.99×10^{-4}	7.07×10^{-5}	2.06×10^{-3}	1.83×10^{-3}	1.68×10^{-1}
	$\sigma(\tau)$	$\sigma(Y_p)$	$\sigma(\Sigma m_\nu)$	$\sigma(r_\nu)$	
Planck + PB-2(0.65) + BAO + H_0	4.43×10^{-3}	5.88×10^{-3}	4.86×10^{-2}	7.41×10^{-1}	
+ SKA1 ($N_{\text{field}} = 4$)	4.38×10^{-3}	5.44×10^{-3}	3.71×10^{-2}	3.91×10^{-1}	
+ SKA1 ($N_{\text{field}} = 8$)	4.34×10^{-3}	5.13×10^{-3}	3.44×10^{-2}	2.98×10^{-1}	
+ SKA2 ($N_{\text{field}} = 4$)	4.15×10^{-3}	4.45×10^{-3}	2.60×10^{-2}	1.27×10^{-1}	
+ SKA2 ($N_{\text{field}} = 8$)	3.97×10^{-3}	3.94×10^{-3}	2.28×10^{-2}	9.04×10^{-2}	
Planck + SA(0.65) + BAO + H_0	4.39×10^{-3}	5.31×10^{-3}	4.43×10^{-2}	6.61×10^{-1}	
+ SKA1 ($N_{\text{field}} = 4$)	4.33×10^{-3}	4.96×10^{-3}	3.43×10^{-2}	3.78×10^{-1}	
+ SKA1 ($N_{\text{field}} = 8$)	4.29×10^{-3}	4.70×10^{-3}	3.16×10^{-2}	2.92×10^{-1}	
+ SKA2 ($N_{\text{field}} = 4$)	4.10×10^{-3}	4.12×10^{-3}	2.33×10^{-2}	1.26×10^{-1}	
+ SKA2 ($N_{\text{field}} = 8$)	3.90×10^{-3}	3.65×10^{-3}	2.05×10^{-2}	9.02×10^{-2}	

Table 33: $f_{\text{sky}} = 0.65$, inverted hierarchy, without the residual foregrounds.

	$\sigma(\Omega_m h^2)$	$\sigma(\Omega_b h^2)$	$\sigma(\Omega_\Lambda)$	$\sigma(n_s)$	$\sigma(A_s \times 10^{10})$
Planck + PB-2(0.65) + BAO + H_0	6.81×10^{-4}	1.08×10^{-4}	4.47×10^{-3}	3.81×10^{-3}	1.97×10^{-1}
+ SKA1 ($N_{\text{field}} = 4$)	6.39×10^{-4}	1.05×10^{-4}	4.29×10^{-3}	3.66×10^{-3}	1.96×10^{-1}
+ SKA1 ($N_{\text{field}} = 8$)	6.04×10^{-4}	1.02×10^{-4}	4.13×10^{-3}	3.54×10^{-3}	1.95×10^{-1}
+ SKA2 ($N_{\text{field}} = 4$)	4.54×10^{-4}	9.81×10^{-5}	2.96×10^{-3}	2.76×10^{-3}	1.88×10^{-1}
+ SKA2 ($N_{\text{field}} = 8$)	3.72×10^{-4}	9.18×10^{-5}	2.38×10^{-3}	2.29×10^{-3}	1.82×10^{-1}
Planck + SA(0.65) + BAO + H_0	6.32×10^{-4}	8.89×10^{-5}	4.33×10^{-3}	3.22×10^{-3}	1.86×10^{-1}
+ SKA1 ($N_{\text{field}} = 4$)	6.01×10^{-4}	8.67×10^{-5}	4.17×10^{-3}	3.12×10^{-3}	1.85×10^{-1}
+ SKA1 ($N_{\text{field}} = 8$)	5.73×10^{-4}	8.46×10^{-5}	4.02×10^{-3}	3.04×10^{-3}	1.84×10^{-1}
+ SKA2 ($N_{\text{field}} = 4$)	4.32×10^{-4}	8.25×10^{-5}	2.92×10^{-3}	2.48×10^{-3}	1.77×10^{-1}
+ SKA2 ($N_{\text{field}} = 8$)	3.55×10^{-4}	7.81×10^{-5}	2.35×10^{-3}	2.10×10^{-3}	1.71×10^{-1}
	$\sigma(\tau)$	$\sigma(Y_p)$	$\sigma(\Sigma m_\nu)$	$\sigma(r_\nu)$	
Planck + PB-2(0.65) + BAO + H_0	4.52×10^{-3}	6.53×10^{-3}	4.34×10^{-2}	7.37×10^{-1}	
+ SKA1 ($N_{\text{field}} = 4$)	4.49×10^{-3}	6.21×10^{-3}	4.22×10^{-2}	6.80×10^{-1}	
+ SKA1 ($N_{\text{field}} = 8$)	4.47×10^{-3}	5.96×10^{-3}	4.12×10^{-2}	6.34×10^{-1}	
+ SKA2 ($N_{\text{field}} = 4$)	4.32×10^{-3}	5.20×10^{-3}	3.33×10^{-2}	4.16×10^{-1}	
+ SKA2 ($N_{\text{field}} = 8$)	4.19×10^{-3}	4.66×10^{-3}	2.94×10^{-2}	3.21×10^{-1}	
Planck + SA(0.65) + BAO + H_0	4.34×10^{-3}	5.37×10^{-3}	3.58×10^{-2}	5.85×10^{-1}	
+ SKA1 ($N_{\text{field}} = 4$)	4.31×10^{-3}	5.18×10^{-3}	3.49×10^{-2}	5.55×10^{-1}	
+ SKA1 ($N_{\text{field}} = 8$)	4.29×10^{-3}	5.02×10^{-3}	3.41×10^{-2}	5.30×10^{-1}	
+ SKA2 ($N_{\text{field}} = 4$)	4.15×10^{-3}	4.51×10^{-3}	2.72×10^{-2}	3.81×10^{-1}	
+ SKA2 ($N_{\text{field}} = 8$)	4.00×10^{-3}	4.09×10^{-3}	2.40×10^{-2}	3.04×10^{-1}	

Table 34: $f_{\text{sky}} = 0.65$, normal hierarchy, with the residual foregrounds.

	$\sigma(\Omega_m h^2)$	$\sigma(\Omega_b h^2)$	$\sigma(\Omega_\Lambda)$	$\sigma(n_s)$	$\sigma(A_s \times 10^{10})$
Planck + PB-2(0.65) + BAO + H_0	7.32×10^{-4}	1.09×10^{-4}	4.53×10^{-3}	3.81×10^{-3}	1.97×10^{-1}
+ SKA1 ($N_{\text{field}} = 4$)	6.39×10^{-4}	1.05×10^{-4}	4.28×10^{-3}	3.67×10^{-3}	1.96×10^{-1}
+ SKA1 ($N_{\text{field}} = 8$)	5.95×10^{-4}	1.02×10^{-4}	4.10×10^{-3}	3.55×10^{-3}	1.96×10^{-1}
+ SKA2 ($N_{\text{field}} = 4$)	4.47×10^{-4}	9.83×10^{-5}	2.96×10^{-3}	2.79×10^{-3}	1.88×10^{-1}
+ SKA2 ($N_{\text{field}} = 8$)	3.67×10^{-4}	9.20×10^{-5}	2.39×10^{-3}	2.33×10^{-3}	1.83×10^{-1}
Planck + SA(0.65) + BAO + H_0	6.67×10^{-4}	8.90×10^{-5}	4.37×10^{-3}	3.22×10^{-3}	1.86×10^{-1}
+ SKA1 ($N_{\text{field}} = 4$)	6.05×10^{-4}	8.67×10^{-5}	4.16×10^{-3}	3.13×10^{-3}	1.85×10^{-1}
+ SKA1 ($N_{\text{field}} = 8$)	5.69×10^{-4}	8.46×10^{-5}	3.99×10^{-3}	3.04×10^{-3}	1.85×10^{-1}
+ SKA2 ($N_{\text{field}} = 4$)	4.27×10^{-4}	8.25×10^{-5}	2.92×10^{-3}	2.50×10^{-3}	1.78×10^{-1}
+ SKA2 ($N_{\text{field}} = 8$)	3.51×10^{-4}	7.82×10^{-5}	2.36×10^{-3}	2.13×10^{-3}	1.73×10^{-1}
	$\sigma(\tau)$	$\sigma(Y_p)$	$\sigma(\Sigma m_\nu)$	$\sigma(r_\nu)$	
Planck + PB-2(0.65) + BAO + H_0	4.52×10^{-3}	6.53×10^{-3}	5.40×10^{-2}	8.36×10^{-1}	
+ SKA1 ($N_{\text{field}} = 4$)	4.50×10^{-3}	6.23×10^{-3}	4.25×10^{-2}	4.68×10^{-1}	
+ SKA1 ($N_{\text{field}} = 8$)	4.47×10^{-3}	5.98×10^{-3}	3.97×10^{-2}	3.60×10^{-1}	
+ SKA2 ($N_{\text{field}} = 4$)	4.33×10^{-3}	5.23×10^{-3}	3.15×10^{-2}	1.41×10^{-1}	
+ SKA2 ($N_{\text{field}} = 8$)	4.20×10^{-3}	4.69×10^{-3}	2.84×10^{-2}	1.01×10^{-1}	
Planck + SA(0.65) + BAO + H_0	4.35×10^{-3}	5.38×10^{-3}	4.47×10^{-2}	6.69×10^{-1}	
+ SKA1 ($N_{\text{field}} = 4$)	4.32×10^{-3}	5.19×10^{-3}	3.62×10^{-2}	4.31×10^{-1}	
+ SKA1 ($N_{\text{field}} = 8$)	4.30×10^{-3}	5.03×10^{-3}	3.34×10^{-2}	3.43×10^{-1}	
+ SKA2 ($N_{\text{field}} = 4$)	4.17×10^{-3}	4.54×10^{-3}	2.50×10^{-2}	1.40×10^{-1}	
+ SKA2 ($N_{\text{field}} = 8$)	4.03×10^{-3}	4.12×10^{-3}	2.24×10^{-2}	1.00×10^{-1}	

Table 35: $f_{\text{sky}} = 0.65$, inverted hierarchy, with the residual foregrounds.

	$\sigma(\Omega_m h^2)$	$\sigma(\Omega_b h^2)$	$\sigma(\Omega_\Lambda)$	$\sigma(n_s)$	$\sigma(A_s \times 10^{10})$
Planck + PB-2(0.016) + BAO + H_0	8.28×10^{-4}	1.65×10^{-4}	4.72×10^{-3}	5.74×10^{-3}	2.12×10^{-1}
+ SKA1 ($N_{\text{field}} = 4$)	6.84×10^{-4}	1.44×10^{-4}	4.34×10^{-3}	5.04×10^{-3}	2.09×10^{-1}
+ SKA1 ($N_{\text{field}} = 8$)	6.09×10^{-4}	1.31×10^{-4}	4.10×10^{-3}	4.59×10^{-3}	2.06×10^{-1}
+ SKA2 ($N_{\text{field}} = 4$)	4.35×10^{-4}	1.20×10^{-4}	2.69×10^{-3}	2.89×10^{-3}	1.95×10^{-1}
+ SKA2 ($N_{\text{field}} = 8$)	3.41×10^{-4}	1.02×10^{-4}	2.10×10^{-3}	2.22×10^{-3}	1.90×10^{-1}
Planck + SA(0.016) + BAO + H_0	7.78×10^{-4}	1.51×10^{-4}	4.67×10^{-3}	5.22×10^{-3}	2.08×10^{-1}
+ SKA1 ($N_{\text{field}} = 4$)	6.66×10^{-4}	1.30×10^{-4}	4.31×10^{-3}	4.59×10^{-3}	2.05×10^{-1}
+ SKA1 ($N_{\text{field}} = 8$)	5.99×10^{-4}	1.18×10^{-4}	4.05×10^{-3}	4.19×10^{-3}	2.02×10^{-1}
+ SKA2 ($N_{\text{field}} = 4$)	4.26×10^{-4}	1.10×10^{-4}	2.68×10^{-3}	2.73×10^{-3}	1.90×10^{-1}
+ SKA2 ($N_{\text{field}} = 8$)	3.34×10^{-4}	9.46×10^{-5}	2.09×10^{-3}	2.11×10^{-3}	1.82×10^{-1}
	$\sigma(\tau)$	$\sigma(Y_p)$	$\sigma(\Sigma m_\nu)$	$\sigma(r_\nu)$	
Planck + PB-2(0.016) + BAO + H_0	4.59×10^{-3}	1.02×10^{-2}	6.03×10^{-2}	9.58×10^{-1}	
+ SKA1 ($N_{\text{field}} = 4$)	4.59×10^{-3}	8.66×10^{-3}	5.53×10^{-2}	7.87×10^{-1}	
+ SKA1 ($N_{\text{field}} = 8$)	4.53×10^{-3}	7.84×10^{-3}	5.19×10^{-2}	6.85×10^{-1}	
+ SKA2 ($N_{\text{field}} = 4$)	4.36×10^{-3}	5.94×10^{-3}	3.88×10^{-2}	3.99×10^{-1}	
+ SKA2 ($N_{\text{field}} = 8$)	4.26×10^{-3}	5.12×10^{-3}	3.17×10^{-2}	2.96×10^{-1}	
Planck + SA(0.016) + BAO + H_0	4.57×10^{-3}	9.05×10^{-3}	4.89×10^{-2}	9.28×10^{-1}	
+ SKA1 ($N_{\text{field}} = 4$)	4.57×10^{-3}	7.73×10^{-3}	4.50×10^{-2}	7.68×10^{-1}	
+ SKA1 ($N_{\text{field}} = 8$)	4.51×10^{-3}	6.98×10^{-3}	4.25×10^{-2}	6.71×10^{-1}	
+ SKA2 ($N_{\text{field}} = 4$)	4.28×10^{-3}	5.50×10^{-3}	3.12×10^{-2}	3.95×10^{-1}	
+ SKA2 ($N_{\text{field}} = 8$)	4.12×10^{-3}	4.72×10^{-3}	2.66×10^{-2}	2.94×10^{-1}	

Table 36: $f_{\text{sky}} = 0.016$, normal hierarchy, with the residual foregrounds of CMB, without those of 21 cm line.

	$\sigma(\Omega_m h^2)$	$\sigma(\Omega_b h^2)$	$\sigma(\Omega_\Lambda)$	$\sigma(n_s)$	$\sigma(A_s \times 10^{10})$
Planck + PB-2(0.016) + BAO + H_0	9.04×10^{-4}	1.65×10^{-4}	4.80×10^{-3}	5.75×10^{-3}	2.12×10^{-1}
+ SKA1 ($N_{\text{field}} = 4$)	6.71×10^{-4}	1.44×10^{-4}	4.31×10^{-3}	5.06×10^{-3}	2.09×10^{-1}
+ SKA1 ($N_{\text{field}} = 8$)	5.89×10^{-4}	1.31×10^{-4}	4.06×10^{-3}	4.62×10^{-3}	2.06×10^{-1}
+ SKA2 ($N_{\text{field}} = 4$)	4.29×10^{-4}	1.20×10^{-4}	2.70×10^{-3}	2.94×10^{-3}	1.96×10^{-1}
+ SKA2 ($N_{\text{field}} = 8$)	3.36×10^{-4}	1.02×10^{-4}	2.12×10^{-3}	2.26×10^{-3}	1.91×10^{-1}
Planck + SA(0.016) + BAO + H_0	8.53×10^{-4}	1.51×10^{-4}	4.75×10^{-3}	5.23×10^{-3}	2.08×10^{-1}
+ SKA1 ($N_{\text{field}} = 4$)	6.55×10^{-4}	1.30×10^{-4}	4.27×10^{-3}	4.59×10^{-3}	2.06×10^{-1}
+ SKA1 ($N_{\text{field}} = 8$)	5.80×10^{-4}	1.18×10^{-4}	4.01×10^{-3}	4.20×10^{-3}	2.03×10^{-1}
+ SKA2 ($N_{\text{field}} = 4$)	4.20×10^{-4}	1.10×10^{-4}	2.68×10^{-3}	2.76×10^{-3}	1.91×10^{-1}
+ SKA2 ($N_{\text{field}} = 8$)	3.29×10^{-4}	9.44×10^{-5}	2.10×10^{-3}	2.14×10^{-3}	1.83×10^{-1}
	$\sigma(\tau)$	$\sigma(Y_p)$	$\sigma(\Sigma m_\nu)$	$\sigma(r_\nu)$	
Planck + PB-2(0.016) + BAO + H_0	4.59×10^{-3}	1.02×10^{-2}	7.30×10^{-2}	1.09	
+ SKA1 ($N_{\text{field}} = 4$)	4.59×10^{-3}	8.68×10^{-3}	5.34×10^{-2}	4.24×10^{-1}	
+ SKA1 ($N_{\text{field}} = 8$)	4.54×10^{-3}	7.88×10^{-3}	4.97×10^{-2}	3.12×10^{-1}	
+ SKA2 ($N_{\text{field}} = 4$)	4.37×10^{-3}	5.98×10^{-3}	3.80×10^{-2}	1.28×10^{-1}	
+ SKA2 ($N_{\text{field}} = 8$)	4.27×10^{-3}	5.16×10^{-3}	3.15×10^{-2}	9.10×10^{-2}	
Planck + SA(0.016) + BAO + H_0	4.57×10^{-3}	9.05×10^{-3}	6.39×10^{-2}	1.05	
+ SKA1 ($N_{\text{field}} = 4$)	4.57×10^{-3}	7.73×10^{-3}	4.20×10^{-2}	4.22×10^{-1}	
+ SKA1 ($N_{\text{field}} = 8$)	4.51×10^{-3}	6.99×10^{-3}	3.88×10^{-2}	3.11×10^{-1}	
+ SKA2 ($N_{\text{field}} = 4$)	4.30×10^{-3}	5.53×10^{-3}	2.93×10^{-2}	1.28×10^{-1}	
+ SKA2 ($N_{\text{field}} = 8$)	4.14×10^{-3}	4.74×10^{-3}	2.55×10^{-2}	9.09×10^{-2}	

Table 37: $f_{\text{sky}} = 0.016$, inverted hierarchy, with the residual foregrounds of CMB, without those of 21 cm line.

	$\sigma(\Omega_m h^2)$	$\sigma(\Omega_b h^2)$	$\sigma(\Omega_\Lambda)$	$\sigma(n_s)$	$\sigma(A_s \times 10^{10})$
Planck + PB-2(0.2) + BAO + H_0	7.53×10^{-4}	1.33×10^{-4}	4.61×10^{-3}	4.60×10^{-3}	2.03×10^{-1}
+ SKA1 ($N_{\text{field}} = 4$)	6.49×10^{-4}	1.21×10^{-4}	4.28×10^{-3}	4.18×10^{-3}	2.02×10^{-1}
+ SKA1 ($N_{\text{field}} = 8$)	5.86×10^{-4}	1.12×10^{-4}	4.05×10^{-3}	3.89×10^{-3}	2.00×10^{-1}
+ SKA2 ($N_{\text{field}} = 4$)	4.16×10^{-4}	1.05×10^{-4}	2.68×10^{-3}	2.65×10^{-3}	1.90×10^{-1}
+ SKA2 ($N_{\text{field}} = 8$)	3.27×10^{-4}	9.21×10^{-5}	2.09×10^{-3}	2.09×10^{-3}	1.85×10^{-1}
Planck + SA(0.2) + BAO + H_0	6.98×10^{-4}	1.14×10^{-4}	4.53×10^{-3}	3.96×10^{-3}	1.94×10^{-1}
+ SKA1 ($N_{\text{field}} = 4$)	6.21×10^{-4}	1.04×10^{-4}	4.21×10^{-3}	3.65×10^{-3}	1.95×10^{-1}
+ SKA1 ($N_{\text{field}} = 8$)	5.68×10^{-4}	9.68×10^{-5}	3.97×10^{-3}	3.41×10^{-3}	1.93×10^{-1}
+ SKA2 ($N_{\text{field}} = 4$)	4.02×10^{-4}	9.28×10^{-5}	2.65×10^{-3}	2.43×10^{-3}	1.82×10^{-1}
+ SKA2 ($N_{\text{field}} = 8$)	3.17×10^{-4}	8.23×10^{-5}	2.07×10^{-3}	1.94×10^{-3}	1.73×10^{-1}
	$\sigma(\tau)$	$\sigma(Y_p)$	$\sigma(\Sigma m_\nu)$	$\sigma(r_\nu)$	
Planck + PB-2(0.2) + BAO + H_0	4.55×10^{-3}	8.10×10^{-3}	4.96×10^{-2}	8.54×10^{-1}	
+ SKA1 ($N_{\text{field}} = 4$)	4.55×10^{-3}	7.15×10^{-3}	4.67×10^{-2}	7.26×10^{-1}	
+ SKA1 ($N_{\text{field}} = 8$)	4.50×10^{-3}	6.59×10^{-3}	4.46×10^{-2}	6.43×10^{-1}	
+ SKA2 ($N_{\text{field}} = 4$)	4.31×10^{-3}	5.33×10^{-3}	3.40×10^{-2}	3.90×10^{-1}	
+ SKA2 ($N_{\text{field}} = 8$)	4.17×10^{-3}	4.65×10^{-3}	2.86×10^{-2}	2.92×10^{-1}	
Planck + SA(0.2) + BAO + H_0	4.46×10^{-3}	6.77×10^{-3}	3.97×10^{-2}	7.36×10^{-1}	
+ SKA1 ($N_{\text{field}} = 4$)	4.46×10^{-3}	6.09×10^{-3}	3.75×10^{-2}	6.48×10^{-1}	
+ SKA1 ($N_{\text{field}} = 8$)	4.41×10^{-3}	5.64×10^{-3}	3.58×10^{-2}	5.87×10^{-1}	
+ SKA2 ($N_{\text{field}} = 4$)	4.19×10^{-3}	4.75×10^{-3}	2.66×10^{-2}	3.75×10^{-1}	
+ SKA2 ($N_{\text{field}} = 8$)	3.98×10^{-3}	4.12×10^{-3}	2.28×10^{-2}	2.85×10^{-1}	

Table 38: $f_{\text{sky}} = 0.2$, normal hierarchy, with the residual foregrounds of CMB, without those of 21 cm line.

	$\sigma(\Omega_m h^2)$	$\sigma(\Omega_b h^2)$	$\sigma(\Omega_\Lambda)$	$\sigma(n_s)$	$\sigma(A_s \times 10^{10})$
Planck + PB-2(0.2) + BAO + H_0	8.15×10^{-4}	1.33×10^{-4}	4.69×10^{-3}	4.61×10^{-3}	2.03×10^{-1}
+ SKA1 ($N_{\text{field}} = 4$)	6.39×10^{-4}	1.21×10^{-4}	4.25×10^{-3}	4.19×10^{-3}	2.03×10^{-1}
+ SKA1 ($N_{\text{field}} = 8$)	5.69×10^{-4}	1.12×10^{-4}	4.01×10^{-3}	3.91×10^{-3}	2.00×10^{-1}
+ SKA2 ($N_{\text{field}} = 4$)	4.10×10^{-4}	1.06×10^{-4}	2.68×10^{-3}	2.69×10^{-3}	1.91×10^{-1}
+ SKA2 ($N_{\text{field}} = 8$)	3.22×10^{-4}	9.23×10^{-5}	2.11×10^{-3}	2.13×10^{-3}	1.85×10^{-1}
Planck + SA(0.2) + BAO + H_0	7.47×10^{-4}	1.14×10^{-4}	4.59×10^{-3}	3.97×10^{-3}	1.95×10^{-1}
+ SKA1 ($N_{\text{field}} = 4$)	6.16×10^{-4}	1.04×10^{-4}	4.18×10^{-3}	3.65×10^{-3}	1.95×10^{-1}
+ SKA1 ($N_{\text{field}} = 8$)	5.55×10^{-4}	9.67×10^{-5}	3.92×10^{-3}	3.42×10^{-3}	1.93×10^{-1}
+ SKA2 ($N_{\text{field}} = 4$)	3.97×10^{-4}	9.27×10^{-5}	2.65×10^{-3}	2.46×10^{-3}	1.83×10^{-1}
+ SKA2 ($N_{\text{field}} = 8$)	3.12×10^{-4}	8.21×10^{-5}	2.08×10^{-3}	1.96×10^{-3}	1.74×10^{-1}
	$\sigma(\tau)$	$\sigma(Y_p)$	$\sigma(\Sigma m_\nu)$	$\sigma(r_\nu)$	
Planck + PB-2(0.2) + BAO + H_0	4.55×10^{-3}	8.11×10^{-3}	6.20×10^{-2}	9.71×10^{-1}	
+ SKA1 ($N_{\text{field}} = 4$)	4.55×10^{-3}	7.17×10^{-3}	4.52×10^{-2}	4.16×10^{-1}	
+ SKA1 ($N_{\text{field}} = 8$)	4.50×10^{-3}	6.61×10^{-3}	4.23×10^{-2}	3.09×10^{-1}	
+ SKA2 ($N_{\text{field}} = 4$)	4.32×10^{-3}	5.37×10^{-3}	3.28×10^{-2}	1.28×10^{-1}	
+ SKA2 ($N_{\text{field}} = 8$)	4.19×10^{-3}	4.67×10^{-3}	2.81×10^{-2}	9.09×10^{-2}	
Planck + SA(0.2) + BAO + H_0	4.47×10^{-3}	6.77×10^{-3}	5.20×10^{-2}	8.39×10^{-1}	
+ SKA1 ($N_{\text{field}} = 4$)	4.47×10^{-3}	6.10×10^{-3}	3.62×10^{-2}	4.03×10^{-1}	
+ SKA1 ($N_{\text{field}} = 8$)	4.41×10^{-3}	5.65×10^{-3}	3.31×10^{-2}	3.03×10^{-1}	
+ SKA2 ($N_{\text{field}} = 4$)	4.21×10^{-3}	4.77×10^{-3}	2.44×10^{-2}	1.27×10^{-1}	
+ SKA2 ($N_{\text{field}} = 8$)	4.01×10^{-3}	4.14×10^{-3}	2.15×10^{-2}	9.06×10^{-2}	

Table 39: $f_{\text{sky}} = 0.2$, inverted hierarchy, with the residual foregrounds of CMB, without those of 21 cm line.

	$\sigma(\Omega_m h^2)$	$\sigma(\Omega_b h^2)$	$\sigma(\Omega_\Lambda)$	$\sigma(n_s)$	$\sigma(A_s \times 10^{10})$
Planck + PB-2(0.65) + BAO + H_0	6.81×10^{-4}	1.08×10^{-4}	4.47×10^{-3}	3.81×10^{-3}	1.97×10^{-1}
+ SKA1 ($N_{\text{field}} = 4$)	6.09×10^{-4}	1.01×10^{-4}	4.19×10^{-3}	3.55×10^{-3}	1.98×10^{-1}
+ SKA1 ($N_{\text{field}} = 8$)	5.60×10^{-4}	9.58×10^{-5}	3.98×10^{-3}	3.36×10^{-3}	1.96×10^{-1}
+ SKA2 ($N_{\text{field}} = 4$)	3.97×10^{-4}	9.15×10^{-5}	2.66×10^{-3}	2.44×10^{-3}	1.87×10^{-1}
+ SKA2 ($N_{\text{field}} = 8$)	3.14×10^{-4}	8.21×10^{-5}	2.08×10^{-3}	1.97×10^{-3}	1.80×10^{-1}
Planck + SA(0.65) + BAO + H_0	6.32×10^{-4}	8.89×10^{-5}	4.33×10^{-3}	3.22×10^{-3}	1.86×10^{-1}
+ SKA1 ($N_{\text{field}} = 4$)	5.78×10^{-4}	8.43×10^{-5}	4.07×10^{-3}	3.05×10^{-3}	1.86×10^{-1}
+ SKA1 ($N_{\text{field}} = 8$)	5.36×10^{-4}	8.06×10^{-5}	3.86×10^{-3}	2.91×10^{-3}	1.85×10^{-1}
+ SKA2 ($N_{\text{field}} = 4$)	3.82×10^{-4}	7.78×10^{-5}	2.62×10^{-3}	2.22×10^{-3}	1.75×10^{-1}
+ SKA2 ($N_{\text{field}} = 8$)	3.03×10^{-4}	7.12×10^{-5}	2.06×10^{-3}	1.82×10^{-3}	1.67×10^{-1}
	$\sigma(\tau)$	$\sigma(Y_p)$	$\sigma(\Sigma m_\nu)$	$\sigma(r_\nu)$	
Planck + PB-2(0.65) + BAO + H_0	4.52×10^{-3}	6.53×10^{-3}	4.34×10^{-2}	7.37×10^{-1}	
+ SKA1 ($N_{\text{field}} = 4$)	4.53×10^{-3}	5.96×10^{-3}	4.15×10^{-2}	6.50×10^{-1}	
+ SKA1 ($N_{\text{field}} = 8$)	4.48×10^{-3}	5.58×10^{-3}	4.00×10^{-2}	5.88×10^{-1}	
+ SKA2 ($N_{\text{field}} = 4$)	4.28×10^{-3}	4.73×10^{-3}	3.08×10^{-2}	3.76×10^{-1}	
+ SKA2 ($N_{\text{field}} = 8$)	4.12×10^{-3}	4.17×10^{-3}	2.63×10^{-2}	2.86×10^{-1}	
Planck + SA(0.65) + BAO + H_0	4.34×10^{-3}	5.37×10^{-3}	3.58×10^{-2}	5.85×10^{-1}	
+ SKA1 ($N_{\text{field}} = 4$)	4.34×10^{-3}	5.01×10^{-3}	3.45×10^{-2}	5.38×10^{-1}	
+ SKA1 ($N_{\text{field}} = 8$)	4.30×10^{-3}	4.75×10^{-3}	3.34×10^{-2}	5.02×10^{-1}	
+ SKA2 ($N_{\text{field}} = 4$)	4.09×10^{-3}	4.14×10^{-3}	2.55×10^{-2}	3.50×10^{-1}	
+ SKA2 ($N_{\text{field}} = 8$)	3.89×10^{-3}	3.67×10^{-3}	2.20×10^{-2}	2.73×10^{-1}	

Table 40: $f_{\text{sky}} = 0.65$, normal hierarchy, with the residual foregrounds of CMB, without those of 21 cm line.

	$\sigma(\Omega_m h^2)$	$\sigma(\Omega_b h^2)$	$\sigma(\Omega_\Lambda)$	$\sigma(n_s)$	$\sigma(A_s \times 10^{10})$
Planck + PB-2(0.65) + BAO + H_0	7.32×10^{-4}	1.09×10^{-4}	4.53×10^{-3}	3.81×10^{-3}	1.97×10^{-1}
+ SKA1 ($N_{\text{field}} = 4$)	6.03×10^{-4}	1.01×10^{-4}	4.16×10^{-3}	3.56×10^{-3}	1.98×10^{-1}
+ SKA1 ($N_{\text{field}} = 8$)	5.46×10^{-4}	9.58×10^{-5}	3.94×10^{-3}	3.37×10^{-3}	1.96×10^{-1}
+ SKA2 ($N_{\text{field}} = 4$)	3.91×10^{-4}	9.16×10^{-5}	2.66×10^{-3}	2.47×10^{-3}	1.87×10^{-1}
+ SKA2 ($N_{\text{field}} = 8$)	3.09×10^{-4}	8.22×10^{-5}	2.09×10^{-3}	1.99×10^{-3}	1.81×10^{-1}
Planck + SA(0.65) + BAO + H_0	6.67×10^{-4}	8.90×10^{-5}	4.37×10^{-3}	3.22×10^{-3}	1.86×10^{-1}
+ SKA1 ($N_{\text{field}} = 4$)	5.76×10^{-4}	8.43×10^{-5}	4.05×10^{-3}	3.06×10^{-3}	1.87×10^{-1}
+ SKA1 ($N_{\text{field}} = 8$)	5.28×10^{-4}	8.05×10^{-5}	3.82×10^{-3}	2.92×10^{-3}	1.86×10^{-1}
+ SKA2 ($N_{\text{field}} = 4$)	3.76×10^{-4}	7.78×10^{-5}	2.62×10^{-3}	2.24×10^{-3}	1.76×10^{-1}
+ SKA2 ($N_{\text{field}} = 8$)	2.99×10^{-4}	7.11×10^{-5}	2.07×10^{-3}	1.84×10^{-3}	1.69×10^{-1}
	$\sigma(\tau)$	$\sigma(Y_p)$	$\sigma(\Sigma m_\nu)$	$\sigma(r_\nu)$	
Planck + PB-2(0.65) + BAO + H_0	4.52×10^{-3}	6.53×10^{-3}	5.40×10^{-2}	8.36×10^{-1}	
+ SKA1 ($N_{\text{field}} = 4$)	4.53×10^{-3}	5.97×10^{-3}	4.07×10^{-2}	4.03×10^{-1}	
+ SKA1 ($N_{\text{field}} = 8$)	4.48×10^{-3}	5.60×10^{-3}	3.81×10^{-2}	3.03×10^{-1}	
+ SKA2 ($N_{\text{field}} = 4$)	4.30×10^{-3}	4.75×10^{-3}	2.94×10^{-2}	1.27×10^{-1}	
+ SKA2 ($N_{\text{field}} = 8$)	4.13×10^{-3}	4.19×10^{-3}	2.55×10^{-2}	9.07×10^{-2}	
Planck + SA(0.65) + BAO + H_0	4.35×10^{-3}	5.38×10^{-3}	4.47×10^{-2}	6.69×10^{-1}	
+ SKA1 ($N_{\text{field}} = 4$)	4.35×10^{-3}	5.02×10^{-3}	3.46×10^{-2}	3.79×10^{-1}	
+ SKA1 ($N_{\text{field}} = 8$)	4.30×10^{-3}	4.75×10^{-3}	3.19×10^{-2}	2.93×10^{-1}	
+ SKA2 ($N_{\text{field}} = 4$)	4.11×10^{-3}	4.16×10^{-3}	2.36×10^{-2}	1.26×10^{-1}	
+ SKA2 ($N_{\text{field}} = 8$)	3.92×10^{-3}	3.69×10^{-3}	2.07×10^{-2}	9.02×10^{-2}	

Table 41: $f_{\text{sky}} = 0.65$, inverted hierarchy, with the residual foregrounds of CMB, without those of 21 cm line.

of Planck + Simons Array + BAO (DESI) + SKA phase 2, we will be able to determine the hierarchy to be inverted or normal at 2σ unless the mass structure is degenerated. By using Omniscope, we can discriminate any mass hierarchies up to $\sum m_\nu \sim 0.1$ eV [52].

Our results indicate that combining the 21 cm line observations with the CMB polarization observations has strong impacts on the determinations of the neutrino property and the origin of matter in the Universe.

Acknowledgments

We thank Kiyotomo Ichiki for a useful correspondence about specifications of SKA, and Maresuke Shiraishi for useful comments about treatments of the residual foregrounds of CMB. This work is supported in part by MEXT KAKENHI Grant Numbers 15H05889 (K.K.), 15H05891 (M.H.), JSPS KAKENHI Grant Numbers 26105520 (K.K.), 26247042 (K.K.) and 26220709 (M.H.). The work of K.K. is also supported by the Center for the Promotion of Integrated Science (CPIS) of Sokendai (1HB5804100).

Note added

While finalizing this manuscript, Ref. [96] appeared which has some overlaps with this work.

References

- [1] B. Aharmim *et al.* [SNO Collaboration], Phys. Rev. Lett. **101**, 111301 (2008).
- [2] P. Adamson *et al.* [MINOS Collaboration], Phys. Rev. Lett. **101**, 131802 (2008) [arXiv:0806.2237 [hep-ex]].
- [3] T. Thummller [KATRIN Collaboration], Phys. Part. Nucl. **42**, 590 (2011); M. Beck [KATRIN Collaboration], J. Phys. Conf. Ser. **203**, 012097 (2010) [arXiv:0910.4862 [nucl-ex]].
- [4] J. J. Gomez-Cadenas, J. Martin-Albo, M. Sorel, P. Ferrario, F. Monrabal, J. Munoz-Vidal, P. Novella and A. Poves, JCAP **1106**, 007 (2011) [arXiv:1010.5112 [hep-ex]].
- [5] INO, India Based Neutrino Observatory, URL <http://www.ino.tifr.res.in/ino/>
- [6] M. Blennow and T. Schwetz, arXiv:1203.3388 [hep-ph].
- [7] E. K. Akhmedov, S. Razzaque and A. Y. Smirnov, arXiv:1205.7071 [hep-ph].
- [8] D. S. Ayres *et al.* [NOvA Collaboration], hep-ex/0503053.
- [9] M. Ishitsuka, T. Kajita, H. Minakata and H. Nunokawa, Phys. Rev. D **72**, 033003 (2005) [hep-ph/0504026].
- [10] K. Hagiwara, N. Okamura and K. -i. Senda, Phys. Lett. B **637**, 266 (2006) [Erratum-ibid. B **641**, 491 (2006)] [hep-ph/0504061].
- [11] A. Badertscher, T. Hasegawa, T. Kobayashi, A. Marchionni, A. Meregaglia, T. Maruyama, K. Nishikawa and A. Rubbia, arXiv:0804.2111 [hep-ph].
- [12] S. K. Agarwalla and P. Hernandez, arXiv:1204.4217 [hep-ph].
- [13] O. Elgaroy and O. Lahav, JCAP **0304**, 004 (2003) [astro-ph/0303089].
- [14] K. Ichikawa, M. Fukugita and M. Kawasaki, Phys. Rev. D **71**, 043001 (2005).
- [15] U. Seljak *et al.* [SDSS Collaboration], Phys. Rev. D **71**, 103515 (2005) [astro-ph/0407372].
- [16] A. Goobar, S. Hannestad, E. Mortsell and H. Tu, JCAP **0606**, 019 (2006) [astro-ph/0602155].
- [17] K. Ichiki, M. Takada and T. Takahashi, Phys. Rev. D **79**, 023520 (2009).
- [18] S. A. Thomas, F. B. Abdalla and O. Lahav, Phys. Rev. Lett. **105**, 031301 (2010) [arXiv:0911.5291 [astro-ph.CO]].

- [19] S. Riemer-Sorensen, C. Blake, D. Parkinson, T. M. Davis, S. Brough, M. Colless, C. Contreras and W. Couch *et al.*, Phys. Rev. D **85**, 081101 (2012) [arXiv:1112.4940 [astro-ph.CO]].
- [20] S. Hannestad, A. Mirizzi, G. G. Raffelt and Y. Y. Y. Wong, JCAP **1008**, 001 (2010).
- [21] S. Saito, M. Takada and A. Taruya, Phys. Rev. D **83**, 043529 (2011).
- [22] P. Crotty, J. Lesgourgues and S. Pastor, Phys. Rev. D **69**, 123007 (2004) [hep-ph/0402049].
- [23] U. Seljak, A. Slosar and P. McDonald, JCAP **0610**, 014 (2006) [astro-ph/0604335].
- [24] M. Fukugita, K. Ichikawa, M. Kawasaki and O. Lahav, Phys. Rev. D **74**, 027302 (2006).
- [25] E. Komatsu *et al.* [WMAP Collaboration], Astrophys. J. Suppl. **180**, 330 (2009) [arXiv:0803.0547 [astro-ph]].
- [26] B. A. Reid, W. J. Percival, D. J. Eisenstein, L. Verde, D. N. Spergel, R. A. Skibba, N. A. Bahcall and T. Budavari *et al.*, Mon. Not. Roy. Astron. Soc. **404**, 60 (2010) [arXiv:0907.1659 [astro-ph.CO]].
- [27] B. A. Reid, L. Verde, R. Jimenez and O. Mena, JCAP **1001**, 003 (2010) [arXiv:0910.0008 [astro-ph.CO]].
- [28] J. Hamann, S. Hannestad, J. Lesgourgues, C. Rampf and Y. Y. Y. Wong, JCAP **1007**, 022 (2010) [arXiv:1003.3999 [astro-ph.CO]].
- [29] E. Komatsu *et al.* [WMAP Collaboration], Astrophys. J. Suppl. **192**, 18 (2011) [arXiv:1001.4538 [astro-ph.CO]].
- [30] E. Di Valentino, S. Galli, M. Lattanzi, A. Melchiorri, P. Natoli, L. Pagano and N. Said, Phys. Rev. D **88**, no. 2, 023501 (2013) [arXiv:1301.7343 [astro-ph.CO]].
- [31] P. A. R. Ade *et al.* [Planck Collaboration], arXiv:1303.5076 [astro-ph.CO].
- [32] P. A. R. Ade *et al.* [Planck Collaboration], arXiv:1502.01589 [astro-ph.CO].
- [33] E. Giusarma, E. Di Valentino, M. Lattanzi, A. Melchiorri and O. Mena, Phys. Rev. D **90**, no. 4, 043507 (2014) [arXiv:1403.4852 [astro-ph.CO]].
- [34] E. Di Valentino, E. Giusarma, M. Lattanzi, O. Mena, A. Melchiorri and J. Silk, arXiv:1507.08665 [astro-ph.CO].
- [35] E. Di Valentino, A. Melchiorri and J. Silk, arXiv:1507.06646 [astro-ph.CO].
- [36] E. Pierpaoli, Mon. Not. Roy. Astron. Soc. **342**, L63 (2003) [astro-ph/0302465].

- [37] P. Crotty, J. Lesgourgues and S. Pastor, Phys. Rev. D **67**, 123005 (2003) [astro-ph/0302337].
- [38] N. Said, E. Di Valentino and M. Gerbino, Phys. Rev. D **88**, no. 2, 023513 (2013) [arXiv:1304.6217 [astro-ph.CO]].
- [39] E. Di Valentino, M. Gerbino and A. Melchiorri, Phys. Rev. D **87**, no. 10, 103523 (2013).
- [40] E. Di Valentino, M. Lattanzi, G. Mangano, A. Melchiorri and P. Serpico, curvaton scenario,” Phys. Rev. D **85**, 043511 (2012) [arXiv:1111.3810 [astro-ph.CO]].
- [41] E. Di Valentino and A. Melchiorri, Phys. Rev. D **90**, no. 8, 083531 (2014) [arXiv:1405.5418 [astro-ph.CO]].
- [42] J. Lesgourgues, L. Perotto, S. Pastor and M. Piat, Phys. Rev. D **73**, 045021 (2006) [astro-ph/0511735].
- [43] R. de Putter, O. Zahn and E. V. Linder, Phys. Rev. D **79**, 065033 (2009).
- [44] K. N. Abazajian *et al.* [Topical Conveners: K.N. Abazajian, J.E. Carlstrom, A.T. Lee Collaboration], Astropart. Phys. **63**, 66 (2015) [arXiv:1309.5383 [astro-ph.CO]].
- [45] W. L. K. Wu, J. Errard, C. Dvorkin, C. L. Kuo, A. T. Lee, P. McDonald, A. Slosar and O. Zahn, Astrophys. J. **788**, 138 (2014) [arXiv:1402.4108 [astro-ph.CO]].
- [46] M. Gerbino, M. Lattanzi and A. Melchiorri, arXiv:1507.08614 [hep-ph].
- [47] M. McQuinn, O. Zahn, M. Zaldarriaga, L. Hernquist and S. R. Furlanetto, Astrophys. J. **653**, 815 (2006) [arXiv:astro-ph/0512263].
- [48] A. Loeb and S. Wyithe, Phys. Rev. Lett. **100**, 161301 (2008).
- [49] J. R. Pritchard and E. Pierpaoli, Phys. Rev. D **78**, 065009 (2008).
- [50] J. R. Pritchard and E. Pierpaoli, Nucl. Phys. Proc. Suppl. **188**, 31 (2009).
- [51] K. N. Abazajian, E. Calabrese, A. Cooray, F. De Bernardis, S. Dodelson, A. Friedland, G. M. Fuller and S. Hannestad *et al.*, Astropart. Phys. **35**, 177 (2011) [arXiv:1103.5083 [astro-ph.CO]].
- [52] Y. Oyama, A. Shimizu and K. Kohri, Phys. Lett. B **718**, 1186 (2013) [arXiv:1205.5223 [astro-ph.CO]].
- [53] Y. Oyama, “Constraints on the neutrino parameters by future cosmological 21cm line and precise CMB polarization observations (PhD thesis, The Graduate University for Advanced Studies (SOKENDAI), 2014)”, arXiv:1510.05161 [astro-ph.CO].

- [54] K. Kohri, Y. Oyama, T. Sekiguchi and T. Takahashi, JCAP **1409**, 014 (2014) [arXiv:1404.4847 [astro-ph.CO]].
- [55] F. Villaescusa-Navarro, P. Bull and M. Viel, arXiv:1507.05102 [astro-ph.CO].
- [56] M. Tegmark and M. Zaldarriaga, Phys. Rev. D **79**, 083530 (2009) [arXiv:0805.4414 [astro-ph]].
- [57] M. Tegmark and M. Zaldarriaga, Phys. Rev. D **82**, 103501 (2010) [arXiv:0909.0001 [astro-ph.CO]].
- [58] K. Kohri, Y. Oyama, T. Sekiguchi and T. Takahashi, JCAP **1310**, 065 (2013) [arXiv:1303.1688 [astro-ph.CO]].
- [59] <http://www.skatelescope.org/>
- [60] <http://desi.lbl.gov/>
- [61] S. Furlanetto, S. P. Oh and F. Briggs, Phys. Rept. **433**, 181 (2006).
- [62] J. R. Pritchard and A. Loeb, arXiv:1109.6012 [astro-ph.CO].
- [63] P. Madau, A. Meiksin and M. J. Rees, Astrophys. J. **475**, 429 (1997) [arXiv:astro-ph/9608010].
- [64] S. Furlanetto, Mon. Not. Roy. Astron. Soc. **371**, 867 (2006) [arXiv:astro-ph/0604040].
- [65] J. R. Pritchard and A. Loeb, Phys. Rev. D **78**, 103511 (2008) [arXiv:0802.2102 [astro-ph]].
- [66] S. A. Wouthuysen, Astron. J. **57**, 31 (1952).
- [67] G. B. Field, Proc. IRE. **46**, 240 (1958).
- [68] Y. Mao, M. Tegmark, M. McQuinn, M. Zaldarriaga and O. Zahn, Phys. Rev. D **78**, 023529 (2008) [arXiv:0802.1710 [astro-ph]].
- [69] M. McQuinn, A. Lidz, O. Zahn, S. Dutta, L. Hernquist and M. Zaldarriaga, Mon. Not. Roy. Astron. Soc. **377**, 1043 (2007) [astro-ph/0610094].
- [70] M. McQuinn, L. Hernquist, M. Zaldarriaga and S. Dutta, Mon. Not. Roy. Astron. Soc. **381**, 75 (2007) [arXiv:0704.2239 [astro-ph]].
- [71] M. Tegmark, A. Taylor and A. Heavens, Astrophys. J. **480**, 22 (1997) [arXiv:astro-ph/9603021].
- [72] E. Chapman, F. B. Abdalla, G. Harker, V. Jelic, P. Labropoulos, S. Zaroubi, M. A. Brentjens and A. G. de Bruyn *et al.*, arXiv:1201.2190 [astro-ph.CO].

- [73] <http://www.lofar.org/>
- [74] G. Mellema, L. V. E. Koopmans, F. A. Abdalla, G. Bernardi, B. Ciardi, S. Daiboo, A. G. de Bruyn and K. K. Datta *et al.*, Exper. Astron. **36**, 235 (2013) [arXiv:1210.0197 [astro-ph.CO]].
- [75] J. Lesgourgues and S. Pastor, Phys. Rept. **429**, 307 (2006) [arXiv:astro-ph/0603494].
- [76] Y. Y. Y. Wong, Ann. Rev. Nucl. Part. Sci. **61**, 69 (2011) [arXiv:1111.1436 [astro-ph.CO]].
- [77] J. Lesgourgues, S. Pastor and L. Perotto, Phys. Rev. D **70**, 045016 (2004) [hep-ph/0403296].
- [78] M. Takada, E. Komatsu and T. Futamase, Phys. Rev. D **73**, 083520 (2006) [astro-ph/0512374].
- [79] A. Slosar, Phys. Rev. D **73**, 123501 (2006) [astro-ph/0602133].
- [80] F. De Bernardis, T. D. Kitching, A. Heavens and A. Melchiorri, Phys. Rev. D **80**, 123509 (2009) [arXiv:0907.1917 [astro-ph.CO]].
- [81] R. Jimenez, T. Kitching, C. Pena-Garay and L. Verde, JCAP **1005**, 035 (2010) [arXiv:1003.5918 [astro-ph.CO]].
- [82] T. Okamoto and W. Hu, Phys. Rev. D **67**, 083002 (2003)[astro-ph/0301031].
- [83] <http://lpsc.in2p3.fr/perotto/>
- [84] D. Baumann *et al.* [CMBPol Study Team Collaboration], AIP Conf. Proc. **1141**, 10 (2009) [arXiv:0811.3919 [astro-ph]].
- [85] L. Verde, H. Peiris and R. Jimenez, JCAP **0601**, 019 (2006) [astro-ph/0506036].
- [86] N. Katayama and E. Komatsu, Astrophys. J. **737**, 78 (2011) [arXiv:1101.5210 [astro-ph.CO]].
- [87] L. Page *et al.* [WMAP Collaboration], Astrophys. J. Suppl. **170**, 335 (2007) [astro-ph/0603450].
- [88] E. M. Leitch, J. M. Kovac, N. W. Halverson, J. E. Carlstrom, C. Pryke and M. W. E. Smith, Astrophys. J. **624**, 10 (2005) [astro-ph/0409357].
- [89] D. P. Finkbeiner, M. Davis and D. J. Schlegel, Astrophys. J. **524**, 867 (1999) [astro-ph/9905128].
- [90] J. Tauber *et al.* [Planck Collaboration], astro-ph/0604069.

- [91] A. Albrecht, G. Bernstein, R. Cahn, W. L. Freedman, J. Hewitt, W. Hu, J. Huth and M. Kamionkowski *et al.*, astro-ph/0609591.
- [92] C. Blake, D. Parkinson, B. Bassett, K. Glazebrook, M. Kunz and R. C. Nichol, Mon. Not. Roy. Astron. Soc. **365**, 255 (2006) [astro-ph/0510239].
- [93] A. Font-Ribera, P. McDonald, N. Mostek, B. A. Reid, H. J. Seo and A. Slosar, JCAP **1405**, 023 (2014) [arXiv:1308.4164 [astro-ph.CO]].
- [94] A. Lewis, A. Challinor and A. Lasenby, Astrophys. J. **538**, 473 (2000) [astro-ph/9911177].
- [95] <http://camb.info/>
- [96] A. Liu, J. R. Pritchard, R. Allison, A. R. Parsons, U. Seljak and B. D. Sherwin, arXiv:1509.08463 [astro-ph.CO].